NANYANG TECHNOLOGICAL UNIVERSITY

THE ELECTRO-OXIDATION OF C1, C2 AND C3 SATURATED ALCOHOLS ON NICKEL-COBALT OXIDES

SUN SHENGNAN

SCHOOL OF MATERIALS SCIENCE AND ENGINEERING

2017

THE ELECTRO-OXIDATION OF C1, C2 AND C3 SATURATED ALCOHOLS ON NICKEL-COBALT OXIDES

SUN SHENGNAN

SCHOOL OF MATERIALS SCIENCE AND ENGINEERING

A thesis submitted to the Nanyang Technological University
in partial fulfilment of the requirement for the degree of
Doctor of Philosophy

2017

Statement of Originality

I hereby certify that the work embodied in this thesis is the result of original research and has not been submitted for a higher degree to any other University or Institution.

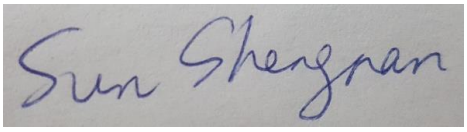

08-Aug-2017

. . . . . .
Date

. . . . . .
Sun Shengnan

Abstract

The energy and environment problems are becoming focus in recent decades. The electro-oxidation of small molecules is attracting an increasing interest in many fields like water splitting, fuel cell, environmental protection, and fine chemical industry. Hydrogen, water, urea, and alcohols is becoming the major objects due to their simple molecule structure and availability in energy and fine chemistry industry. Water splitting is based on the bond cleavage of hydrogen and the bond formation of oxygen and oxygen by applying external energy to obtain hydrogen as clean energy. In fuel cells, the oxidation of fuels like hydrogen and alcohol plays the key role in obtaining high voltage and high efficiency. In the field of environmental protection, the substance with potential toxicity can be converted into environment-friendly substance by electro-oxidation. In fine chemical industry, converting alcohols to value-added chemicals by electrochemical method has also become the hot topic.

This thesis is focused on the electro-oxidation of small molecular (C1, C2, and C3) alcohols on Ni-Co hydroxides and Ni-Co oxides in alkaline. The Ni-Co hydroxides with various Ni contents were prepared by electrodeposition, and Ni-Co oxides were obtained by calcinating the corresponding Ni-Co hydroxides. For C1 alcohol methanol, the investigation was given to the Ni effect in Ni-Co hydroxides and Ni-Co oxides for methanol oxidation reaction. Cyclic voltammetry (CV) and chronoamperometry (CA) methods were used to compare the methanol oxidation activity. The results show that as the Ni content increases, the methanol oxidation activity on Ni-Co hydroxides increases, while the activity on Ni-Co oxides exhibits a volcano-shaped trend. The highest activity on Ni-Co oxides was found at the atomic ratio of Ni / (Ni + Co) = 46%. By conducting electrochemical impedance spectroscopy (EIS), it was found that Ni can promote the adsorption of intermediate products. It suggests that this best ratio of 46% for the methanol electro-oxidation was due to the balance of the adsorption of intermediate products and methanol oxidation onset potential. For C2 alcohols, ethanol and ethylene glycol, the study was performed to reveal the Ni effect of Ni-Co oxides on the oxidation activity and the

product selectivity. The similar volcano-shaped trend was also obtained, i.e. the ratio of 46% is the optimal one for the two alcohol oxidation reactions. The oxidation products were analyzed by nuclear magnetic resonance (NMR) technique and it was found that the functional groups were converted from -OH to -COOH. The electro-oxidation of C3 saturated alcohols was studied on Co_3O_4. It shows that C3 saturated alcohols had different reaction rates on Co_3O_4, which presented the following order: glycerol (GLY) > 1,2-propanediol (1,2-P) > 1,3-propanediol (1,3-P) > 1-propanol (1-P) > 2-propanol (2-P). Through NMR analysis, we found that for the adjacent hydroxyl groups, the C-C bond can be readily broken up.

In future work, we plan to compare Ni/Co effect in different coordination environments on alcohol oxidation. $Ni_xCo_{1-x}Al_2O_4$, $ZnCo_{2-x}Ni_xO_4$, and $LaCo_{1-x}Ni_xO_3$, three systems were chosen to fix Ni and Co in tetrahedral sites and octahedral sites, respectively. The glycerol oxidation will be compared on cobalt based oxides with cobalt in different coordination environments to investigate the coordination effect. Finally, dihydric alcohol (C2-C4) oxidation on Co_3O_4 will be compared to study the position effect of hydroxyl group on oxidation rate.

Acknowledgements

I would like to appreciate my supervisor Prof. Jason Xu Zhichuan for his advice and guidance during my PhD study. Prof. Xu made me know what is research and how to do research in a correct way. During these years, Prof. Xu gave me a lot of help on my research and he helped me open another door.

I would like to thank my TAC members Prof. Alex Yan Qingyu and Prof. Zhang Qichun for their comments on my work. I would like to thank Dr. Sun Libo, Dr. Wang Zilong, and Dr. Ren Xiao for their help for characterization.

A great gratitude will be given to all the group members, technical staffs, and administrative staffs.

Table of Contents

Figure Captions

curves of (b) Ni-Co hydroxides and (d) Ni-Co oxides in 1.0 M + 0.5 M methanol; (e) summary for the background, MOR and the net current densities; (f) summary for the MOR onset potentials.

Figure 4.7 EIS results of methanol oxidation on Ni-Co hydroxides with various Ni contents: 0% (a-c), 15% (d-f), 27% (g-i), 46% (j-l), 75% (m-o) and 100% (p-r).

Figure 4.8 EIS results of methanol oxidation on Ni-Co oxides with various Ni contents: 0% (a-c), 15% (d-f), 27% (g-i), 46% (j-l), 75% (m-o) and 100% (p-r).

Figure 4.9 Equivalent circuits for simulating MOR on Ni-Co hydroxides and Ni-Co oxides.

Figure 4.10 The relationship between double layer capacitance corrected current and Ni content.

Figure 4.11 The MOR j-t curves on Ni-Co hydroxides (a) and Ni-Co oxides (b) from EIS at 0.56 V; the MOR j-t curves on Ni-Co hydroxides (c) and Ni-Co oxides (d) from EIS at 0.60 V; summary of current densities on Ni-Co hydroxides (e) and Ni-Co oxides (f) with various Ni contents at the 120th second (solid lines) and 780th second (dash lines).

Figure 5.1 (a) The relationship of Ni content between in solution and in sample; (b) the mass loadings of Ni-Co oxides on stainless steel meshes.

Figure 5.2 (a) NCO CV curves in 1.0 M KOH solution; NCO CV curves in 1.0 M KOH + 0.5 M EG (b) or 0.5 M EtOH (c); (d) summary for currents at 0.60 V against the Ni content.

Figure 5.3 CV curves of (a) EG and (b) EtOH oxidation on NCO-46 at different scan rates in 1.0 M KOH solution.

Figure 5.4 EIS results of EG oxidation on NCOs: NCO-0 (a-c), NCO-15 (d-f), NCO-27 (g-i), NCO-46 (j-l), NCO-75(m-o) and NCO-100 (p-r).

Figure 5.5 EIS results of EtOH oxidation on NCOs: NCO-0 (a-c), NCO-15 (d-f), NCO-27 (g-i), NCO-46 (j-l), NCO-75(m-o) and NCO-100 (p-r).

Figure 5.6 The impedance Z vs the bias potential for EG (a) and EtOH (b) oxidation on NCOs.

Figure 5.7 Different concentrations of EG oxidation on NCO-46: (a) LSV curves; (b) the current at 0.60 V vs. concentration; (c) the potential at 2 mA vs. concentration; (d) DPV curve.

Figure 5.8 Different concentrations of EtOH oxidation on NCO-46: (a) LSV curves; (b) the current at 0.60 V vs. concentration; (c) the potential at 2 mA vs. concentration; (d) DPV curve.

Figure 5.9 The ^{13}C NMR spectra of solution after EG (a) and EtOH (b) oxidation.

Figure 5.10 (a) The Q obtained from the CA tests in Figure A.1; (b) the Q(EG)/Q(EtOH) value from Figure 5.10a; (c) the net Q(EG) and net Q(EtOH) from 0.42 V to each specific potential. The inset: CV anodic sweeps of NCO-46 in the absence and the presence of EG at 80 mV s^{-1}; (d) the value of the net Q(EG) / net Q(EtOH) from 0.42 V to each specific potential (blue line) and the value of the net Q(EG) / net Q(EtOH) within every 0.03 V step from 0.42 V (pink line).

Figure 6.1 The continuous CV cycles of Co_3O_4 in 1.0 M KOH in the absence (a) and the presence (b-f) of C3 saturated alcohols.

Figure 6.2 (a) CV curves of C3 saturated alcohol oxidation. (b) The oxidation potentials for C3 saturated alcohols. (c) The oxidation currents for C3 saturated alcohols. (d) Tafel plots of C3 saturated alcohol oxidation.

Figure 6.3 XANES profiles of Co_3O_4 under electrochemical conditions: Co_3O_4 in 1.0 M KOH solution (a) and KOH and GLY solution (b) at various potential; the relationship between energy edge and valence state of cobalt in 1.0 M KOH solution without (c) and with (d) GLY at various potential.

Figure 6.4 The ^{1}H (a, c, e) and ^{13}C (b, d, f) NMR spectra of the electrolyte solutions after 24-hour oxidation of GLY, 1,2-P and 1-P at 0.60 V. The dots represent the peaks from alcohol substrates.

Figure 6.5 CV curves of C3 saturated alcohol oxidation on Co_3O_4 in different concentrations of KOH solution: (a) no alcohol; (b) GLY; (c) 1,2-P; (d) 1,3-P; (e) 1-P; (f) 2-P.

Figure 6.6 Summary of the relationship between (a) oxidation potentials and KOH concentrations; (b) oxidation potentials and C3 saturated alcohol; (c) oxidation currents (at 1.524 V vs. RHE) and KOH concentrations; (d) oxidation currents (at 1.524 V vs. RHE) for C3 saturated alcohols.

Figure 7.1 The crystal structure of AB_2O_4. The A atoms are located in the yellow tetrahedral sites and the B atoms are located in the blue octahedral site.

Figure 7.2 XRD patterns of $Ni_xCo_{1-x}O$.

Figure 7.3 XRD patterns of $LaCo_{1-x}Ni_xO_3$.

Figure 7.4 Ideal cubic ABO_3 perovskite-type structure.

Figure 7.5 The crystal structure of rock salt.

Figure 7.6 The crystal structure of $LiCoO_2$. The small (purples), mid-sized (blue) and large (red) spheres are Li, Co and O atoms, respectively.

Figure 7.7 Layer structure of (a) $Co(OH)_2$, (b) CoO(OH), and (c)CoO_2.

Figure 7.8 The structure of dihydric alcohols to be investigated in future work.

Abbreviations

HER	Hydrogen evolution reaction
OER	Oxygen evolution reaction
EDS	Energy Dispersive X-ray Spectroscopy
XRD	X-ray Diffraction
SEM	Scanning Electron Microscopy
SEI	Secondary Electron Images
EIS	Electrochemical impedance spectrum
XRD	X-ray Diffraction
CV	Cyclic voltammetry
CA	Chronoamperometry
MOR	Methanol oxidation reaction
XAFS	X-ray absorption fine structure
XANES	X-ray absorption near edge structure
EXAFS	Extended X-ray absorption fine structure
SHE	Standard hydrogen electrode
RHE	Reversible hydrogen electrode
IHP	The inner Helmholtz plane
OHP	The outer Helmholtz plane
DPV	Differential pulse voltammetry
CPE	Constant phase elements
NMR	Nuclear magnetic resonance

Chapter 1

Introduction

The chapter will introduce the background and motivation of the electro-oxidation of C1, C2, and C3 saturated alcohols. Hydrogen production, fuel cell, and fine chemical industry are mentioned. The objects and scope lists the electro-oxidation of alcohols from C1 alcohol (methanol), C2 alcohols (ethylene glycol and ethanol), to C3 alcohols (glycerol, 1,2-propanediol, 1,3-propanediol, 1-propanol, and 2-propanol). The dissertation overview, findings and outcomes will be stressed at last.

1.1 Background

The increase of population, the acceleration of urbanization, and the rising living standards are rapidly increasing global energy consumption and environmental burdens in the last century. Energy consumption is expected to continue increasing dramatically in the coming years along with its associated environmental issues.[1, 2] Although till now there is no universal solution to solve all the problems related to energy and environment, catalysis is indeed playing a critical role in minimizing the energy consumption and waste generation, maximizing the value of the starting material, and optimizing reaction processes.[2-4] Metal-based catalysts, in this regard, have been of immerse importance in a wide range of diverse catalytic applications with high efficiency. However, fine-tuning of the structure and the properties of these catalyst is highly desirable to meet the stringent requirements in energy and environmental applications.[5-7]

Electrocatalysis as the optimization of electrode process by electrode choice becomes the ultimate goal in electrochemistry.[8] Electrocatalysis can be categorized into the homogeneous and heterogeneous electrocatalysis. The homogeneous electrocatalysis is referred to as a pre- or post-process involving a species in solution. If the electrode is not involved, it is not a typical electrocatalytic process. Electrocatalysis can be strictly defined as the effect of electrode materials on the electrode reaction rate.[8] Electrocatalysis have been used for water treatment like metal recovery and removal[9-11], electrocoagulation[12-14], electroflotation[15-17], electrochemical oxidation[18-20], nitrogen removal[21-23]. Also, electrocatalytic engineering can be used for manufacturing of chlorine[24-26], hydrogen[27-29], oxygen[30-32], ammonia[33-35], some other chemicals[36-38], and the practical application like fuel cell[39-41]. Low-cost and highly durable and fault-tolerant catalyst is still challenging.[41]

1.2 Electrochemical Oxidation of small Molecules

The energy and environment problems are becoming focus in recent decades. The electrochemical oxidation of small molecules is attracting an increasing attention in such fields as water splitting[27-32], fuel cell[42-44], environmental protection, and fine chemical

industry[36-38]. Hydrogen[45-47], water[30-32], and alcohols[48-50] is becoming the major objects due to their simple molecule structure and availability in energy and fine chemistry industry. For example, water splitting is based on the cleavage of hydrogen and oxygen bond and the formation of oxygen and oxygen bond by applying external force such as light emission and potential, to obtain hydrogen as clean energy.[27-32] In this case, water oxidation becomes the major obstacle for hydrogen production due to the high overpotential of oxygen evolution reaction in anodes. For the fuel cell field, the oxidation of fuels like hydrogen and alcohol plays the key role in terms of high voltage and high efficiency. High overpotential, catalyst poisoning, and high cost are becoming the limiting factors for the practical use. In fine chemical industry, the purpose is to convert alcohols to value-added chemicals by using electrochemical method, particularly for glycerol oxidation.[50-52]

1.2.1 Hydrogen Evolution

Owing to zero emission of carbon oxide species in practical utilization, hydrogen is an ideal candidate for the replacement of fossil fuels in the future. Water splitting is a dependable link between hydrogen energy and primary renewable energy.[53] During water splitting process, the hydrogen evolution reaction (HER) occurs in the cathode and the oxygen evolution reaction (OER) occurs in the anode (Figure 1.1). Compared HER in the cathode, OER in the anode needs a higher overpotential to activate. This higher overpotential becomes the major obstacle for water splitting.[3, 4, 54] Accordingly, to increase the efficiency of water splitting, more and more attention is concentrated on the development of electro-catalysts with low overpotential for oxygen evolution. The development of highly active electrocatalysts for oxygen OER is the crucial factor for renewable energy conversion and application. Though IrO_2 and RuO_2 are known as the most efficient catalyst for OER, due to their low reserve and high cost restrict their practical applications. Accordingly, designing and developing alternatives with excellent efficiency for OER and low cost is important, which is hot topic in 21st century.[55]

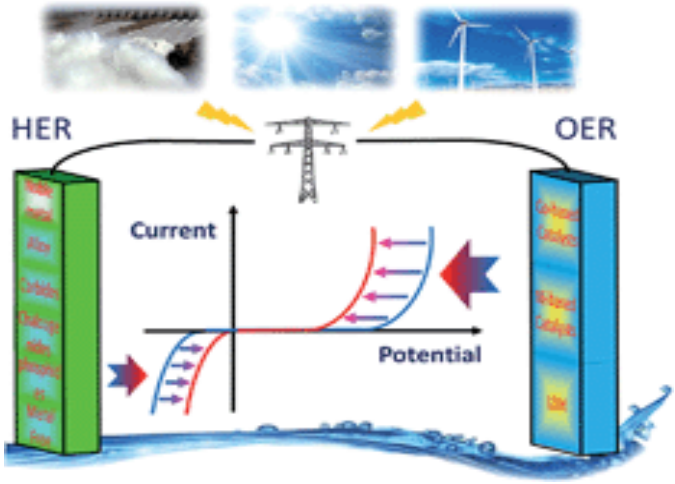

Figure 1.1 The scheme of hydrogen evolution reaction and oxygen evolution reaction[54]

For HER process, except for lowering OER overpotential and facilitating water oxidation directly, another strategy can help to increase HER efficiency. People are gradually utilizing the oxidation of another additives, which is easier to be oxidized than water thermodynamically. For example, for increase HER efficiency, some small organic molecules such as ethanol, benzyl alcohol, 4-nitrobenzyl alcohol, 4-methylbenzyl alcohol, 5-hydroxymethylfurfural widely under investigation in recent years.[3, 4, 54]

1.2.2 Fuel Cell

Nowadays, the development of alternative power sources is an important issue. A fuel cell is a device that convert fuel into electricity without direct combustion. Various fuels can be used in fuel cell to generate electricity. Some common fuels like hydrogen[45-47], alcohols[48-50], and urea[56] can be found in literatures and practical applications. The direct alcohol fuel cell (Figure 1.2) has attracted a great deal of interest since they have high energy conversion efficiencies and power density, low pollution emissions, low-cost and convenient storage. However, several problems restrict its practical commercialization such as materials and technical shortcomings.[57] In the electro-oxidation aspect, Pt is the best known monometallic electrocatalyst for small organic molecules because it has a capability to catalyze C-H bond cleavage and CO oxidation at a comparatively low overpotential.[58-60] However, the low utilization, high cost and decaying activity restrain their wide application. Therefore, Pt alloys[61-65] and non-Pt catalysts[66-72] are frequently

studied for alcohol oxidation to lower cost and decrease the activity loss. In terms of fuels, methanol is the most widely investigated fuel due to the high current density and good kinetics.[72, 73] Meanwhile, alcohols with higher molecule weight, like C2 alcohols (ethylene glycol and ethanol)[61] and C3 alcohols (glycerol, 1,2-propanol, 1,3-propanol, 1-proponal, and 2-proponal)[75-77] are less toxic and of higher boiling points and energy densities, making them alternatives for the application for fuel cell.[57, 59]

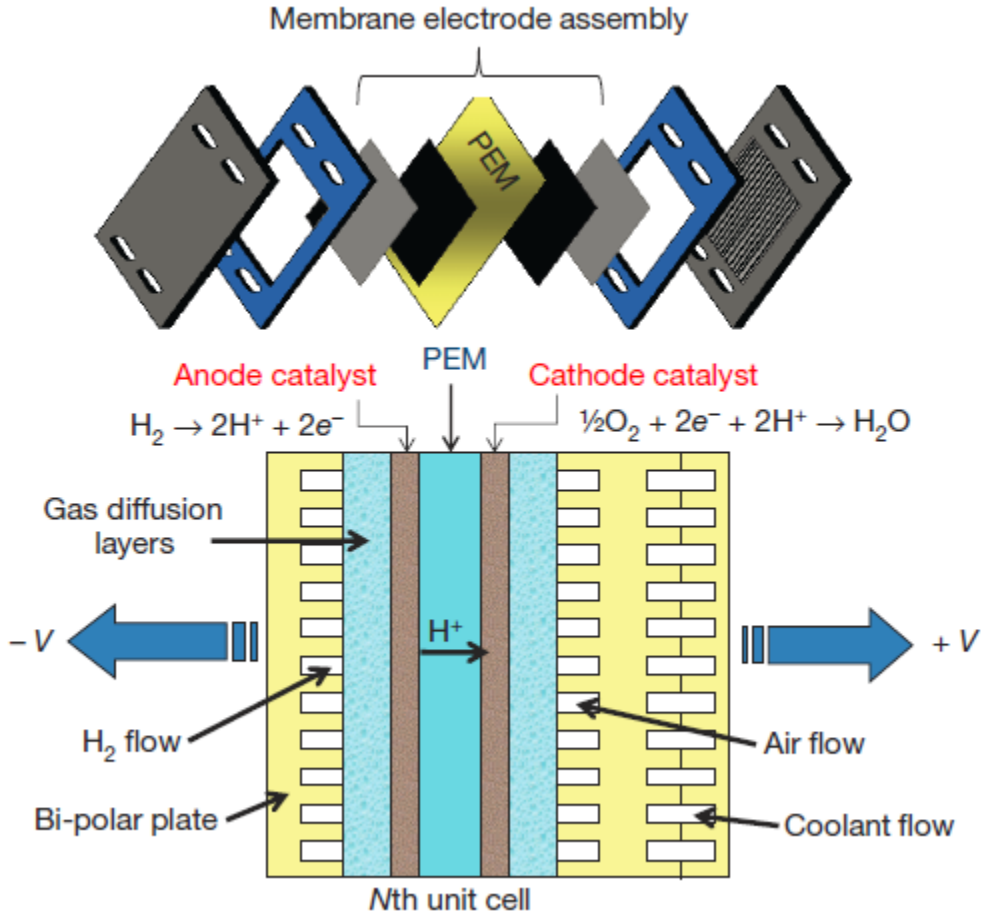

Figure 1.2 Fuel cell components. Unit cell cross-section of the Nth unit cell in a fuel cell stack, showing the components of an expanded MEA.[41]

1.2.3 Value-added Products from C3 Saturated Alcohol Oxidation

Besides the application in fuel cells, the oxidation of alcohol is also a good approach to value-added products.[50-52] In this aspect, C3 saturated alcohols are attracting an increasing interest due to its ability to convert into value-added product based on C-C-C structure.[78,

[79] Among C3 saturated alcohols, glycerol is becoming the focus in recent years.[50-52, 78] Glycerol is one of the byproduct in bio-diesel production. Driven by political decision, the amount of glycerol, as one of the byproduct from bio-diesel production, is constantly increasing.[80] In general, main use of glycerol can be divided into production of food additives, cosmetics, pharmaceuticals, and personal care product, and also various industrial applications, like the production of triacetin, detergents, explosives, cellophane, tobacco, the synthesis of alkyd resins, polyethers, and polyols, etc.[80] However, the use low-quality glycerol from biodiesel production in most of these sectors is just avoided. Simple refining of crude glycerol, usually by means of vacuum distillation followed by fractional distillation, is common but rather expensive. Therefore, the most promising and interesting from industrial point of view is to utilize glycerol as a building block for more valuable C3 molecules. Just due three hydroxyl groups in one glycerol molecule, glycerol can be used as a potential starting material for a lot of value-added products, especially by oxidation reaction (Figure 1.3).[80]

Though all derivatives from glycerol oxygenates are of practical value, selective oxidation is particularly difficult because the hydroxy groups have the similar reactivity in the triol molecule.[81] Glyceric acid and tartronic acid are commercially useful compounds, which can be obtained after the oxidation of primary hydroxy groups of glycerol. Dihydroxyacetone, one inportant fine chemical, can be obtained after the oxidation of the secondary hydroxy group. Mesoxalic acid is one derivative, where all three hyddroxy groups affords the highly functionlized.[81] Conventionally, glycerol derivatives can be produced by oxidation reaction on noble metal based catalysts. For example, the aerobic oxidation of glycerol in water over Au/C and Pt/C yields glyceric acid.[82-84] Tartronic acid is obtained by the catalytic oxidation of both prmary hydroxy groups on Pt-CeO_2.[85] Besides, mesoxalic acid can be produced by the homogeneous and heterogeneous oxidation of all the hydroxy groups of glycerol by using the organic nitroxyl 2,2,6,6-tetramethylpiperidin-1-oxyl and NaOCl.[86] Recently, the conversion of glycerol to value-added products are attracting more and more attention.[50-52]

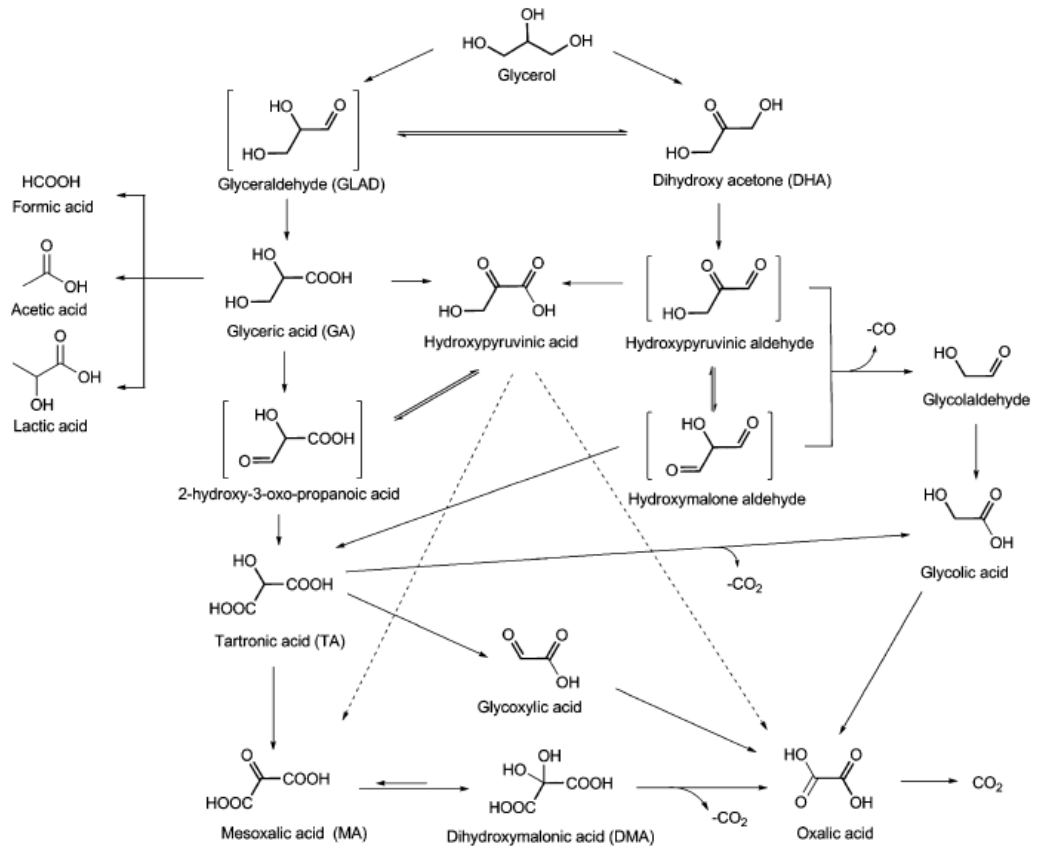

Figure 1.3 Products from the oxidation of glycerol[80]

1.2.4 Investigation Goal and Motivation

Based on the statements above, the electro-oxidation of alcohol can be utilized in three aspects. For hydrogen evolution reaction, alcohol oxidation can be used to replace water oxidation to low the anode overpotential further to promote the hydrogen production. For fuel cell, alcohols can be converted into electricity directly. For fine chemical industry, the electro-oxidation of C3 saturated alcohols is one of the method to synthesize value-added products. In these three aspects, there is no doubt that electrocatalysts play a key role in anodes. For hydrogen evolution and fuel cell, good electrocatalysts increase the efficiency of hydrogen production and export voltage, respectively. For fine chemical industry, the choice of electrocatalysts determine the conversion rate and selectivity of products.

In this report, the saturated alcohols with low carbon atom numbers are used as objectives, and they are methanol with one carbon atom (C1), ethanol and ethylene glycol with two

carbon atoms (C2), and glycerol, 1,2-propanol, 1,3-propanol, 1-proponal, and 2-proponal with three carbon atoms (C3). In terms of electrocatalysts, Pt and Pt based materials are considered as the best catalysts for alcohol oxidation. However, the low reserve and high price of noble metal limits their practical usage. Under this circumstance, non-noble metal based material are attracting much more attention. Among them, transition metal oxides are widely investigated. Here, cobalt based oxide is chosen as electrocatalyst for the oxidation of C1, C2 and C3 alcohols. As for C1 and C2 alcohols, nickel modified cobalt oxides were studied, and the effect of nickel was clarified. As for C3 saturated alcohols, Co_3O_4 was chosen as electrocatalysts, and different oxidation rates and oxidation products for C3 saturated alcohols were studied.

1.3 Dissertation Overview

According to the statements above, this report addresses the following three questions. Firstly, the report addresses the methanol oxidation reaction on Ni-Co hydroxides and Ni-Co oxides in alkaline. The results show that as the Ni content increased methanol oxidation activity exhibits an increasing activity on Ni-Co hydroxides, while a volcano-shaped trend on Ni-Co oxides. The Ni effect on methanol oxidation was also be investigated in Ni-Co oxides. Secondly, the volcano-shaped activity-composition relationship was also found for ethanol and ethylene glycol oxidation. Thirdly, the report compares the electro-oxidation rates and detect the oxidation products on Co_3O_4 using C3 saturated alcohols as example to investigate the influence of the number and position of hydroxyl groups in carbon chain on electro-oxidation.

Chapter 1 provides a rationale for the research and outlines the goals and scope. It gives the background and motivation of the electro-oxidation of C1, C2, and C3 saturated alcohols. It gives a dissertation overview and summarize the findings and outcome in the current research.

Chapter 2 reviews the literature concerning the mechanism and development of C1 and C2 alcohol oxidation on noble metals Pt and Pt-based materials. Also, the C3 saturated alcohol

oxidation for value-added products is introduced. Besides, this chapter demonstrates the alcohol oxidation on non-noble metal based materials and the recent progress.

Chapter 3 introduces the mechanism of preparing Ni-Co hydroxide and Ni-Co oxide electrodes by electrodeposition and the reason why we chose it. Also, this chapter introduces the principle of characterization (XRD, XAFS, SEM, NMR) and the basic knowledge of electrochemistry and electrochemical test.

Chapter 4 elaborates the C1 alcohol methanol oxidation reaction on Ni-Co hydroxides and Ni-Co oxides in alkaline. The results show that as the Ni content increases, the methanol oxidation activity on Ni-Co hydroxides increases, while the activity on Ni-Co oxides exhibits a volcano-shaped trend. The highest activity on Ni-Co oxides was found at the atomic ratio of Ni / (Ni + Co) = 46%.

Chapter 5 elaborates the C2 alcohols ethanol and ethylene glycol oxidation on Ni-Co oxides in alkaline. The similar volcano-shaped trend like methanol oxidation on Ni-Co oxides was also obtained, i.e. the ratio of 46% is the optimal one for the two alcohol oxidation reactions. The oxidation products were analyzed by nuclear magnetic resonance (NMR) technique and it was found that the functional groups were converted from -OH to -COOH.

Chapter 6 elaborates the C3 saturated alcohol (glycerol, 1,2-propanediol, 1,3-propanediol, 1-propanol, 2-propanol) oxidation on Co_3O_4 in alkaline. The results show that C3 saturated alcohols had different reaction rates on Co_3O_4, which presented the following order: glycerol (GLY) > 1,2-propanediol (1,2-P) > 1,3-propanediol (1,3-P) > 1-propanol (1-P) > 2-propanol (2-P). Through NMR analysis, we found that for the adjacent hydroxyl groups, the C-C bond can be readily broken up.

Chapter 7 gives a general discussion on the results in Chapter 4-6. Three future work based on the results are brought up. They are (1) Alcohol oxidation on Ni/Co in different coordination; (2) Glycerol oxidation on Co in different coordination; (3) Dihydric alcohol

oxidation on Co_3O_4, respectively.

1.4 Findings and Outcomes/Originality

This thesis provides several novel outcomes as follow:

1. For C1 alcohol methanol, the study was performed to explore the Ni effect in Ni-Co hydroxides and Ni-Co oxides for methanol oxidation reaction. The result shows that as the Ni content increased, the methanol oxidation activity on Ni-Co hydroxides increased, while the activity on Ni-Co oxides exhibited a volcano-shaped trend. The highest activity was found at the atomic ratio of Ni / (Ni + Co) = 46%. By conducting electrochemical impedance spectroscopy, it was found that Ni can promote the adsorption of intermediate products. It suggests that this best ratio of 46% for the methanol electro-oxidation was due to the balance of the adsorption of intermediate products and onset potential.

2. For C2 alcohols, ethanol and ethylene glycol, the study was performed to reveal the Ni effect in Ni-Co oxides on the oxidation activity and the product selectivity. The similar result was also obtained, i.e. the ratio of 46% is the optimal one for the two alcohol oxidation reactions. By conducting electrochemical impedance spectroscopy, it was found that Ni can promote the oxidation of intermediate products. Such a promoted oxidation caused by Ni was more dramatic from alcohol to intermediate products than from intermediate products to final products. It suggests that this best ratio of 46% for the ethanol and ethylene glycol electro-oxidation was due to the balance of the reaction rate between from alcohol to intermediate products and from intermediate products to final products. The oxidation products were analyzed by nuclear magnetic resonance (NMR) technique and it was found that the functional groups were converted from -OH to -COOH.

3. The electro-oxidation of C3 saturated alcohols (glycerol, 1,2-propanediol, 1,3-propanediol, 1-proponal, and 2-proponal) was studied on Co_3O_4. It shows that C3 saturated alcohols had different reaction rates on Co_3O_4, which presented the following order: glycerol (GLY) > 1,2-propanediol (1,2-P) > 1,3-propanediol (1,3-P) > 1-propanol (1-P) > 2-propanol (2-P). Through NMR analysis, we found that for the adjacent hydroxyl groups,

the C-C bond can be readily broken up.

References:

[1] X. Deng and H. Tüysüz. *ACS Catalysis*. **2014**, 4, 3701-3714.

[2] M. S. Faber and S. Jin. *Energy & Environmental Science*. **2014**, 7, 3519-3542.

[3] B. You, N. Jiang, X. Liu and Y. Sun. *Angewandte Chemie*. **2016**, 55, 9913-9917.

[4] B. You, X. Liu, X. Liu and Y. Sun. *ACS Catalysis*. **2017**, 4564-4570.

[5] S. De, J. Zhang, R. Luque and N. Yan. *Energy & Environmental Science*. **2016**, 9, 3314-3347.

[6] J. Suntivich, K. J. May, H. A. Gasteiger, J. B. Goodenough and Y. Shao-Horn. *Science*. **2011**, 334, 1383-1385.

[7] J. Suntivich, H. A. Gasteiger, N. Yabuuchi, H. Nakanishi, J. B. Goodenough and Y. Shao-Horn. *Nature Chemistry*. **2011**, 3, 546-550.

[8] S. Trasatti. *Electrochimica Acta.* **2000**, 45, 2377-2385.

[9] D. N. Bennion. *Journal of applied electrochemistry*. **1972**, 2, 113-122.

[10] M. Mohsen-Nia, P. Montazeri and H. Modarress. *Desalination*. **2007**, 217, 276-281.

[11] F. Fu and Q. Wang. *Journal of Environmental Management*. **2011**, 92, 407-418.

[12] M. Y. A. Mollah, R. Schennach, J. R. Parga and D. L. Cocke. *Journal of Hazardous Materials*. **2001**, B84, 29-41.

[13] J. N. Hakizimana, B. Gourich, M. Chafi, Y. Stiriba, C. Vial, P. Drogui and J. Naja. *Desalination*. **2017**, 404, 1-21.

[14] P. Krystynik and D. N. Tito. *Chemical Engineering & Processing: Process Intensification*. **2017**, 117, 106-112.

[15] M. Murugananthan, G. B. Raju and S. Prabhakar. *Separation and Purification Technology*. **2004**, 40, 69-75.

[16] A. Y. Hosny. *Separations Technology*. **1996**, 6, 9-17.

[17] X. Chen, G. Chen and P. L. Yue. *Environmental Science & Technology*. **2002**, 36, 778-783.

[18] Ch. Comninellis and C. Pulgarin. *Journal of Applied Electrochemistry*. **1993**, 23, 108-112.

[19] C. A. Martinez-Huitle and S. Ferro. *Chemical Society Review*. **2006**, 35, 1324-1340.

[20] E. Brillas, J. C. Calpe and J. Casado. *Water Research*. **2000**, 34, 2253-2262.

[21] W. T. Mook, M. H. Chakrabarti, M. K. Aroua, G. M. A. Khan, B. S. Ali, M. S. Islam and M. A. Abu Hassan. *Desalination*. **2012**. 285. 1-13.

[22] P. Clauwaert, J. Desloover, C. Shea. R. Nerenberg, N. Boon and W. Verstraete. *Biotechnology Letters*. **2009**, 31, 1537-1543.

[23] L. Li and Y. Liu. *Journal of Hazardous Materials*. **2009**, 161, 1010-1016.

[24] R. K. B. Karlsson and A. Cornell. *Chemical Reviews*. **2016**, 116, 2982-3028.

[25] K. S. Exner, J. Anton, T. Jacob and H. Over. *Angewandte Chemie International Edition*. **2014**, 53, 11032-11035.

[26] R. K. B. Karlsson, H. A. Hansen, T. Bligaard, A. Cornell and L. G. M. Pettersson. *Eelctrochimica Acta*. **2014**. 146. 733-740.

[27] P. Xiao, W. Chen and X. Wang. *Advanced Energy Materials*. **2015**, 5, 1500985-1500997

[28] M. Gong, D.-Y. Wang, C.-C. Chen, B.-J. Hwang and H. Dai. *Nano Research*. **2016**, 9, 28-46.

[29] F. Safizadeh, E. Ghali, G. Houlachi. *International Journal of Hydrogen Energy*. **2015**, 40, 256-274.

[30] M. Gong and H. Dai. *Nano Research*. **2015**, 8, 23-29.

[31] K. A. Stoerzinger, L. Qiao, M. D. Biegalski and Y. Shao-Horn. *The Journal of Physical Chemistry Letters*. **2014**, 5, 1636-1641.

[32] I. C. Man, H.-Y. Su, F. Calle-Vallejo, H. A. Hansen, J. I. Martinez, N. G. Inoglu, J. Kitchin, T. F. Jaramillo, J. K. Norskov and J. Rossmeisl. *ChemCatChem*, **2011**, 3, 1159-1165.

[33] S. Giddey, S. P. S. Badwal and A. Kulkarni. *International Journal of Hydrogen Energy*. **2013**, 38, 14575-14594.

[34] V. Kyriakou, I. Garagounis, E. Vasileiou, A. Vourros and M. Stoukides. *Catalysis Today*. **2017**, 286, 2-13.

[35] S. Klinsrisuk and J. T. S. Irvine. *Catalysis Today*. **2017**, 286, 41-50.

[36] S. Kongjao, S. Damronglerd and M. Hunsom. *Journal of Applied Electrochemistry*. **2011**, 41, 215-222.

[37] D. J. Chadderdon, L. Xin, J. Qi, B. Brady, J. A. Miller, K. Sun, M. J. Janik and W. Li. *ACS Catalysis*. **2015**, 5, 6926-6936.

[38] J. Mahmoudian, M. Bellini, M. V. Pagliaro, W. Oberhauser, M. Innocenti, F. Vizza and H. A. Miller. *ACS Sustainable Chemistry & Engineering*. **2017**, 5, 6090-6098.

[39] O. Sorsa, H. Romar, U. Lassi and T. Kallio. *Electrochimica Acta*. **2017**, 230, 49-57.

[40] D. A. Cantane and F. H. B. Lima. *Electrocatalysis*. **2012**, 3, 324-333.

[41] M. K. Debe. *Nature*. **2012**, 486, 43-51.

[42] R. Parsons. T. VanderNoot. *Interfacial Electrochemistry*. **1988**, 257, 9-45.

[43] J. T. Muller, P. M. Urban, W. F. Holderich, K. M. Colbow, J. Zhang and D. P. Wilkinson. *Journal of The Electrochemical Society*. **2000**, 147, 4058-4060.

[44] E. S. Steigerwalt, G. A. Deluga, D. E. Cliffel and C. M. Lukehart. *The Journal of Physical Chemistry B*. **2001**, 105, 8097-8101.

[45] W. Sheng, H. A. Gasteiger and Y. Shao-Horn. *Journal of The Electrochemical Society*. **2010**, 157, B1529-B1536.

[46] D. Strmcnik, M. Uchimura, C. Wang, R. Subbaraman, N. Danilovic, D. van der Vliet, A. P. Paulikas, V. R. Stamenkovic and N. M. Markovic. *Nature Chemistry*. **2013**, 5, 300-306.

[47] J. Durst, A. Siebel, C. Simon, F. Hasche, J. Herranz and H. A. Gasteiger. *Energy & Environmental Science*. **2014**, 7, 2255-2260.

[48] T. Iwasita. *Electrochimica Acta*. **2002**, 47, 3663-3674.

[49] F. Vigier, C. Coutanceau, A. Perrard, E. M. Belgsir and C. Lamy. *Journal of Applied Electrochemistry*. **2004**, 34, 439-446.

[50] R. Ciriminna, G. Palmisano, C. D. Pina, M. Rossi and M. Pagliaro. *Tetrahedron Letters*. **2006**, 47, 6993-6995.

[51] Z. Zhang, L. Xin and W. Li. *Applied Catalysis B: Environmental*. **2012**, 119-120, 40-48.

[52] J. Qi, L. Xin, D. J. Chadderdon, Y. Qiu, Y. Jiang, N. Benipal, C. Liang, W. Li. *Applied Catalysis B: Environmental*. **2014**, 154-155, 360-368.

[53] X. Li, X. Hao, A. Abudula and G. Guan. *Journal of Materials Chemistry A*. **2016**, 4, 11973-12000.

[54] B. You, X. Liu, N. Jiang and Y. Sun. *J Am Chem Soc*. **2016**.138, 13639-13646.

[55] A. R. Jadhav, H. A. Bandal, A. A. Chaugule and H. Kim. *Electrochimica Acta*. **2017**, 240, 277-287.

[56] V. Vedharathinam and G. G. Botte. Electrochimica Acta. **2012**, 81, 292-300.

[57] M. Guo, Y. Yu and J. Hu. *Journal of The Electrochemical Society*. **2017**, 164, H198-H2

[58] M. Betowska-Brzezinska, T. Uczak and R. Holze. *Journal of Applied Electrochemistry*. **1997**, 27, 999-1011.

[59] A. Santasalo-Aarnio, Y. Kwon, E. Ahlberg, K. Kontturi, T. Kallio and M. T. M. Koper. *Electrochemistry Communications*. **2011**, 13, 466-469.

[60] E. Sitta, B. C. Batista and H. Varela. *Chemical communications*. **2011**, 47, 3775-3777.

[61] M. Chatterjee, A. Chatterjee, S. Ghosh and I. Basumallick. *Electrochimica Acta*. **2009**, 54, 7299-7304.

[62] F. Vigier, C. Coutanceau, F. Hahn, E. M. Belgsir and C. Lamy. *Journal of Electroanalytical Chemistry*. **2004**, 563, 81-89.

[63] A. V. Tripkovic, K. D. Popovic, J. D. Momcilovic and D. M. Drazic. *Journal of Electroanalytical Chemistry*. **1996**, 418, 9-20.

[64] A. V. Tripkovic, K. D. Popovic, J. D. Momcilovic and D. M. Drazic. *Journal of Electroanalytical Chemistry*. **1998**, 448, 173-181.

[65] A. V. Tripkovic, K. D. Popovic, J. D. Momcilovic and D. M. Drazic. *Electrochimica Acta*. **1998**, 44, 1135-1145.

[66] A. K. Das, R. K. Layek, N. H. Kim, D. Jung and J. H. L. Lee. *Nanoscale*. **2014**, 6, 10657-10665.

[67] R. Ding, L. Qi, M. Jia and H. Wang. *Catal. Sci. Technol.*. **2013**, 3, 3207-3215.

[68] J. B. Wu, Z. G. Li, X. H. Huang and Y. Lin. *Journal of Power Sources*. **2013**, 224, 1-5.

[69] X. Tarrús, M. Montiel, E. Vallés and E. Gómez. *International Journal of Hydrogen Energy*. **2014**, 39, 6705-6713.

[70] J. M. Skowronski and A. Wazny. *Journal of New Materials for Electrochemical Systems*. **2006**, 9, 345-351.

[71] R. N. Singh, T. Sharma, A. Singh, Anindita, D. Mishra and S. K. Tiwari. *Electrochimica Acta*. **2008**, 53, 2322-2330.

[72] M. U. A. Prathap, B. Satpati and R. Srivastava. *Electrochimica Acta*. **2014**, 130, 368-380.

[73] Y. X. Chen, A. Miki, S. Ye, H. Sakai and M. Osawa. *Journal of the American Chemical Society*. **2003**, 125, 3680-3681.

[74] J. L. Cohen, D. J. Volpe and H. D. Abruna. *Physical chemistry chemical physics*. **2007**, 9, 49-77.

[75] M. E. M. Chbihi, D. Takky, F. Hahn, H. Huser, J. M. Leger and C. Lamy. *Journal of Electroanalytical Chemistry*. **1999**, 463, 63-71.

[76] I. d. A. Rodrigues, J. P. I. De Souza, E. Pastor and F. C. Nart. *Langmuir*. **1997**, 13, 6829-6835.

[77] J. Ye, J. Liu, C. Xu, S. Jiang and Y. Tong. *Electrochemistry Communications*. **2007**, 9, 2760-2763.

[78] C. S. Lee, M. K. Aroua, W. M. A. W. Daud, P. Cognet, Y. Pérès-Lucchese, P. L. Fabre, O. Reynes and L. Latapie. *Renewable and Sustainable Energy Reviews*. **2015**, 42, 963-972.

[79] J. L. Bott-Neto, A. C. Garcia, V. L. Oliveira, N. E. de Souza and G. Tremiliosi-Filho. *Journal of Electroanalytical Chemistry*. **2014**, 735, 57-62.

[80] B. Katryniok, H. Kimura, E. Skrzyńska, J.-S. Girardon, P. Fongarland, M. Capron, R. Ducoulombier, N. Mimura, S. Paul and F. Dumeignil. *Green Chemistry*. **2011**, 13, 1960.

[81] M. Pagliaro, R. Ciriminna, H. Kimura, M. Rossi and C. Della Pina. *Angewandte Chemie*. **2007**, 46, 4434-4440.

[82] S. Carrettin, P. McMorn, P. Johnston, K. Griffin, C. J. Kiely, G. A. Attard and G. J. Hutchings. *Topics in Catalysis*. **2004**, 27, 131-136

[83] R. Garcia, M. Besson and P. Gallezot. *Applied Catalysis A: General*. **1995**, 127, 165-176.

[84] N. Dimitratos, J. A. Lopez-Sanchez, D. Lennon, F. Porta, L. Prati and A. Villa. *Catalysis Letters*. **2006**, 108, 147-153.

[85] P. Fordham, M. Besson and P. Gallezot. *Applied Catalysis A: General*. **1995**, 133, L179-L184.

[86] R. Ciriminna and M. Pagliaro. *Advanced Synthesis & Catalysis*. 2003, 345, 383-388

Chapter 2

Literature Review

This chapter gives a comprehensive literature review on the mechanism of C1, C2, and C3 alcohols' electro-oxidation on noble metals and the recent progress on non-noble metal based materials. The electro-oxidation of alcohols on transition metal based material is given more details, especially for cobalt and nickel based materials. Based on the literature review, we learned about the reaction mechanism of C1 and C2 alcohol oxidation on Pt based materials, and the value-added production from C3 saturated alcohols (glycerol, 1,2-propanediol, and 1,3-propanediol) on noble metals. Due to the high cost and low reserve of noble metals, the transition metal based materials with low cost are attracting an increasing interest, especially for Ni and Co based oxides. From literature review, it can be found that Ni doped Co_3O_4 can promote the alcohol oxidation reaction, and however, it has no systematic investigation on alcohol oxidation on Ni-Co hydroxides and oxides and to explore Ni effect. From literature review, though there are many reports on the oxidation and conversion from C3 alcohols to value-added products, few investigations report the C3 alcohol oxidation on transition metal oxides. Thus, in this thesis, we finished the C1 alcohol, methanol oxidation on Ni-Co hydroxides and oxides, and further C2 alcohols, ethanol and ethylene glycol oxidation on Ni-Co oxides, and finally C3 saturated alcohol oxidation on Co_3O_4.

2.1 Alcohol Electro-oxidation

2.1.1 Methanol Oxidation on Pt

The electro-oxidation of methanol, as a simplest alcohol, is widely investigated due to its practical application as a fuel in fuel cell. The complete methanol oxidation forms CO_2 through a $6e^-$ oxidation process. This oxidation process can take place in both acid and alkaline media in the anode. In the anode, Pt based materials are studied as the most efficient electrocatalyst for methanol oxidation. The reaction process of methanol oxidation on Pt in acid and alkaline are given in Equation 2.1 and 2.2.[1]

In acid solution

$$CH_3OH + H_2O \rightarrow CO_2 + 6H^+ + 6e^- \qquad E^0 = 0.016 \text{ V vs. SHE pH} = 0 \qquad (2.1)$$

In alkaline solution

$$CH_3OH + 6OH^- \rightarrow CO_2 + 5H_2O + 6e^- \quad E^0 = -0.810 \text{ V vs. SHE pH} = 14 \qquad (2.2)$$

For methanol oxidation in alkaline,[1-3] the mechanism can be described as following (Figure 2.1). The cleavage of O-H bond in CH_3OH was assumed to be the first step in alkaline, followed by the cleavage of one of the C-H bond in CH_3O_{ads} as the second step to form CH_2O_{ads}. The further dehydrogenation of CH_2O_{ads} forms CHO_{ads}. In the subsequence step, CHO_{ads} will proceed to form CO_{ads} and $COOH_{ads}$. CO_{ads} was accepted as a poison species, which can be oxidized to CO_2 at high potential. As for those $COOH_{ads}$, they can react with OH^- to form $HCOO^-$ ions in solution or are further oxidized to CO_2. In acid, the first two steps are the dehydrogenation of CH_3OH_{ads}. Different from the dehydrogenation in alkaline, the reactions occur on C-H bond instead of the cleavage of O-H bond followed by C-H bond until $CHOH_{ads}$ forms. $CHOH_{ads}$ will proceed along two paths. One is the formation of HCOOH in solution. The other one is the formation of CHO_{ads}. The subsequent oxidation pathway is the same with that in alkaline. It is noticed that almost each step after CHO_{ads} needs the participation of OH_{ads}, especially for the removal of Co_{ads}. Thus, OH_{ads} becomes the key step to eliminate the CO_{ads} and facilitate the overall reaction. It is also reported that methanol oxidation has a higher rate on Pt in alkaline than in acid. Such phenomena can be ascribed to two factors. One is the lack of specifically-adsorbing spectator ions in alkaline. The other one is the higher coverage of adsorbed OH at low potential. Such two

factors above is required for methanol oxidation.[4]

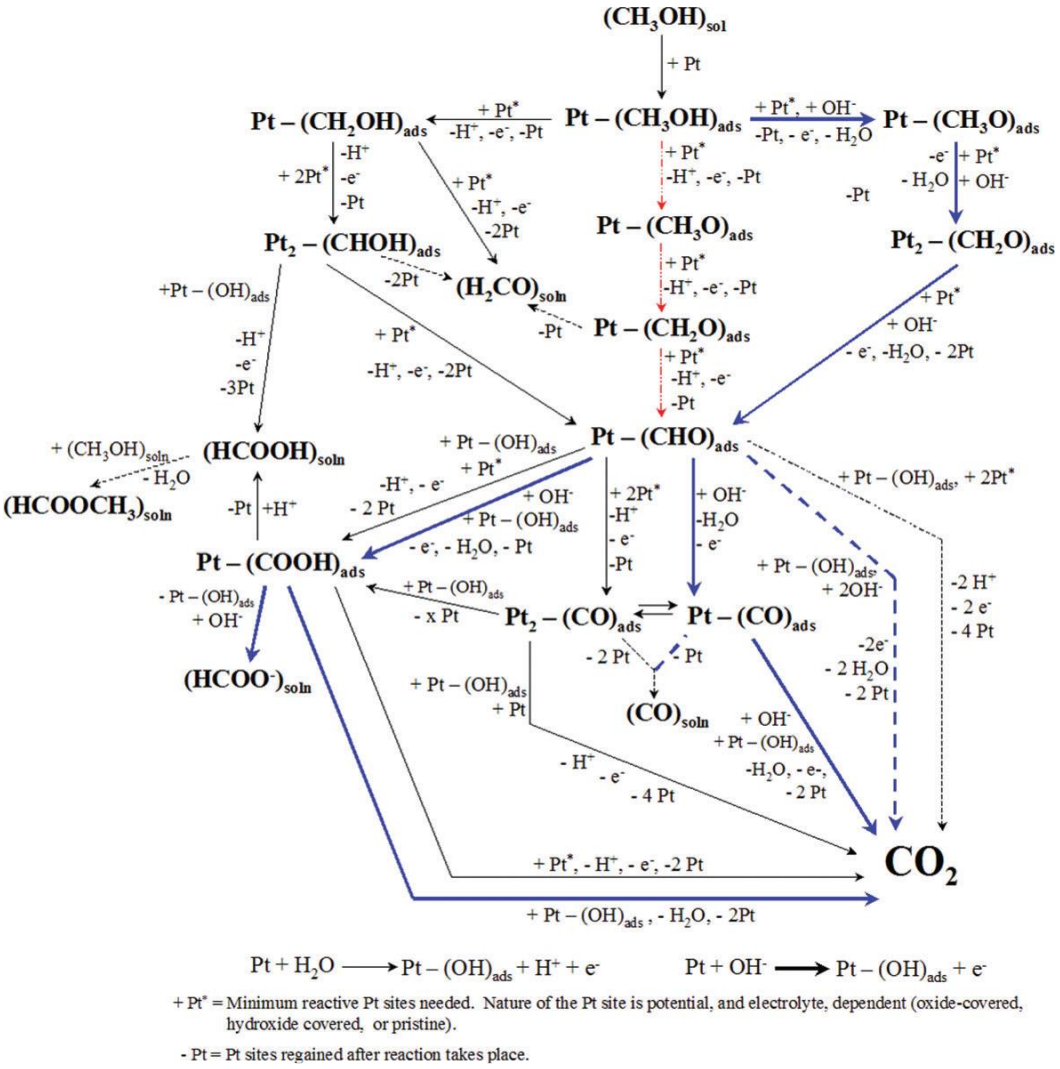

Figure 2.1 The mechanism of methanol oxidation on Pt in acid and alkaline solution. The methanol oxidation process is shown in black solid line in acid and in blue solid line in alkaline. Dashed lines represent pathways suggested in the literature for acid and alkaline solution, but are impossible to happen under typical experiment conditions. The pathway (red line) represents the initial dehydrogenation pathway determined by UHV experiments.[5]

According the statement above, CO is a poison species produced as an intermediates methanol oxidation, and CO can form a strong bond with Pt. Its removal requires an adjacent Pt(OH) by activating H_2O, and this activation of H_2O become the key step:

$$H_2O + Pt \rightarrow Pt(OH)_{ads} + H^+ + e^- \quad E > 0.4\ V \text{ vs. SHE} \qquad (2.3)$$

To decrease CO poisoning and increase the methanol oxidation efficiency on Pt, one strategy is employed to lower the activation energy of H_2O. Researchers synthesized Pt

alloy or used another metal to modify the Pt surface. Among them PuRu shows a better methanol oxidation activity than Pt. When PtRu is used, the activation of H_2O takes place at much lower potential

$$Ru + H_2O \rightarrow Ru(OH)_{ads} + H^+ + e^- \quad E \sim 0.2\text{-}0.3 \text{ V vs. SHE} \qquad (2.4)$$

Thus, the oxidation of adsorbed CO can be achieved under energetically favorable condition in the presence of Ru.

$$Ru(OH)_{ads} + Pt(CO)_{ads} \rightarrow Pt + Ru + CO_2 + H^+ + e^- \qquad (2.5)$$

As shown in Figure 2.1 and Equation 2.4, 2.5, and 2.5, the Pt function as catalyst is dehydrogenation and activation of H_2O at high potential and Ru functions as H_2O activator at low potential. When these two functions act cooperatively, synergistic reactions occur and the overall reaction rates are faciliated. In addition, when Ru is present in PtRu alloy, electrons will transfer from Ru to Pt, making density of states near the Fermi level of Pt lower and electron density of $2\pi^*$ MO of adsorbed CO is reduced and this makes Pt-CO bond weaker. Due to Ru-O having similar bonding energy of Ru-O with Pt-C, Ru easily oxidizes this loosely CO to CO_2. The relative contribution of bifunctional and electronic effect towards effective removal of CO is a subject of great controversy. However, in a very recent paper Wieckowski et al, suggested that for methanol electro-oxidation onto PtRu surface, bifunctional path contributes about 80% and the rest is through electronic effect.[6]

2.1.2 Ethanol and Ethylene Glycol Oxidation on Pt

When ethanol oxidation takes place on Pt in alkaline, there are also two pathways proposed, through reactive intermediates (C2 pathway, no poisoning) and poisoning species (C1 pathway, poisoning) shown below, respectively.[7]

C2 pathway: $CH_3CH_2OH \rightarrow$ reactive intermediates $\rightarrow CH_3CHO$ or CH_3COO^-

C1 pathway: $CH_3CH_2OH \rightarrow$ reactive intermediates $\rightarrow CO_{ad} \rightarrow CO_2$

No matter the ethanol oxidation occurs through Path A or Path B, the first step is the adsorption of ethanol on Pt (Equation 2.5), and then reacts with OHads (Equation 2.6) to form CH_3CO_{ads} (Equation 2.7). As for Path A, the CH_3CO_{ads} continues to react with OH_{ads} to form CH_3COOH (Equation 2.8), which exists in CH_3COO^- ions in alkaline (Equation

2.9). In Path B, poisoning species CO_{ad} reacts with OH_{ads} and OH^- to form CO_3^{2-} (Equation 2.10).

$$CH_3CH_2OH_{sol} \rightarrow CH_3CH_2OH_{ad} \quad (2.6)$$

$$OH^- \rightarrow OH_{ad} + e^- \quad (2.7)$$

$$CH_3CH_2OH_{ad} + 3OH_{ad} \rightarrow CH_3CO_{ad} + 3H_2O + 3e^- \quad (2.8)$$

$$CH_3CO_{ad} + OH_{ad} \rightarrow CH_3COOH \quad (2.9)$$

$$CH_3COOH + OH^- \rightarrow CH_3COO^- + H_2O \quad (2.10)$$

For the poisoning species CO_{ad}

$$CO_{ad} + 2OH_{ad} + 3OH^- \rightarrow CO_3^{2-} + 2H_2O + e^- \quad (2.11)$$

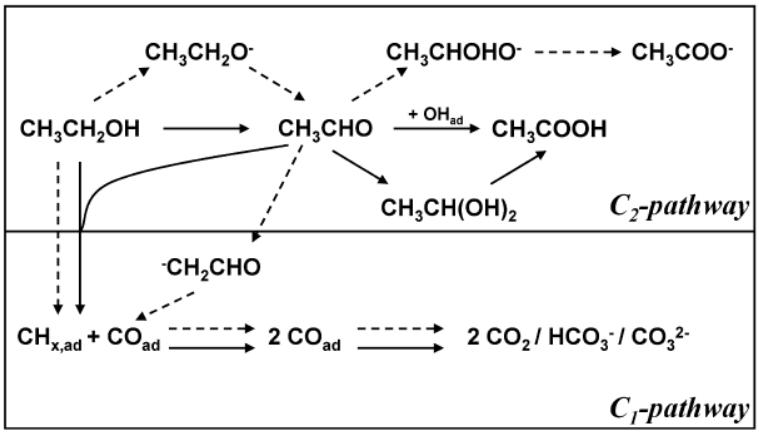

Figure 2.2 Scheme of ethanol oxidation on Pt in low (solid arrows) and high (dashed arrows) pH electrolyte.[8]

The effect of pH on ethanol oxidation activity on Pt is also reported. Ethanol oxidation activity was promoted dramatically when the solution pH value was higher than 10. The detailed reaction pathways of ethanol oxidation in low and high electrolyte are illustrated in Figure 2.2.[8]

The ethylene glycol oxidation on Pt in alkaline has been widely reported and the reaction pathway has been unrevealed. There are also two pathways in ethylene glycol oxidation (Figure 2.3). During oxidation, ethylene glycol mainly undergoes partial oxidation to glycol aldehyde and then to glycolate. In non-poisoning path, ethylene glycol can be oxidized to oxalate; in poisoning path, ethylene glycol can be oxidized to formate, where CO is formed as a reaction intermediate.[9, 10]

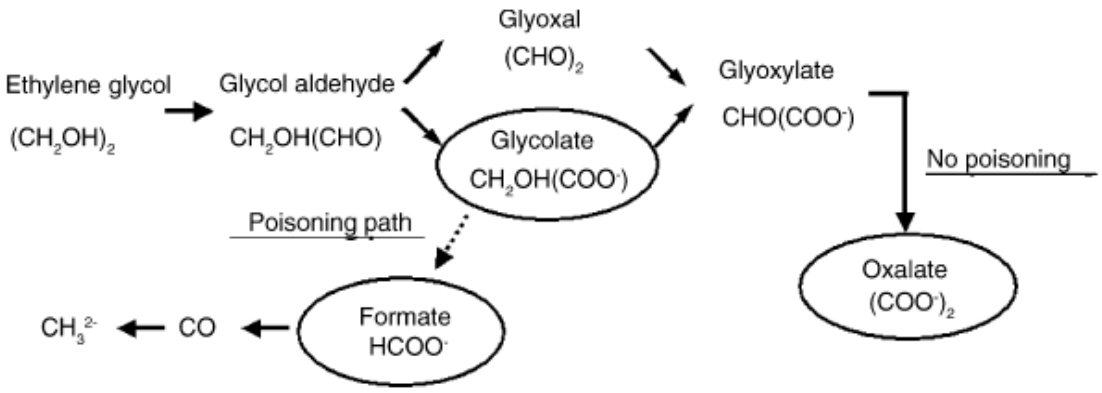

Figure 2.3 Scheme of ethylene glycol oxidation on Pt in alkaline solution.[9]

Besides, it has been found that the cleavage of C-C bond is hardly detected in ethylene glycol oxidation. The reason can be attributed to strong adsorption between Pt and CO_{ads}, which can be described as follow. The intermediates with carbonyl group C=O interact most strongly with Pt, and the cleavage of C-C bond is facile, resulting in fast decomposition to CO_{ads}. Nevertheless, the interaction between Pt and hydroxyl group OH is much weaker than that between Pt and C=O. Thus, as the potential increases, the CO_{ads} is facile to reach a maximum of saturation coverage, and the further dissociative adsorption is blocked by CO_{ads} at higher CO_{ads} coverages. Accordingly, the dissociation rate is low. Besides, the carboxyl group COOH exhibits a weak interaction with Pt, and no cleavage of C-C bond can be detected in the potential from ca. 0.1 to 0.95 V.[11, 12]

2.1.3 Value-added Products from C3 Saturated Alcohol Oxidation

In this area, the selectivity and conversion degree become the major interest. C3 saturated alcohol oxidation on Pt and Au are widely investigated and compared in acid and alkaline solution.,. Electro-oxidation of glycerol has been widely investigated by many groups. Koper's group has found that glycerol oxidation has different pathways on Au and Pt in alkaline, neutral and acid solutions. In alkaline solution, glyceric acid is the primary oxidation products on Pt and glyceraldehyde is the intermediate species, while on Au the main oxidation product is glyceric acid, which can be further oxidized to glycolic acid and formic acid when the potential is higher than 0.8 V (Figure 2.4). In neutral solution, glycerol oxidation rate is significantly sluggish on Pt and Au. Under this condition,

glyceraldehyde is the major oxidation product, especially on gold (Figure 2.5). In acid solution, glyceraldehyde is the main product with a low conversion rate. At more positive potential, Pt surface oxide formed, which can catalyze the conversion of glyceraldehyde to formic acid and CO_2 (Figure 2.6). In acid solution, gold shows little catalytic activity (Figure 2.6).[13]

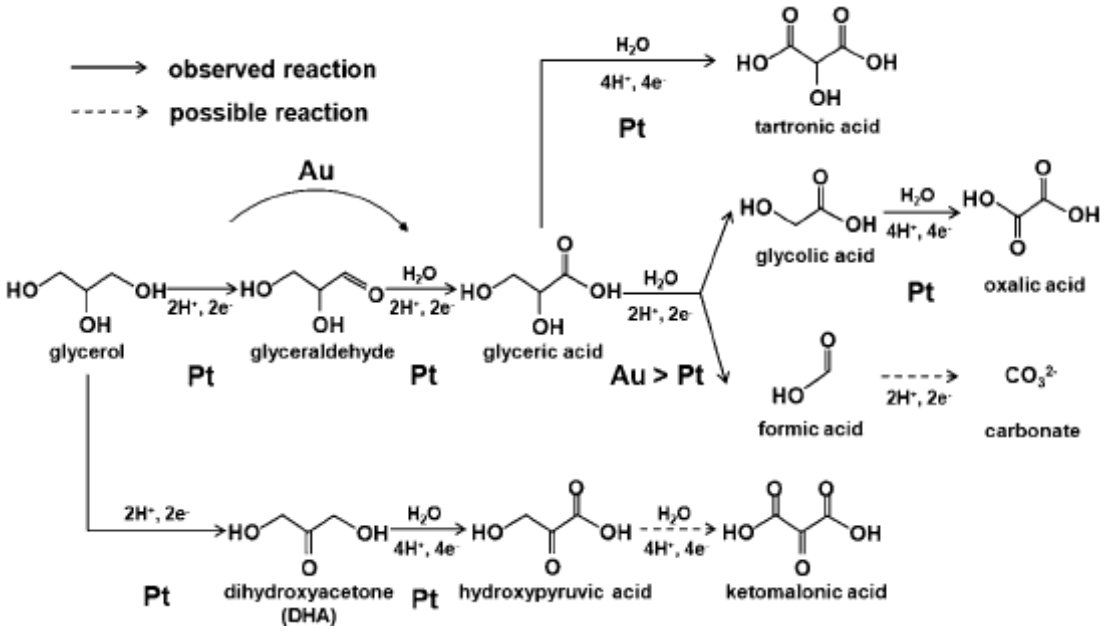

Figure 2.4 Scheme of glycerol oxidation on Au and Pt in alkaline solution.[13]

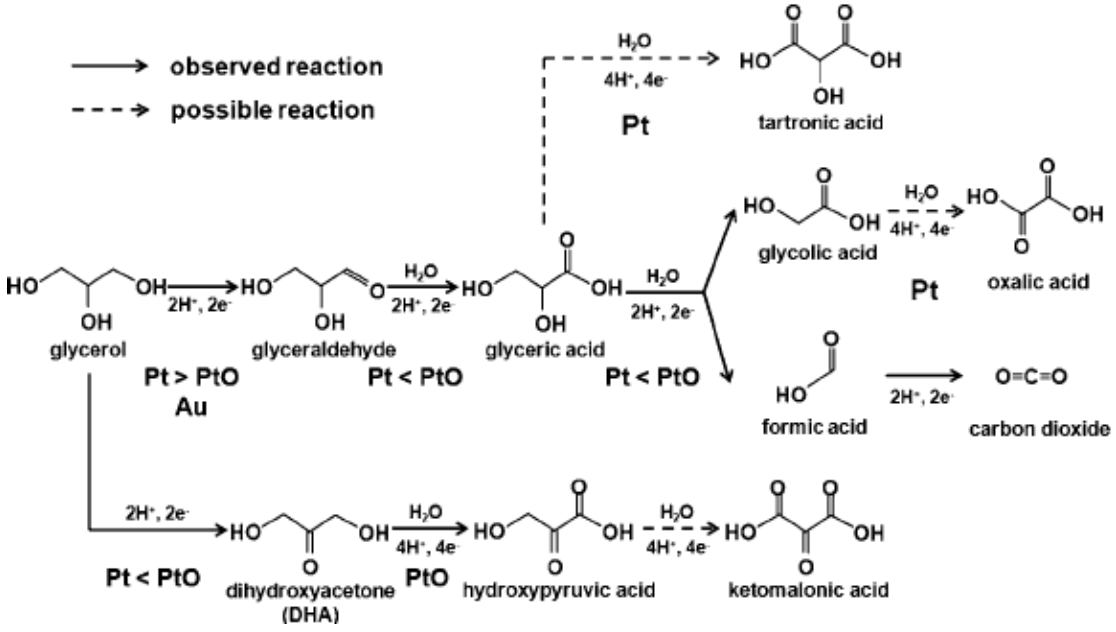

Figure 2.5 Scheme of glycerol oxidation on Au and Pt in neutral solution.[13]

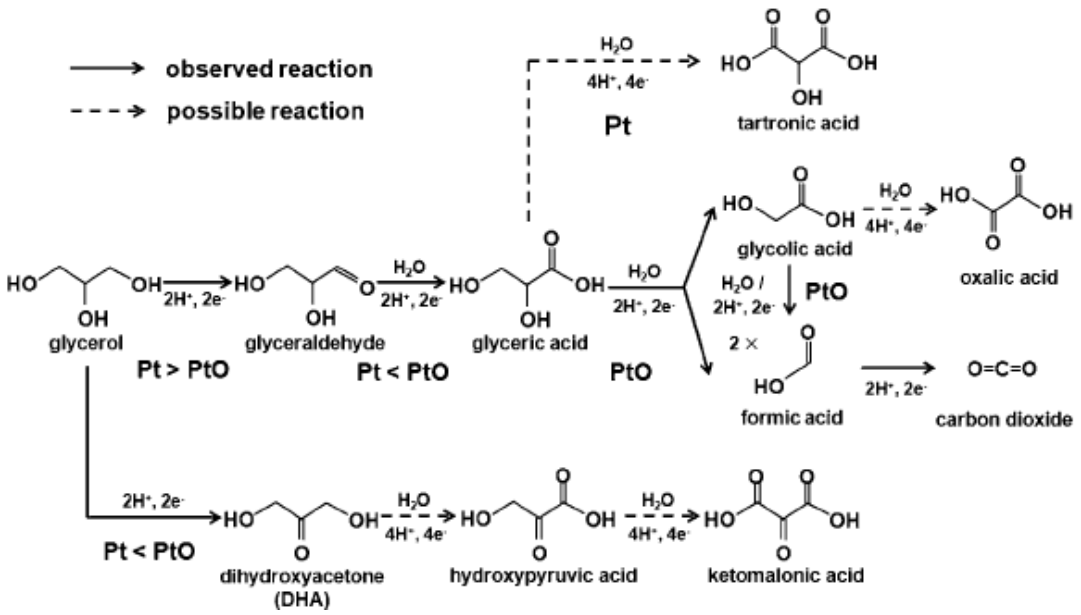

Figure 2.6 Scheme of glycerol oxidation on Pt in acid solution.[13]

The electro-oxidation of 1,2-propanediol on Au and Pt has been widely investigated in alkaline. The reaction mechanism is displayed in Figure 2.8. It has been concluded that on Au the oxidation rate was determined by the rate of C-H bond cleavage in 1,2-propanediol molecules interacting with the OH_{ads}. Lactic, formic and acetic acid ions are the major oxidation products of 1,2-propanediol.[12] It can be observed that 1,2-propanediol oxidation can proceed in two different pathways. One is methylglyoxal serves as intermediates and the other one is the anion of lactic acid as intermediates to the anion of pyruvic acid. Methylglyoxal may be also partially transformed into the anion of lactic acid. After cleavage of the C-C bond in pyruvic and lactic acid ions, the formic, acetic and carbonic acid ions may be formed.[12]

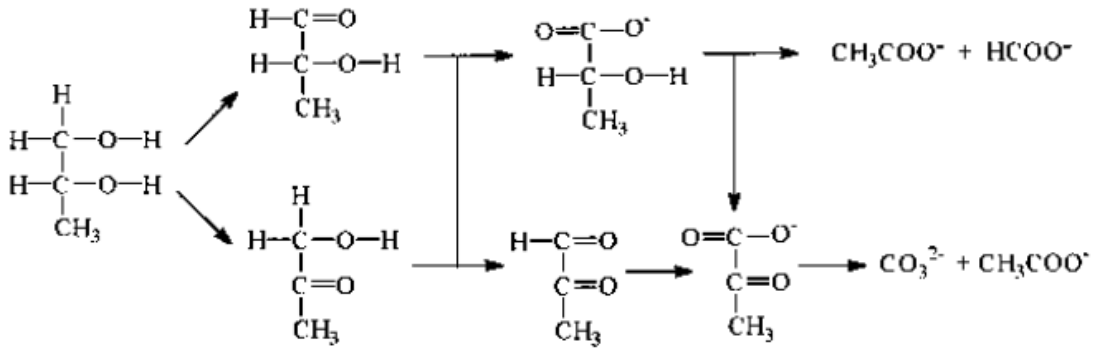

Figure 2.7 The mechanism of 1,2-propanediol oxidation on Au and Pt in alkaline[12]

Besides, Li et al. also did a systematic product analysis on 1,2-propanediol oxidation on Pt and Au (Figure 2.8).[14] They found that Pt/C is preferable to oxidize the primary alcohol group of 1,2-propanediol via the O1 pathway in Figure 2.9. Lactate is the major product with high selectivity. Lactaldehyde was not observed in the liquid product analysis probably due to its much slower formation rate than its oxidation rate. Lactate accumulating in the bulk liquid forms pyruvate through secondary alcohol oxidation slowly. C-C bond cleavage occurs with low selectivity to form acetate, formate, or carbonate. When 1,2-propanediol oxidation occurs on Au/C, lactate is the major product at low potentials. At higher potential, pyruvate becomes more abundant via O2 pathway.[14]

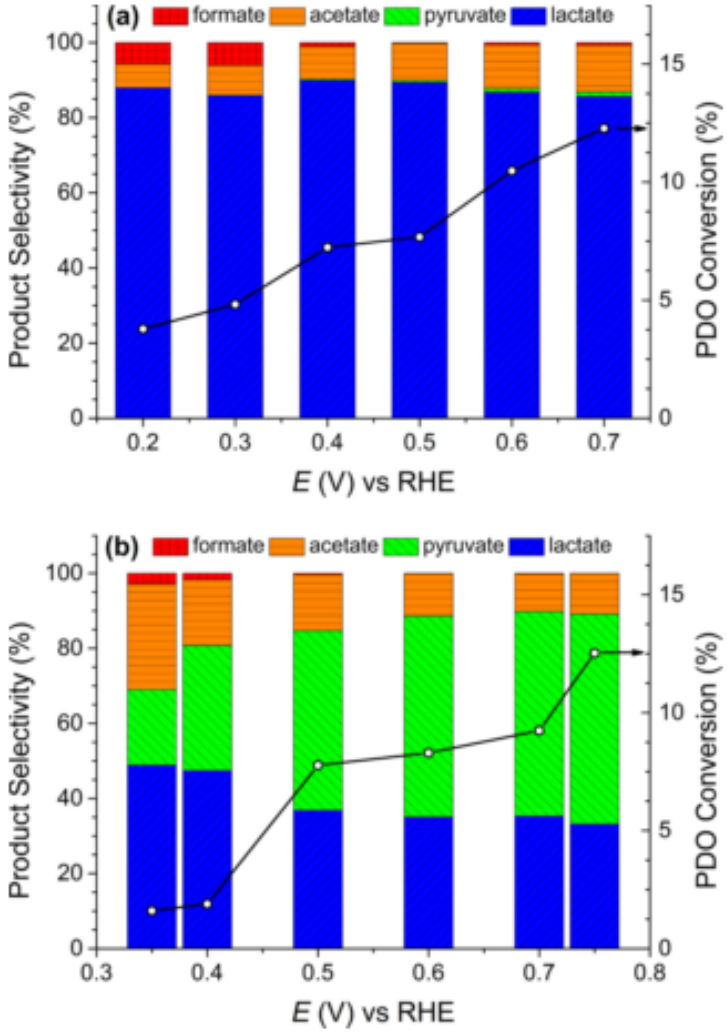

Figure 2.8 Potential-controlled 1,2-propanediol oxidation on (a) Pt/C and (b) Au/C in alkaline[14]

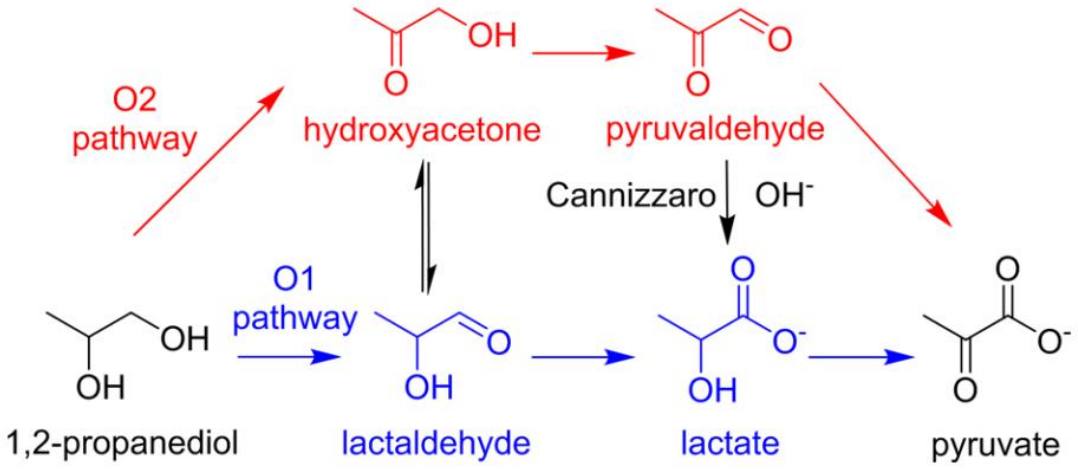

Figure 2.9 The schematic illustration of 1,2-propanediol oxidation[14]

Microbial-derived 1,3-propandiol is a convenient starting material as it is currently produced from glycose or glycerol and hence is a cheap and renewable resource. Acylic acid is one of the most commonly used materials in the organic chemical industry. Current petrochemical-based AA is produced by the oxidation of propylene. Bioacrylic acid can be obtained through both chemical or biochemical routes starting from renewable compounds such as glycerol, lactic acid or C6 sugars, and ethanol.[15] The oxidation of 1,3-propanediol is one of methods to obtain acrylic acid. The 1,3-propanediol oxidation can proceed through different pathways on Au and Pt (Figure 2.10). In the first adsorption step two possibilities can be considered. One is the adsorption by the terminal C, $OH\text{-}CH_2\text{-}CH_2\text{-}\dot{C}H\text{-}OH$ and/or adsorption by oxygen in hydroxyl group, $OH\text{-}CH_2\text{-}CH_2\text{-}CH_2\text{-}\dot{O}$. The other one is the adsorption by the central carbon can be excluded totally due to steric hindrance. By considering the adsorption by one carbon atom, there are two pathways. One is Pathway A, where no dissociation of C-C-C bond occurs, resulting in the formation 3-hydroxyl propanal, β-lactic acid and malonic acid. The other one is Pathway B, including more complex adsorption situation, leading to the cleavage of the C-C bond in 1,2-propanediol and then the formation of CO_{ads}, formaldehyde and formic acid formed. When considering the adsorption is via O atom, there is only one possible path, Path C. 3-hydroxypropanal can form same as in Path A. A fourth path, Pathway D can be proposed to explain the formation of acrylic acid by 1,3-propanediol dehydrogenation followed by oxidation. As for Au and Pt, the electro-oxidation paths are different. For the 1,3-propanediol oxidation

on Au, there is one possible path, Pathway A. For the 1,3-propanediol oxidation on Pd, malonate, 3-hydroxypropanoate, and acrylate can be detected.[15] While on Pt, 1,3-propanediol oxidation proceeds along Pathway B and Pathway C due to the dissociative chemisorption of diol.[16]

2.1.4 Alcohol Oxidation on Ni and Co Based Materials

Compared with the alcohol oxidation on noble metals, non-noble metal based material, particularly transition metal oxides (TMOs) and transition metal hydroxides (TMHOs) are attracting more and more attention as alternatives for oxidation due to rich reserve and comparably cheap price. Among them, Co_3O_4[17], NiO[17], MnO_x, $Co(OH)_2$[18] and $Ni(OH)_2$[19]

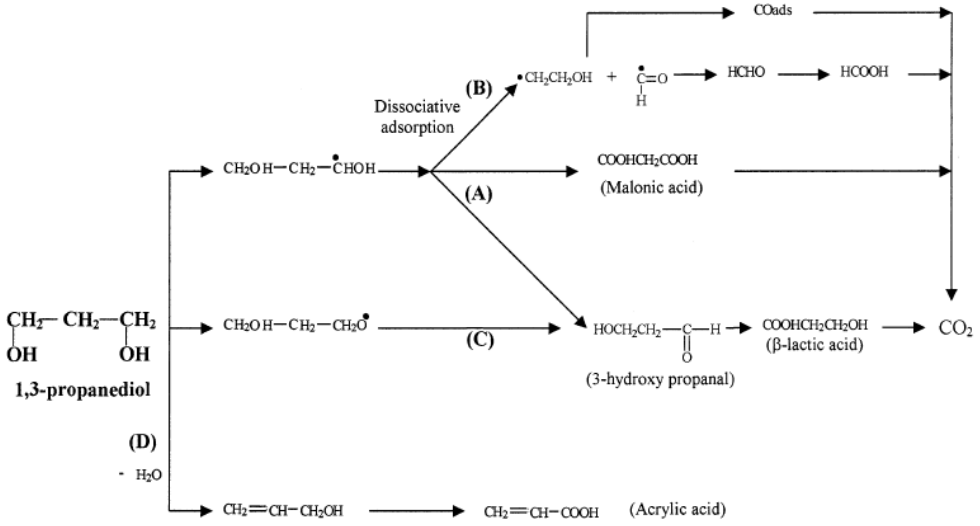

Figure 2.10 The mechanism of 1,3-propanediol oxidation on Pt, Au, and Pd[15, 16]

have brought about the interest on the electro-oxidation activity for small molecules, such as water, urea, and alcohols in alkaline. These TMOs and TMHOs are usually utilized as energy-storage materials based on their unique cation redox chemistry. The redox chemistry of these cations may also lead to the alcohol oxidation under proper conditions. Among these catalysts, Ni and Co oxides and hydroxides have shown greater potential for alcohol oxidation. This finding has evoked much interest and effort to explore these materials in recent years. Most work on alcohol oxidation on these TMOs and TMHOs are concentrated on methanol, and the simplest alcohol (methanol) was used to compare the electro-oxidation activity of different TMOs and TMHOs. For example, Jafarian et al.

investigated methanol oxidation on $Co(OH)_2$ and they found that the generation and consumption of Co^{4+} ions electrochemically were related to methanol oxidation activity. As for oxides, some investigations have shown that the combination of two oxides can increase the methanol oxidation activity and improve the catalyst stability. For example, the combination of Co_3O_4 and NiO exhibited a lower overpotential and stable activity compared with the pure Co_3O_4 and NiO during methanol oxidation. Wu et al. prepared Co_3O_4/NiO nanowire with core/shell structure, showing a higher electrochemical activity and better stability than Co_3O_4. Some studies also showed that nickel and cobalt ternary oxides might have an enhanced activity for methanol oxidation than their binary counterparts. For instance, $NiCo_2O_4$ was found to be more active for methanol oxidation than pure NiO, pure Co_3O_4 and Co_3O_4/NiO complex structure.[20] High methanol oxidation activity on $NiCo_2O_4$ was attributed intriguing mesoporous structures and high electron conductivity by Ding et al.[20] The conductivity improvement induced by Ni are often ascribed to Ni^{3+} in octahedral sites in spinel structure.[21] It is generally accepted that in $NiCo_2O_4$ with spinel structure, Ni ions lie in octahedral sites and Co ions are equally distributed in tetrahedral and octahedral sites. Ni ions exist in the state of Ni^{2+}, and Co ions exist in the state of Co^{3+} in octahedral sites and Co^{2+} in tetrahedral sites. However, it is also found that a little amount of Ni^{3+} ions exist in octahedral sites. Additionally, some reports reported that the Ni doping in Co_3O_4 can increase the conductivity to four-five orders of magnitude compared with Co_3O_4.[21] The highest conductivity of Ni doped Co_3O_4 was found at atomic Ni / (Ni + Co) is close to 0.5.[22] Besides, there are more comparative reports with regarding to methanol oxidation on NiO, Co_3O_4, and $NiCo_2O_4$[23, 24] electrodes. The conclusions are highly consistent that no matter the electrodes were in the form of powder or film, $NiCo_2O_4$ had a higher activity for methanol oxidation than NiO and Co_3O_4. To improve to methanol oxidation activity, Ni-Co oxides were further combined with other materials. For instance, reduced graphene oxide was used to combine $NiCo_2O_4$ to improve the activity and stability.[23] β-$Ni(OH)_2$ was also used to modify the surface of $NiCo_2O_4$ surface to improve the methanol oxidation activity.[25] Besides nickel and cobalt-based oxides and hydroxides, some nickel and cobalt metals and alloys were also studied for methanol oxidation.[26] Asgari et al. synthesized Ni-Co alloy and reported that increasing Ni amount in the alloy could enhance the methanol oxidation activity. Their work found that

the cobalt addition could increase the charge-acceptance ability of Ni, further enabling Ni^{2+}/Ni^{3+} peak shift to more negative direction. Nanosized Ni/Ti and Ni electrodes were also prepared for studying methanol, and nanosized Ni/Ti exhibits a higher activity than pure Ni for methanol oxidation. Except for the work mentioned above, the Ni^{3+}/Ni^{2+} ratio was considered to contribute to the methanol oxidation activity. For example, $La_{2-x}Sr_xNiO_4$ ($0 \leqslant x \leqslant 1$) has shown an increasing methanol oxidation activity with the increase of Ni^{3+}/Ni^{2+} ratio by increasing Sr amount in alkaline solution, and no poisoning phenomenon can be observed caused by oxidation intermediates and products.[27]

2.1.5 Alcohol Oxidation Mechanism on Ni and Co Based Materials

Electro-oxidation of alcohol is a kinetically controlled process, which can be considered as the process of hydrogen abstraction. In different schemes, the abstraction of hydrogen from the carbon atom in the α and β position with respect to the alcohol group is considered as the rate-determining step, respectively.[28, 29] Thus, the overall electrochemical process is significantly influenced by molecular dimensions, preferred orientation, and steric hindrance. Here, NiO serves as an example to illustrate alcohol oxidation.

At high pH, the α hydrogen abstraction occurs by base catalysis[29]:

$$RCH_{2,\beta}\text{-}OH_{\alpha} \rightleftharpoons RCH_{2,\beta}\text{-}O^{-} + H_{\alpha}^{+} \quad (2.12)$$

$$RCH_{2,\beta}\text{-}O^{-} \rightleftharpoons RCH_{\beta}O + H_{\beta}^{+} + 2e^{-} \quad (2.13)$$

Aldehydes are not stable in alkaline, and will react quickly in the presence of oxygen and other electron acceptors like the positively electrode.

In this scheme, pK_a, depending on the nature of R, dominates the overall reactivity. RCH_2O^- is more reactive than RCH_2OH. Alcohols with a low pK_a (e.g. glycerol and sugar alcohols) have a high oxidation reactivity, whereas alcohols with a high pK_a (e.g. isopropanol and isobutanol) are less active.[29]

In the scheme of the abstraction of β hydrogen can be considered to occur on the electrode, and low valence state of Ni acts as adsorption sites for alcohol, and meanwhile the low valence state of Ni is oxidized to high valence state, which further the oxidizes the adsorbed alcohol[27]. The steps can be described as follows[28]:

$$NiO + OH^- \leftrightarrow NiOOH + e^- \quad (2.14)$$

$$NiO + RCH_{2,\beta}OH \rightarrow NiO(RCH_{2,\beta}OH)_{ads} \quad (2.15)$$

$$NiOOH + NiO(RCH_{2,\beta}OH)_{ads} \rightarrow NiO + NiO(RCH_{\beta}OH)_{ads} + H_2O \quad (2.16)$$

$$NiOOH + NiO(RCH_{\beta}OH)_{ads} \rightarrow NiO + NiO(RCOH)_{ads} + H_2O \quad (2.17)$$

2.1.6 Effect of OH^- Concentration on Electro-oxidation Reaction in Alkaline

The OH^- concentration will lead to two aspects in electro-oxidation reaction. One is for the electrolyte conductivity. The other one is the utilization of active materials. Here, take $Ni(OH)_2$ as an example. The increase of OH^- concentration can increase the electrolyte conductivity, which means that when applying a fixed potential, more potential can be applied in the working electrode. It will increase the energy efficiency. The increase of OH^- concentration mainly determined the upper limit in utilizing active nickel species. It is due to that $Ni(OH)_2$ and OH^- are main reactants involved in the redox process. Meanwhile, the approach to reaching upper limit of active nickel species can be facilitated by increasing the conductivity.[30]

2.1.7 Effect of Cations on Electro-oxidation Reaction in Alkaline

Except for the effect of OH^- concentration on electrocatalysis, the choice of cations also has an obvious effect on electrocatalysis in alkaline solution. In terms of the choice of cations, the common cations are Li^+, Na^+, K^+, and Cs, and the corresponding electrolytes are LiOH, NaOH, KOH, and CsOH, respectively. N. M. Markovic's group found that methanol oxidation on Pt has an increasing activity in alkaline solution in the order LiOH << NaOH < KOH < CsOH.[31] This difference can be explained as follow shown in Figure 2.10. The non-covalent interactions between $M^+(H_2O)_x$ and OH_{ad} species increase in the same order as the hydration energies of the corresponding cations ($Cs^+ < K^+ < Na^+ << Li^+$), and also corresponding to an increase in $M^+(H_2O)_x$-OH_{ad} cluster concentration at the interface. These clusters will block the active sites for methanol oxidation reaction. Similar with electro-oxidation reaction on Pt, the electro-oxidation reaction on non-noble metal oxides has a similar behavior in terms of the choice of cations. For example, the electro-

oxidation of benzyl alcohol and urea showed an increasing catalytic activity in the order $Li^+ < Na^+ < K^+$.[32]

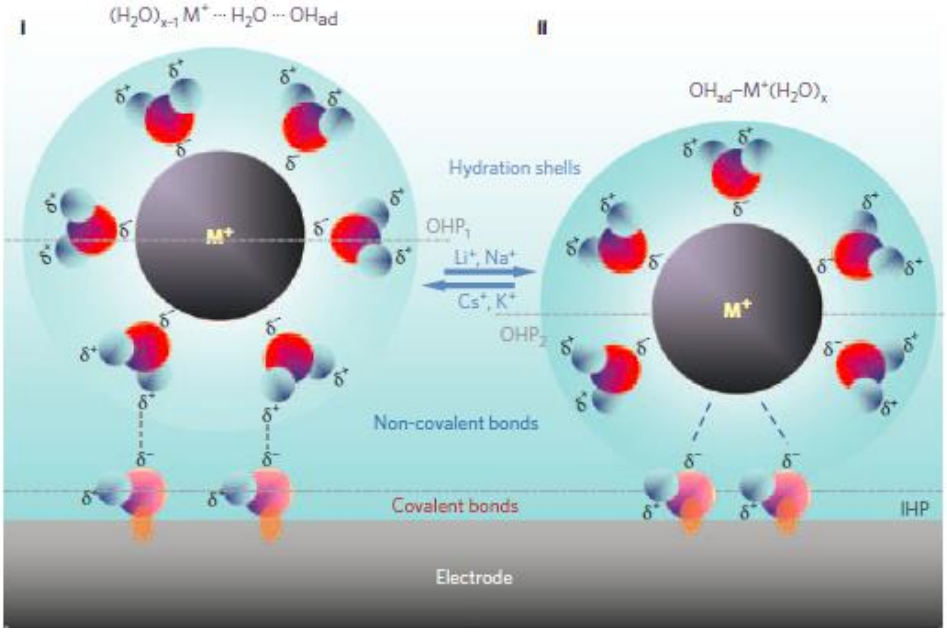

Figure 2.11 Models for non-covalent interactions between $M^+(H_2O)_x$ and OH_{ad}: i, $(H_2O)_{x-1}M^+\cdots H_2O\cdots OH_{ad}$ clusters; ii, $OH_{ad}\cdots M^+(H_2O)_x$ clusters.[31]

2.2 Question: Effect of Ni on Alcohol Oxidation in Ni-Co Hydroxides and Ni-Co Oxides

Based on the literature review, even though there have been numerous report on methanol oxidation on Ni-Co oxides and hydroxides, we cannot find a systematic study on methanol oxidation on Ni-Co hydroxides ($Ni_xCo_{1-x}(OH)_2$) and Ni-Co oxides (Ni doped Co_3O_4). The effect of Ni gradual increase in Ni-Co hydroxides and Ni-Co oxides on methanol oxidation are not revealed. Whether there will be an optimal Ni/Co value in Ni-Co hydroxides and Ni-Co oxides towards methanol oxidation is significantly expected.

The methanol molecule is a molecule with one carbon atom. The relationship between oxidation activity and Ni/Co is applicable for C2 alcohols, ethanol and ethylene glycol. Comparing the molecule structure of ethanol and ethylene glycol, ethylene glycol has one more hydroxyl group than ethanol in one molecule. It is expected to investigate the difference of electro-oxidation of ethanol and ethylene glycol.

2.3 Question: Electro-oxidation of C3 Alcohols on Co_3O_4

Based on the literature on C3 alcohol derived value-added products, it is found that most investigations are based on C3 alcohol oxidation on noble metal, there are few report on C3 alcohol oxidation on non-noble metal electrode. Besides, no systematic comparison investigations on C3 saturated alcohols (glycerol, 1,2-propanediol, 1,3-propanediol, 1-propanol, and 2-propanol) are reported. For C3 saturated alcohols, the number of hydroxyl groups can increase from one to three in one molecule, and the position of hydroxyl group can change. Thus, it is necessary to compare the electro-oxidation rate on the same electrode to uncover the relationship between oxidation rate and the number and position of hydroxyl groups. Some comparison has been done among some C3 alcohols, and however, few systematic comparisons are found among these five alcohols, especially on non-noble metal oxides. Thus, Co_3O_4, a normal spinel, was chosen as electrode to compare the C3 alcohol oxidation rate, and meanwhile the oxidation products will be analyzed.

Thus, in Chapter 4, the methanol oxidation will be investigated on Ni-Co hydroxides and oxides, and the Ni/Co composition dependence of methanol oxidation activity on Ni-Co hydroxides and oxides will be determined. In Chapter 5, the electro-oxidation of C2 alcohols (ethanol and ethylene glycol) was conducted on Ni-Co oxides. The relationship between alcohol oxidation activity and Ni/Co composition will be investigated, and the ethanol and ethylene glycol oxidation will be investigated and compared. In Chapter 6, the electro-oxidation of C3 saturated alcohols will be compared and the oxidation products will be analyzed.

2.4 PhD in context of literature

In this thesis, based on the literature review, three major objectives will be achieved.

1. Investigating the relationship between methanol oxidation activity and Ni/Co ratio in Ni-Co hydroxides and Ni-Co oxides.
2. Investigating the relationship between ethanol and ethylene glycol oxidation and Ni/Co ratio in Ni-Co oxides. Comparing ethanol and ethylene glycol oxidation on Ni-Co

oxides.

3. Comparing C3 saturated alcohols' oxidation rates on Co_3O_4. Detecting and analyzing the oxidation products.

References:

[1] J. L. Cohen, D. J. Volpe and H. D. Abruna. *Physical chemistry chemical physics : PCCP*. **2007**, 9, 49-77.

[2] A. V. Tripkovic, K. D. Popovic, J. D. Momcilovic and D. M. Drazic. *Journal of Electroanalytical Chemistry*. **1996**, 418, 9-20.

[3] A. V. Tripkovic, K. D. Popovic, J. D. Momcilovic and D. M. Drazic. *Journal of Electroanalytical Chemistry*, **1998**, 448, 173-181.

[4] A. V. Tripkovic, K. D. Popovic, J. D. Momcilovic and D. M. Drazic. *Electrochimica Acta*. **1998**, 44, 1135-1145.

[5] J. S. Spendelow and A. Wieckowski. *Physical chemistry chemical physics : PCCP*. **2007**, 9, 2654-2675.

[6] M. Chatterjee, A. Chatterjee, S. Ghosh and I. Basumallick, *Electrochimica Acta*, 2009, **54**, 7299-7304.

[7] L. Jiang, A. Hsu, D. Chu and R. Chen. *International Journal of Hydrogen Energy*. **2010**, 35, 365-372.

[8] S. C. S. Lai, S. E. F. Kleijn, F. T. Z. Öztürk, V. C. van Rees Vellinga, J. Koning, P. Rodriguez and M. T. M. Koper. *Catalysis Today*. **2010**, 154, 92-104.

[9] K. Matsuoka, Y. Iriyama, T. Abe, M. Matsuoka and Z. Ogumi. *Electrochimica Acta*. **2005**, 51, 1085-1090.

[10] E. Sitta, R. Nagao and H. Varela. *Plos One*, **2013**, 8, e75086.

[11] A. Serov and C. Kwak. *Applied Catalysis B: Environmental*. **2010**, 97, 1-12.

[12] M. Betowska-Brzezinska, T. Uczak and R. Holze. *Journal of Applied Electrochemistry*. **1997**, 27, 999-1011.

[13] Y. Kwon, K. J. P. Schouten and M. T. M. Koper. *ChemCatChem*. **2011**, 3, 1176-1185.

[14] D. J. Chadderdon, L. Xin, J. Qi, B. Brady, J. A. Miller, K. Sun, M. J. Janik and W. Li. *ACS Catalysis*. **2015**, 5, 6926-6936.

[15] J. Mahmoudian, M. Bellini, M. V. Pagliaro, W. Oberhauser, M. Innocenti, F. Vizza and H. A. Miller. *ACS Sustainable Chemistry & Engineering*. **2017**, 5, 6090-6098.

[16] M. E. M. Chbihi, D. Takky, F. Hahn, H. Huser, J. M. Leger and C. Lamy. *Journal of Electroanalytical Chemistry*. **1999**, 463, 63-71.

[17] J. B. Wu, Z. G. Li, X. H. Huang and Y. Lin, *Journal of Power Sources*, 2013, **224**, 1-5.

[18] M. Jafarian, M. G. Mahjani, H. Heli, F. Gobal, H. Khajehsharifi and M. H. Hamedi. *Electrochimica Acta*. **2003**, 48, 3423-3429.

[19] J. M. Skowronski and A. Wazny. *Journal of New Materials for Electrochemical Systems*. **2006**, 9, 345-351.

[20] R. Ding, L. Qi, M. Jia and H. Wang. *Catal. Sci. Technol.*. **2013**, 3, 3207-3215.

[21] Y. Li, P. Hasin and Y. Wu. *Advanced materials*. **2010**, 22, 1926-1929.

[22] C. F. Windisch Jr., G. J. Exarhos, K. F. Ferris, M. H. Engelhard and D. C. Stewart. *Thin Solid Films*. **2001**, 398-399, 45-52.

[23] A. K. Das, R. K. Layek, N. H. Kim, D. Jung and J. H. L. Lee. *Nanoscale*. **2014**, 6, 10657-10665.

[24] L. Qian, L. Gu, L. Yang, H. Yuan and D. Xiao. *Nanoscale*. **2013**, 5, 7388.

[25] M. U. A. Prathap, B. Satpati and R. Srivastava. *Electrochimica Acta*. **2014**, 130, 368-380.

[26] X. Tarrús, M. Montiel, E. Vallés and E. Gómez. *International Journal of Hydrogen Energy*. **2014**, 39, 6705-6713.

[27] R. N. Singh, T. Sharma, A. Singh, Anindita, D. Mishra and S. K. Tiwari. *Electrochimica Acta*. **2008**, 53, 2322-2330.

[28] A. Domenech-Carbo. *Electrochemistry of Porous Materials*. **2010**. p63

[29] Y. Kwon, S. C. S. Lai, P. Rodriguez, M. T. M. Koper. *Journal of The American Chemical Society.* **2011**, 133, 6914-6917.

[30] C.-C. Hu, K.-H. Chang and T.-Y. Hsu. *Journal of The Electrochemical Society*. **2008**, 155, F196.

[31] D. Strmcnik, K. Kodama, D. van der Vliet, J. Greeley, V. R. Stamenkovic and N. M. Markovic. *Nature Chemistry*. **2009**, 1, 466-472.

[32] W. Zhang, S. Yin, X. Li, G. Xu and T. Xie. *Electrochemistry Communications*. **2016**, 63, 1-4.

Chapter 3

Experimental Methodology

This chapter introduces the sample preparation principles and methods and gives the rationale for selecting electrodeposition as preparation method. The advantage of electrode preparation by electrodeposition is stressed. The principles of material characterizations such as X-ray absorption fine structure (XAFS), scanning electron microscope-energy dispersive X-ray (SEM-EDX), and etc. are introduced. XAFS is used to determine the change of valence state. SEM-EDX is employed to characterize the morphology of the materials and to determine the element ratio. The fundamental knowledge and principles of electrochemistry and electrochemical characterizations such as cyclic voltammetry (CV), chronoamperometry (CA), Differential pulse voltammetry (DPV), electrochemical impedance spectroscopy (EIS) are also described. CV and CA are used for comparing the alcohol oxidation rates. DPV is used to investigate the redox properties of materials. EIS is utilized for studying the alcohol oxidation mechanism.

3.1 Rationale for Selection of Methods/Materials

In this thesis, we chose the electrodeposition method to prepare materials using three-electrode system. In traditional electrode preparation process, binders are necessary to avoid the loss of electrocatalysts. However, the electrochemical performance will greatly be decreased due to the presence of the binder. Firstly, the kinetics of the transport of electrons and ions at the electrode and at the electrode-electrolyte interface will be hindered by binders. Secondly, a larger portion of the binder-enriched electrocatalyst surface of is blocked from contact with the electrolyte. One of the efficient methods to solve this problem is the direct growth of catalysts on the electrode. Thus, electrodeposition (followed by calcination) were used for directly preparing electroactive materials on conductive substrates. This binder-free electrode has several obvious advantages. Since every nanostructure of electrocatalysts is directly adhered to the electrode, the electronic resistance and ion diffusion resistance does not become a big concern, the electrolyte can easily penetrate into the electrode material. In the absence of binder, almost all the surfaces of electrocatalysts are exposed, and are thus able to participate in the electrochemical reaction, maximizing their utilization as electrocatalytic materials.[1]

In this thesis, the stainless steel meshes (SSM) or graphite papers (GPE) served as the substrates for working electrode. A saturated calomel electrode (SCE) was used as reference electrode. A Pt wire or plate were used as auxiliary electrode. The electrolyte was comprised of $Ni(NO_3)_2$ and $Co(NO_3)_2$ aqueous solution. The total metal ion amount was kept 0.1 M to guarantee the enough ion concentration and electrolyte conductivity. A potentiostat (Biologic SP-150) was utilized to keep a fixed potential -0.85 V against SCE electrode to guarantee the reduction of nitrate. The passing charge was kept the same to obtain the similar mass loading of Ni-Co hydroxides on substrates. The Ni-Co hydroxides were calcinated at 300 °C at a slow ramping rate to obtain the corresponding Ni-Co oxides.

In C1 alcohol (methanol) oxidation section, Ni-Co hydroxides and Ni-Co oxides were chosen as electrodes for studying. Stainless steel mesh (500 mesh, ~ 0.5 × 1.0 cm^2) was

used as the substrate. The electrodeposition potential and passing charge was fixed at -0.85 V and 0.6 C.

In C2 alcohol (ethanol and ethylene glycol) oxidation section, the Ni-Co oxides were used as electrodes for studying. Stainless steel mesh (500 mesh, ~ 1.0 × 1.0 cm^2) was chosen as the substrate. The electrodeposition potential and passing charge was fixed at -0.85V and 1.8 C, respectively. Ni-Co oxides were prepared to compare the C2 alcohol oxidation activity.

In C3 saturated alcohol (glycerol, 1,2-propanediol, 1,3-propanediol, 1-propanol, and 2-propanol) oxidation section, Co_3O_4 was used as the electrode for investigating the electrochemical oxidation of C3 saturated alcohols. The graphite paper (1.0 × 1.0 cm^2) was chosen as the substrate. The reason for using graphite paper rather than stainless steel as the substrates is to avoid the influence of stainless steel mesh on oxidation product analysis. The electrodeposition potential and passing charge was fixed at -0.85 V and 1.8 C, respectively.

3.2 Electrode Preparation

The preparation method in this report is electrodeposition. Electrodeposition is a common preparation method electrochemically. Electrodeposition has become a science and technology able to produce materials atom by atom with controllable, sophisticated structures and properties. In an electrochemical cell, when current is flowing through an electrode, the potential of this electrode is different from its equilibrium potential. If the equilibrium potential of the electrode is E_0 and the same electrode potential due to the current flowing is E(I), then the potential difference η between these two potentials is called overpotential, which can be given

$$\eta = E(I) - E \quad (3.1)$$

For our preparation method, the $Ni(NO_3)_2$ and $Co(NO_3)_2$ were used as precursor. The $Ni(OH)_2$ and $Co(OH)_2$ were prepared first according to the nitrate reduction under applying potential. The mechanism is shown in Equation 3.2-3.4.[1, 2]. Then the Ni-Co oxides can be obtained by calcinating the corresponding Ni-Co hydroxides (Equation 3.5-3.7).

$NO_3^- + H_2O + 2e^- \rightarrow NO_2^- + 2OH^-$ (3.2)

$NO_3^- + 6H_2O + 8e^- \rightarrow NH_3 + 9OH^-$ (3.3)

$NO_2^- + 6H_2O + 6e^- \rightarrow NH_4^+ + 8OH^-$ (3.4)

$6Co(OH)_2 + O_2 \rightarrow 2Co_3O_4 + 6H_2O$ (3.5)

$Ni(OH)_2 \rightarrow NiO + H_2O$ (3.6)

$2Ni(OH)_2 + 4Co(OH)_2 + O_2 \rightarrow 2NiCo_2O_4 + 6H_2O$ (3.7)

3.3 Material Characterization

3.3.1 X-ray Absorption Fine Structure

X-ray absorption fine structure (XAFS) is a very useful technique in the field of charactering the material structure and electronic states. It can be used in many research regions such as catalysts, magnetic materials, semiconductors, sensors, biological assemblies.[3] XAFS spectroscopy refers to the details of how X-rays are absorbed by an atom at the energy close to and above the atom's core-level binding energies. At some certain energies, the absorption increases drastically and produce an absorption edge.[4] Generally, this fine structure is separated into two energy parts. One is called as X-ray absorption near edge structure (XANES), which takes place in the part from the edge to ~40 eV above the edge. The other one is called as the extended X-ray absorption fine structure (EXAFS), which is in the part from 40 eV to 1000 eV above the edge. XANES and EXAFS has different applications for analyzing the materials XANES is strongly sensitive to coordination chemistry and oxidation states, while EXAFS is employed to determine the coordination number, atom distance and species of the neighbors.[4]

In the XAFS test, the simplest mode is transmission (Figure 3.2). In a transmission experiment, the X-ray beam intensity is measured before (I_0) and after (I_1) a sample and the absorbance (μ) calculated using the expression:

$\mu x = -\ln(I_1/I_0)$ (3.8)

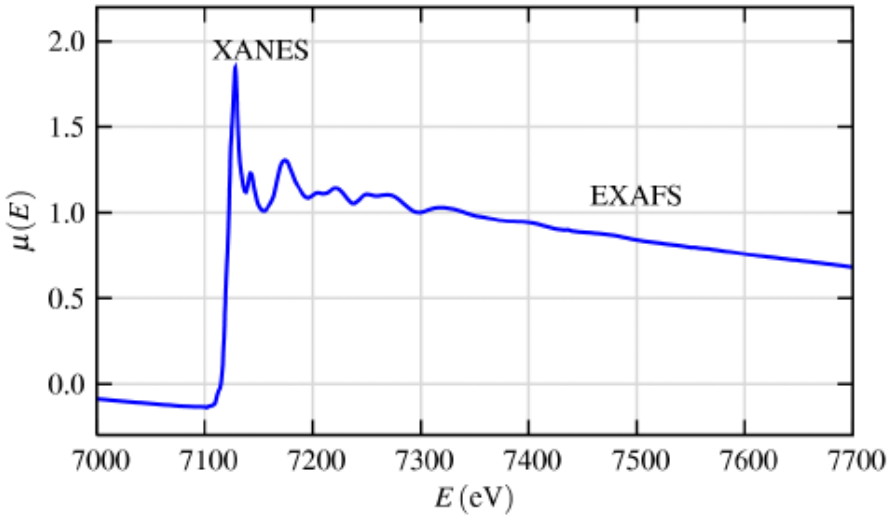

Figure 3.1 XAFS μ(E) for FeO[5].

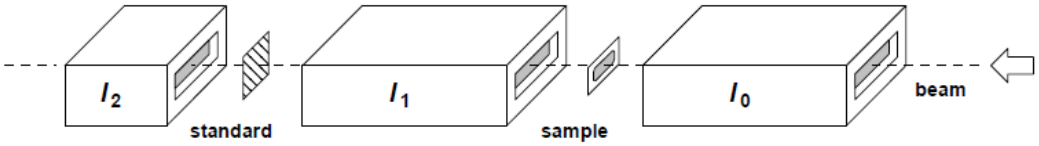

Figure 3.2 Typical setup for XAFS transmission mode. I_0, I_1 and I_2 are ionization detectors.[6]

The fluorescence modes are much more sensitive than transmission mode and are typically used for samples where absorbing atoms are dilute. In the fluorescence mode (Figure 3.3), the absorbance of the sample is measured by testing the intensity of the X-ray fluorescence. If F is the intensity of the fluorescence X-rays, the adsorption coefficient is given:

$$\mu = C(F/I_0) \quad (3.9)$$

where C is approximately constant.

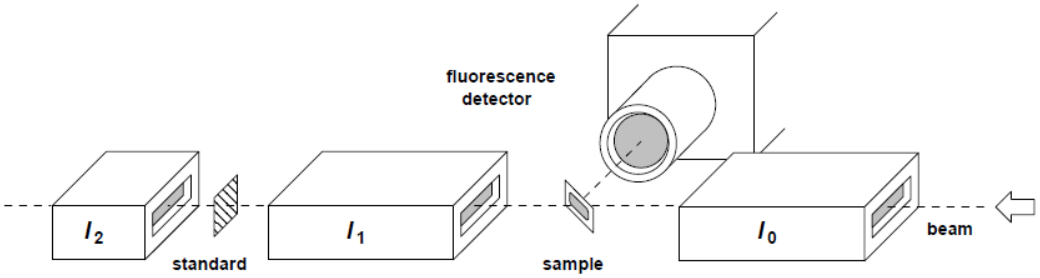

Figure 3.3 Typical setup for XAFS fluorescence mode.[6]

In this report, the XAFS tested was carried out at XAFCA beamline of Singapore Synchrotron Light Source (SSLS). The fluorescence mode was used.

3.3.2 Scanning Electron Microscopy

A scanning electron microscope (SEM) is a tool for observing those invisible micro-space and nano-space worlds by using a focused beam of electrons scanning the sample's surface. It can reveal the details and complexity inaccessible by light microscopy. SEM can achieve a resolution better than 1 nm. The principle of SEM is based on the interaction between electron beams with the sample surface. When a focused electron beam interacts the sample's surface, various types of signals are produced such as secondary electrons, reflected or back-scattered electrons, characteristic X-rays and light, absorbed current and transmitted electrons (Figure 3.4). The secondary electrons emerge from very close to the sample surface (≤ 1 nm), and thus secondary electrons are often used to obtain SEM images. Back-scattered electrons emerge from deeper location in samples, and the back-scattering electron signal intensity is strongly related to the atomic number of samples. Thus, the distribution information of different elements can be obtained by back-scattering electron signal.[7, 8] In this report, JSM-7600F and 6340F were used for obtaining the SEM images and energy dispersive X-ray data.

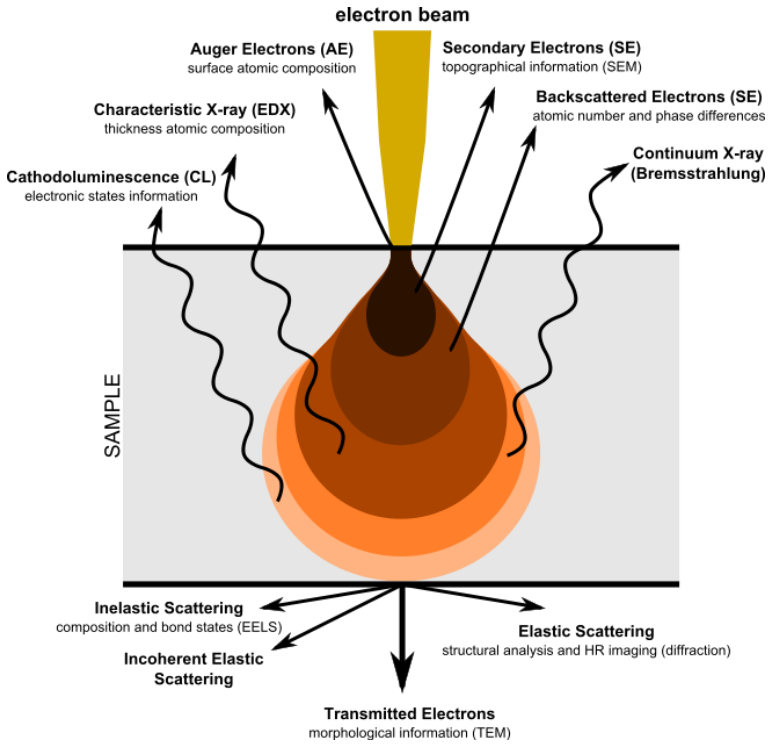

Figure 3.4 Scheme of the interaction between focused beam and sample surface[7]

3.4 Electrochemical Setup

Three-electrode system is commonly used in electrochemical tests. The investigated electrode is called working electrode, which potential and current can be measured and recorded by a potentiostat. Usually, the working electrode potential is against the reference electrode. The reference electrode is an electrode with a well-known and stable potential. There are various commercial reference electrodes in practical applications, and different reference electrodes can be used in different environments. For example, Ag/AgCl electrode and Hg/Hg_2SO_4 electrode (MSE) are often used in acid solution. Ag/AgCl electrode and saturated calomel electrode (SCE) are used in neutral solution. SCE and Hg/HgO electrode are often used in alkaline solution. Each reference electrode has its own electrode potential. To compare their potentials, standard hydrogen electrode (SHE) is often used. Standard hydrogen electrode becomes a basis for comparison with all other electrode reactions. The SHE potential is declared to be zero volts. The determination of standard hydrogen electrode potential is based on the redox reaction on a platinized platinum:

$$2H^+(aq) + 2e^- \rightarrow H_2(g) \quad (3.10)$$

This redox reaction occurs in acid solution with the activity of hydrogen ions unity and pure hydrogen gas is bubbled with a 100 kPa of gas pressure. Except for the standard hydrogen electrode, the reversible hydrogen electrode (RHE) is also used to exclude the effect from pH. The conversion from SHE to RHE can be given

$$E(RHE) / V = E(SHE) / V + 0.059\ V \times pH \quad (3.11)$$

The auxiliary electrode, also called counter electrode, provides circuit for current. The auxiliary electrode potential is usually not measured. The auxiliary electrode potential is only adjusted in order to make the working potential against the reference electrode. In our report, Pt wire and Pt plate were used as auxiliary electrodes.

3.5 Electrochemical Test

3.5.1 Cyclic Voltammetry

The cyclic voltammetry (CV) is a type of potentiodynamic electrochemical measurement method. In a CV test, the working electrode potential is ramped linearly with time from initial potential to a set potential. Once reaching the set potential, the working electrode potential is ramped to the initial potential in the opposite direction. The current at the electrode and the measured current is against the counter electrode. In CV tests, different scan rates can be employed for different purposes. For example, to exclude the effect of mass transfer, a higher scan rate in the CV test is used. To obtain the oxidation and

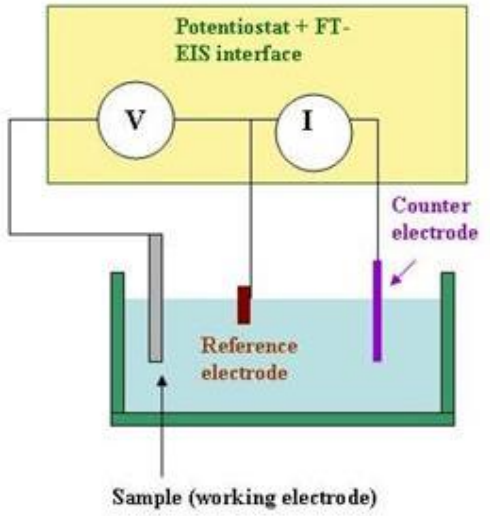

Figure 3.5 The schematic diagram of three-electrode system electrochemical cell[9]

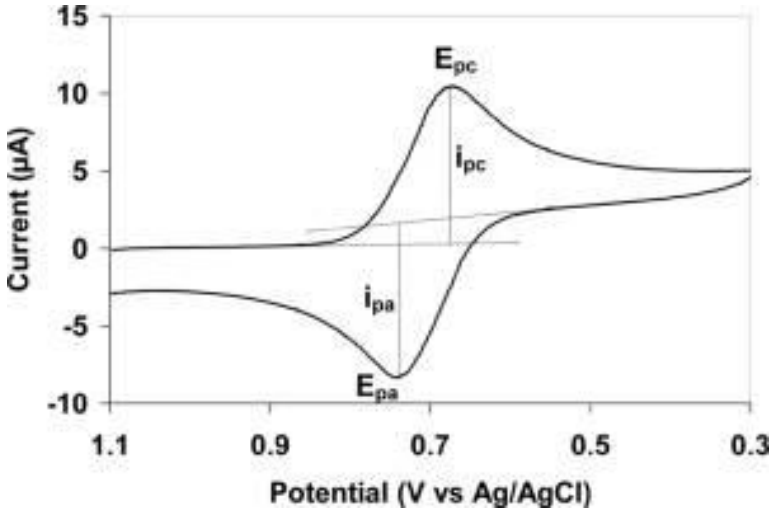

Figure 3.6 The sample of CV plot.[10]

potential of a species, a lower scan rate in the CV test is used. To obtain the information of double layer capacitance, different scan rates of CV curves should be employed. In the CV test, the electrode reaction can be divided into non-Faradic reaction and Faradic reaction. In the non-Faradic reaction, the current primary comes from the process of charging and discharging of the double layer. In the Faradic reaction, the current primary comes from the charge transfer in the interface between electrode and solution.

3.5.2 Non-Faradic Reaction

The non-Faradic reaction primary occurs on the double layer. The double layer solution side is thought to consist of some layers (Figure 3.7). The layer closest to the electrode is called Helmholtz or Stern layer, which includes solvent molecules and other ions or molecules specifically adsorbed. The plane of the charge centers of the specifically adsorbed is called the inner Helmholtz plane (IHP). The plane of the charge centers of these nearest solvated ions is called the outer Helmholtz plane (OHP). In the region from the OHP to the bulk solution is called the diffuse layer, where the solvated ions are nonspecifically adsorbed and distributed.[10]

The double layer capacitance is the electrical energy storage by the double layer effect. This electrical phenomenon appears at the interface between an electrode and an adjacent electrolyte. When applying a potential, two layers of ions exhibit opposite polarity and are separated by a layer of solvent molecules, which adheres to the electrode surface and acts like a dielectric in a conventional double layer capacitor. In the electrochemical cell, electric elements can be used to represent the interaction between the working electrode and reference electrode (i.e. SCE) shown in Figure 3.8. R_s represents the solution resistance; C_d represents the double layer of the interface between the working electrode and reference electrode; C_{SCE} represents the capacitance of SCE. Due to the series capacitance of C_d and C_{SCE} and $C_{SCE} \geq C_d$, C_{SCE} can be neglected in the circuit. When applying voltage in the series circuit, this voltage will be distributed on the solution resistance and double layer capacitance. The voltage on R_s and C_d can be represented E_R and E_C. Thus,

$$E = E_R + E_C = i_c R_s + q/C_d = (dq/dt)R_s + q/C_d \quad (3.12)$$

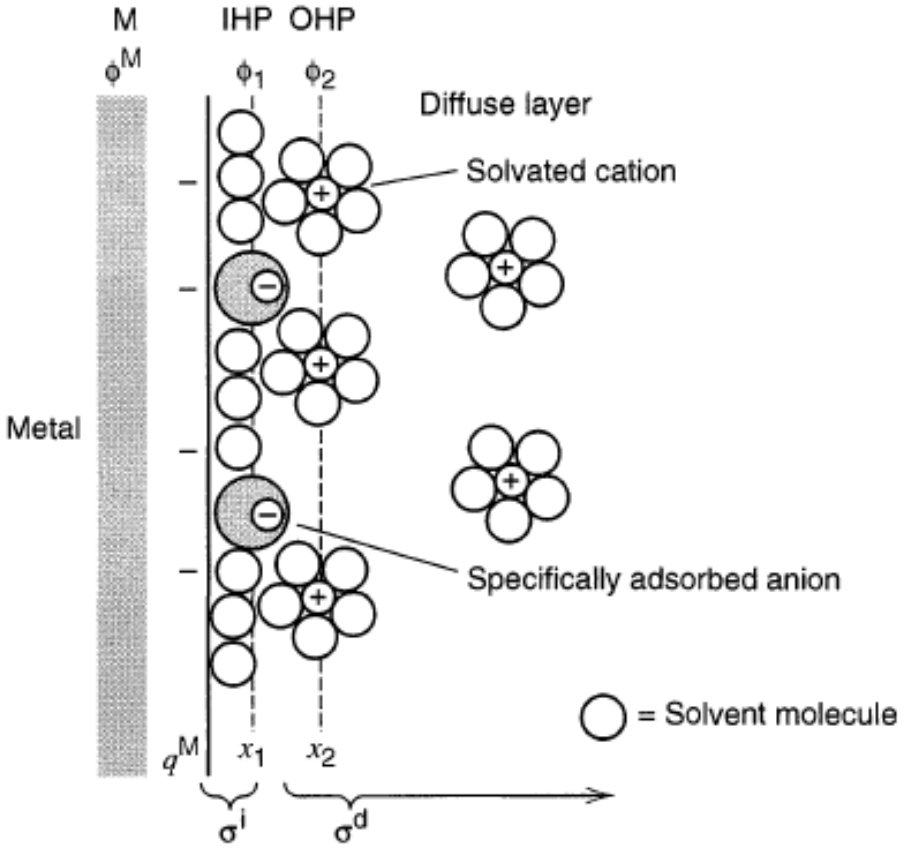

Figure 3.7 The model of double layer where anions are specifically adsorbed.[10]

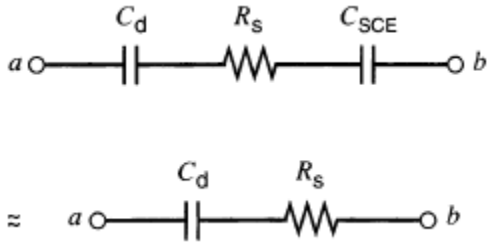

Figure 3.8 Representation of the cell by using circuit elements.[10]

In CV tests, the potential increases linearly with time at a scan rate (v) from some initial potential value, and here the potential value is assumed to be zero. The potential can be described as

$$E = vt \quad (3.13)$$

and thus,

$$vt = (dq/dt)R_s + q/C_d \quad (3.14)$$

If q equals to zero when t is zero,

$$i = vC_d [1 – \exp(-t/R_sC_d)] \quad (3.15)$$

When the potential scan starts, the current rises from zero and finally attains a steady-state value, vC_d (Figure 3.9).

3.5.3 Morphology Factor

Based on the double layer capacitance test, the double layer capacitance C_d can be attained by the relationship between the current i_c and the scan rate v. However, the linear dependence of current i_c against scan rate v is only suitable for a short scan rate range.[11, 12] As the scan rate v increases, there will be a distortion for the linear relationship between current i_c and scan rare v, due to the inhomogeneous potential distribution in the layer and the difficult response of hardly accessible surface regions, especially for highly porous or rugged materials. Thus, the current i_c can be rewritten as

$$i_c = i_i + i_e \quad (3.16)$$

and the corresponding double layer capacitance can be rewritten as

$$C_d = C_{di} + C_{de} \quad (3.17)$$

Where the i_i and C_{di} are attributed to the contribution from the internal interface of electrode, and i_e and C_{de} are attributed to the contribution from the external interface of electrode. Thus, C_d can be obtained by fitting the $i_c \sim v$ plot in low scan rates and C_{de} can be obtained by fitting the $i_c \sim v$ plot in high scan rates. A sample can be found in Figure 3.10. According to the statement above, a new factor, morphology factor φ, can be used to described the roughness or porosity degree, which can be defined as

$$\varphi = C_{di} / C_d = (C_d - C_{de}) / C_d \quad (3.18)$$

when φ is close to zero, it means that the electrode is close to the well-defined planar surface. When φ is bigger, it means that the electrode is more rough or porous.

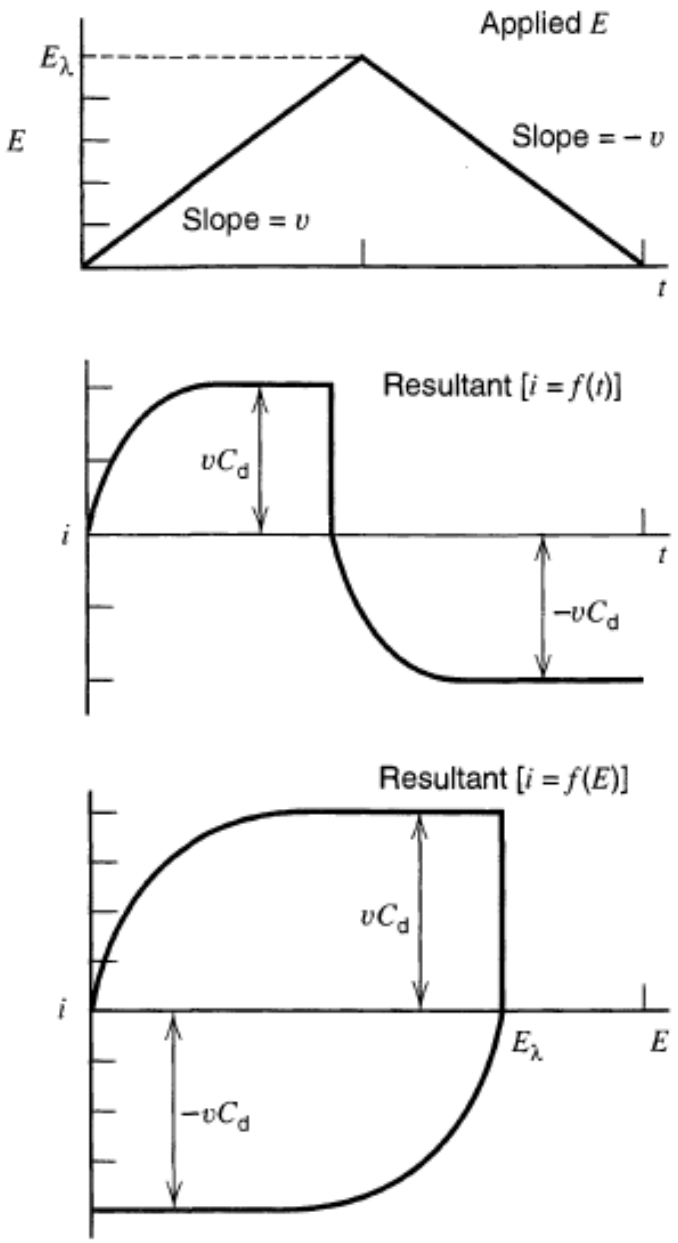

Figure 3.9 The relationship among current, potential, and time based on the series circuit shown in Figure 3.8.[10]

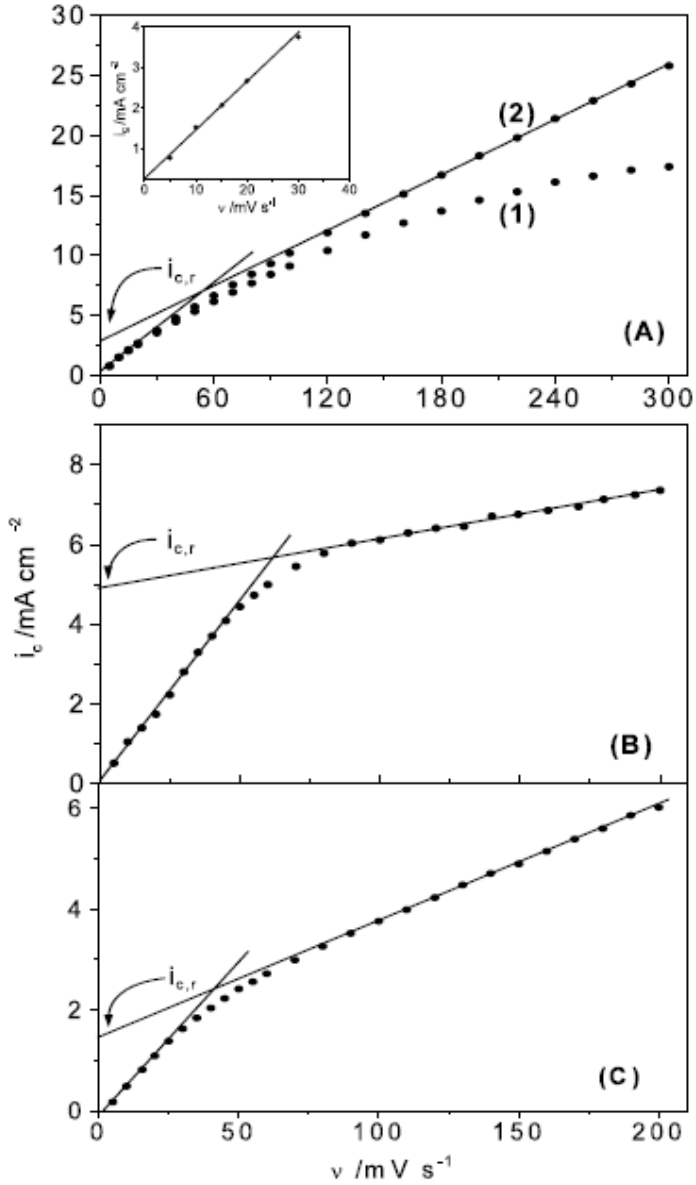

Figure 3.10 Dependence of the capacitance current on scan rates: (A) II-Ti/RuO_2 electrode in 0.5 M H_2SO_4; (B) I-Ti/Pt/β-PbO_2 electrode in 3.0 M H_2SO_4; (c) Ti/Co_3O_4 electrode in 1.0 M NaOH.[11]

3.5.4 Faradic Reaction

Except for the non-Faradic reaction contribution from double layer, Faradic current is also an important direction on the electrode reaction. For Faradic reactions, charges transfer across the interface between the electrode and solution. The oxidation and reduction can be caused by charge transfer. In Faradaic reactions, the chemical reaction amount is

proportional to the passing charge amount. When applying a potential on the working electrode against reference electrode, it is equivalent to controlling the electron energy in the working electrode. Applying a more negative potential means that the electron energy level is raised. When the electrons have an enough high energy, they will transfer into the vacant state of species in the electrolyte, and a reduction current occurs. Similarly, applying a more positive potential means that the energy level is lowered. When the electron energy level is enough low, the electrons from electrolyte species will transfer to the electrode, and the oxidation current occurs.[10] The critical potential where the reduction or oxidation reaction occurs is related to the standard potential E^0 for the specific chemical species.

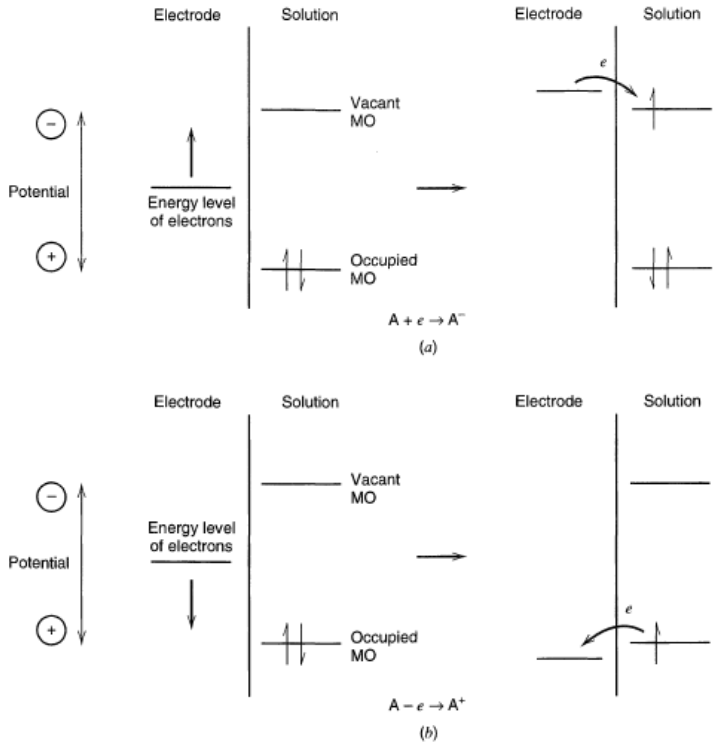

Figure 3.11 The schematic diagram of reduction reaction and oxidation reaction in electrochemical system.[10]

3.5.5 Chronoamperometry

Chronoamperometry (CA) is a technique where the working electrode potential is fixed or stepped and the current at the working electrode is measured and recorded with time. In CA tests, the current from non-faradaic reaction is eliminated as the test proceeds (Figure

3.12). Unlike CV test, chronoamperometry cannot give the information of oxidation and reduction potential of species. However, as a pulsed technique, it can generate high charging current, which decays exponentially with time. In potential-controlled experiment, the current has an obvious response when the potential changes in a step function. In this case, the measured current is diffusion controlled and depends on the rate at which the analyzed species diffuses to the electrode. The most useful equation in CA is the Cottrell equation, describing the current after a large potential step.

$$I = (nFACD^{1/2}) / (\pi^{1/2}t^{1/2}) \quad (3.19)$$

Where n and F represents the electron number in one reaction and Faraday's constant 96,485 C mol^{-1}, respectively; A and C represents the electrode area and the electroactive species concentration, respectively; D is the diffusion constant of electroactive species.

Besides, in the electrocatalysis area, CA is used to study the stability of catalysis. In water splitting and small molecule oxidation aspect, chronoamperometry is widely used.[13-15]

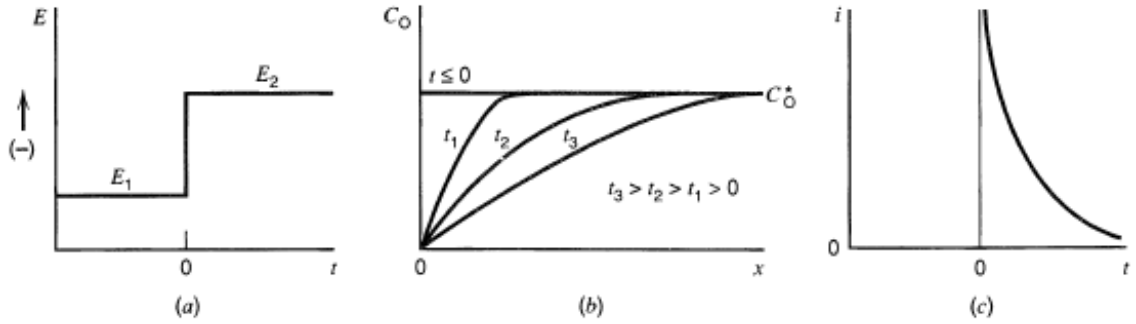

Figure 3.12 The schematic illustration of chronoamperometry test in the electrochemical reduction system: (a) potential vs. time; (b) electroactive species concentration vs. time; (c) current vs. time.[10]

3.5.6 Differential Pulse Voltammetry

Differential pulse voltammetry (DPV) is a technology derived from linear sweep or stair voltammetry, with regular voltage pulses applied on the linear sweep or stairsteps in potential. The current at the working electrode is monitored and recorded immediately before and after each potential change, and the relationship between current difference and potential is plotted. The basis of DPV is the difference in decay rates of the non-faradaic

(charging) and the faradaic currents before and after a potential step or pulse. The non-faradaic current decays exponentially, while the faradaic current under diffusion control decays in $t^{-1/2}$. It means that the decay rate of the non-faradaic current is considerably faster than the that of the faradaic current. Considering a reaction ($Ox + e^- = Red$), when the applied potential is in the positive of the redox potential, no faradaic reaction occurs in response to the pulse, and hence the difference in current is zero. When the applied potential is around the redox potential, the difference in current first reaches a maximum, and then decreases to zero as a result of diffusion control. Therefore, the current response presents a symmetric peak.[16]

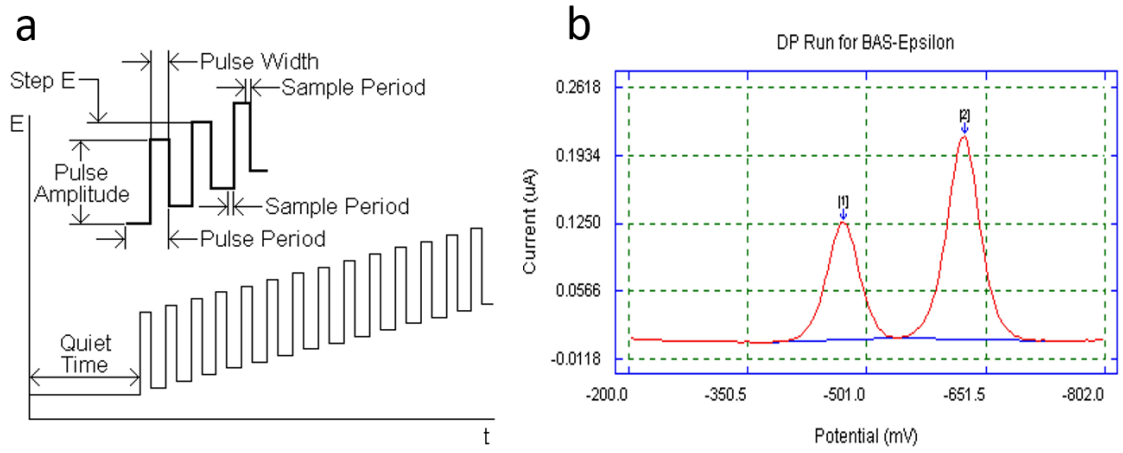

Figure 3.13 (a) Potential wave form in DPV; (b) a typical DPV curve[17]

3.5.7 Electrochemical Impedance Spectroscopy

Electrochemical impedance spectroscopy (EIS) is a powerful tool to characterize the electrochemical mechanism and determine the kinetics of processes, resistance, capacitance, inductance and so on. EIS is often used in the following three types of studies. The first one is the interfacial process. It involves the redox reaction at the electrode, adsorption and desorption, mass transfer and so on.[13, 18-20] The second one is related to the electrode geometric effect.[21, 22] For example, the shape of the electrode, such as line, sphere, and cylinder, can be estimated. The volume-limited, highly porous, and rugged electrodes can be determined. The third one is the practical applications in power source like fuel cell,

battery, and supercapacitor.[23-29] In the fields of coating[30], corrosion[31], electrocatalysis[20], sensor[32], EIS is also widely used.

The principle of EIS is based on the frequency scan under an alternating current (ac) signal. In consecutive frequency scans, different electrochemical circuit elements, representing different electrochemical reactions, gives different responses. Usually, the imposing signal can be given by

$$E = E_0 + E_m \times \sin\omega t \quad (3.20)$$

where E_0 is direct current (dc) bias potential, E_m is the amplitude of pure ac signal, and ω is the scan frequency.

When imposing the ac signal on different electric elements, different results can be recorded. Here, we simplify the imposing signal

$$E = E_m \times \sin\omega t \quad (3.21)$$

When this signal is imposed on a pure resistance (R), based on Ohm's law the current is given

$$i = (E_m/R) \times \sin\omega t = (1/R)E \quad (3.22)$$

Thus, the impedance of pure resistor is R.

When this signal is imposed on a pure capacitance (C), the current can be written

$$i = dq/dt = d(CE)/dt = \omega CE_m \times \cos\omega t = \omega CE_m \times \sin(\omega t + \pi/2) = -j\omega CE \quad (3.23)$$

Thus, the impedance of pure capacitance is $1 / (j\omega C)$.

When this ac signal is imposed on the R + C circuit in series

$$E = E_R + E_C = i\,(R + 1 / (j\omega C)) \quad (3.24)$$

Thus, the impedance Z of R + C circuit in series is $R + 1 / (j\omega C)$.

Generally, the impedance can be represented as

$$Z(\omega) = Z_{Re} - jZ_{Im} \quad (3.25)$$

where Z_{Re} and Z_{Im} are the real and imaginary parts of the impedance, respectively. For instance, for R + C circuit in series, Z_{Re} equals to R and Z_{Im} equals to $1/(\omega C)$. The magnitude of impedance is given by

$$|Z|^2 = Z_{Re}^2 + Z_{Im}^2 = R^2 + 1 / (\omega C)^2 \quad (3.26)$$

The phase angle, φ, is given by

$$\tan\varphi = Z_{Im}/Z_{Re} = 1 / (R\omega C) \quad (3.27)$$

Impedance measurements produce numerical results, usually as Z_{Re} vs. Z_{Im}, and |Z| vs. frequency phase vs. frequency. These three types of relationship are plotted as Nyquist plot (Figure 3.14a), Bode-Z plot (Figure 3.14b), and Bode-phase plot (Figure 3.14c)

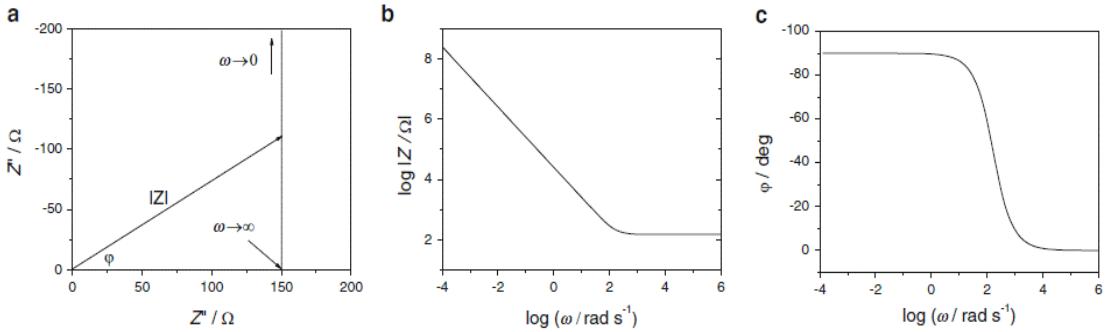

Figure 3.14 Complex plane (a), Bode-Z plot (b), Bode-phase (c) for R + C circuit in series, where R equals to 150 Ω and C equals to 40 μF.[10]

To interpret the EIS data results, equivalent circuit modeling is used to extract and interpret physical properties in the electrochemical system. Some ideal electrical elements are often used in the equivalent circuit. They are resistors (R), capacitors (C), and inductors (L). However, real electrochemical systems do not behave like ideal electric elements because the electrochemical processes occur and distribute in time and space. Some specialized circuit elements suitable for electrochemical system need to be used. These include the generalized constant phase element (CPE) and Warburg element (Z_w). In equivalent circuits, resistors (R) often represent the solution resistance or reaction resistance; the capacitor (C) is related to the double layer capacitance or the adsorption capacitance; the inductor (L) is often involved in the process of adsorption-desorption-adsorption; the Warburg element (Z_w) is used to represent the diffusion or mass transport impedance. Constant phase elements (CPE) are often used to replace the capacitor (C) to indicate the deviation from a perfect capacitor. The impedance of CPE is given by

$$Z(\omega) = 1 / [(j\omega)^{a}Q] \quad (3.28)$$

Where a and Q represent the deviation from an ideal behavior and the frequency-independent parameter, respectively. When a equals to 1, CPE behaves as an ideal capacitor; when a equals to 0, CPE behaves as a pure resistor; when a equals to -1, CPE equals to a pure inductor.[20]

In the electro-oxidation system, two types of equivalent circuits (Figure 3.15) are often used to analyze the EIS data. In the equivalent circuit, R_s represents the solution resistance; R_{ct} represents the charge transfer resistance; R_{ads} represents the intermediate adsorption resistance. CPE1 is related to the double layer capacitance; CPE2 is related to the reaction on intermediate product adsorption. When only considering the charge transfer and double layer capacitance, the equivalent circuit in Figure 3.15a is used; when considering the charge transfer, double layer capacitance and the adsorption reaction, the equivalent circuit in Figure 3.15b is used.

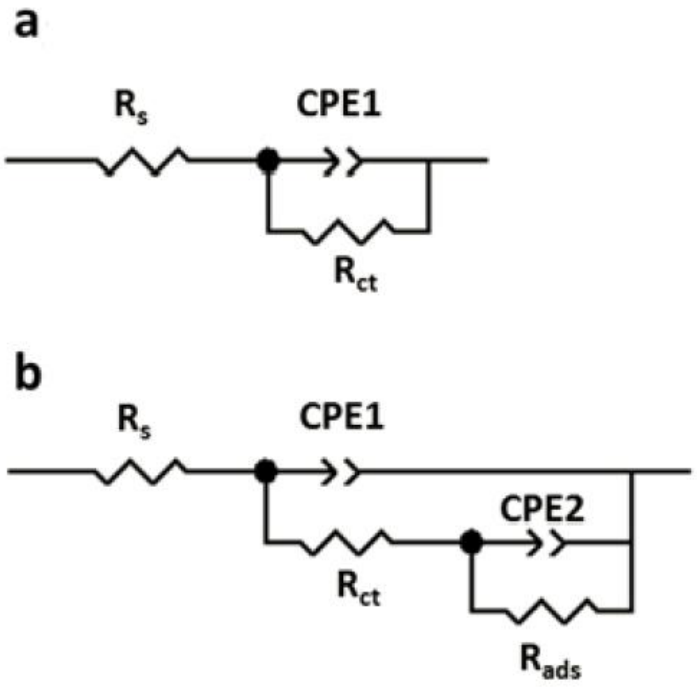

Figure 3.15 The equivalent circuit for analyzing the EIS data in electro-oxidation system: (a) the intermediates adsorption is not considered; (b) the intermediates adsorption is considered.

3.7 Overview of Methodologies

In this thesis, the electrodeposition was used to prepare electrode materials. XRD, SEM, EDX, and XAFS were used to characterize the prepared materials. CV, CA, DPV, and EIS approaches were employed to characterize their electrochemical properties. NMR was used to analyze the oxidation products.

References:

[1] L. Qian, L. Gu, L. Yang, H. Yuan and D. Xiao. *Nanoscale*. **2013**, 5, 7388.

[2] J. R. S. Brownson and C. Lévy-Clément. *Electrochimica Acta*. **2009**, 54, 6637-6644.

[3] Y. Iwasawa, *World Scientific Publishing Co. Pte. Ltd.*

[4] B. D. Shrivastava. *Journal of Physics: Conference Series*. **2012**, 365, 012002.

[5] M. Newville. *Consortium for Advanced Radiation Sources*. University of Chicago, Chicago, IL, 2004.

[6] http://smb.slac.stanford.edu/~ellis/Thesis/Chapter1.pdf.

[7] https://en.wikipedia.org/wiki/Scanning_electron_microscope.

[8] http://www.ammrf.org.au/myscope/sem/background/

[9] http://cn.bing.com/image/search?view=detailV2&ccid=fXGfSwxU&id=40D459E59825BE40D459E59825BE9D36D1AA4D93A5E78E0E6ED60D&thid=OIP.fXGfSwxU0NvDCJ83zqUrVQEmEs&q=three+electrode+electrochemical+cell&simid=607994446690648146&selectedindex=16&mode=overlay&first=1.

[10] A. J. Bard and L. R. Faulkner. Electrochemical Methods-Fundamentals and Applications Second edition.

[11] L. M. Da Silva, L. A. De Faria and J. F. C. Boodts. *Electrochimica Acta*. **2001**, 47, 395-403.

[12] S. Palmas, F. Ferrara, A. Vacca, M. Mascia and A. M. Polcaro. *Electrochimica Acta*. **2007**, 53, 400-406.

[13] S. Sun, Y. Zhou, B. Hu, Q. Zhang and Z. J. Xu. *Journal of The Electrochemical Society*. **2015**, 163, H99-H104.

[14] S. Sun, L. Sun, S. Xi, Y. Du, M. U. Anu Prathap, Z. Wang, Q. Zhang, A. Fisher and Z. J. Xu. *Electrochimica Acta*. **2017**, 228, 183-194.

[15] C. A. Kent, J. J. Concepcion, C. J. Dares, D. A. Torelli, A. J. Rieth, A. S. Miller, P. G. Hoertz and T. J. Meyer. *J Am Chem Soc*. **2013**, 135, 8432-8435.

[16] K. Aoki, J. Osteryoung and R. A. Osteryoung. *Journal of Electroanalytical Chemistry*. **1980**, 110, 1-18.

[17] https://www.basinc.com/manuals/EC_epsilon/Techniques/Pulse/pulse.

[18] M. Asgari, M. G. Maragheh, R. Davarkhah, E. Lohrasbi and A. N. Golikand. *Electrochimica Acta*. **2012**, 59, 284-289.

[19] H. Y. Wang, S. F. Hung, H. Y. Chen, T. S. Chan, H. M. Chen and B. Liu. *J Am Chem Soc*. **2016**, 138, 36-39.

[20] S. Sun and Z. J. Xu. *Electrochimica Acta*. **2015**, 165, 56-66.

[21] J.-B. Jorcin, M. E. Orazem, N. Pébère and B. Tribollet. *Electrochimica Acta*. **2006**, 51, 1473-1479.

[22] H.-K. Song, Y.-H. Jung, K.-H. Lee and L. H. Dao. *Electrochimica Acta*. **1999**, 44, 3513-3519.

[23] P. L. Taberna, C. Portet and P. Simon. *Applied Physics A*. **2005**, 82, 639-646.

[24] Z. He and F. Mansfeld. *Energy Environ. Sci.*. **2009**, 2, 215-219.

[25] A. K. Manohar, O. Bretschger, K. H. Nealson and F. Mansfeld. *Bioelectrochemistry*. **2008**, 72, 149-154.

[26] P. L. Taberna, P. Simon and J. F. Fauvarque. *Journal of The Electrochemical Society*. **2003**, 150, A292.

[27] Z. Deng, Z. Zhang, Y. Lai, J. Liu, J. Li and Y. Liu. *Journal of the Electrochemical Society*. **2013**, 160, A553-A558.

[28] R. Makharia, M. F. Mathias and D. R. Baker. *Journal of The Electrochemical Society*. **2005**, 152, A970.

[29] J.-M. Le Canut, R. M. Abouatallah and D. A. Harrington. *Journal of The Electrochemical Society*. **2006**, 153, A857.

[30] A. Ghasemi, V. S. Raja, C. Blawert, W. Dietzel and K. U. Kainer. *Surface and Coatings Technology*. **2008**, 202, 3513-3518.

[31] F. Mansfel. *Electrochimica Acta*. **1990**, 35, 1533-1544.

[32] S. Qiu, S. Gao, Q. Liu, Z. Lin, B. Qiu and G. Chen. *Biosensors & bioelectronics*. **2011**, 26, 4326-4330.

Chapter 4*

Methanol Oxidation on Ni-Co Hydroxides and Oxides

This chapter discusses methanol oxidation reaction (MOR) on Ni-Co hydroxides and Ni-Co oxides. The MORs were conducted on Ni-Co hydroxides and Ni-Co oxides with different Ni/Co ratios. It can be found that the MOR activity on Ni-Co hydroxides increased with Ni increase, while the MOR activity on Ni-Co oxides exhibited a volcano-shaped trend with the best activity at atomic 46/54 of Ni/Co. The role of Ni in promoting the oxidation reaction was investigated by EIS measurements. It can be found that the Ni in Ni-Co hydroxides and Ni-Co oxides can facilitate MOR. At a low potential, increasing Ni leads to higher adsorption of intermediate products.

* This chapter published substantially as Sun et al., Composition dependence of methanol oxidation activity in nickel–cobalt hydroxides and oxides: an optimization toward highly active electrodes, *Electrochimica Acta*, **2015**, 165, 56–66.

4.1 Introduction

Using methanol as a proton resource is attracting an increasing attention in the fuel cell due to that methanol is easier to store and less problematic than hydrogen gas.[1-4] It has encouraged an intensive effort on the development of direct methanol fuel cells. The exiting MOR efficient catalysts are mainly noble metals, like Pt and its alloys.[5-7] Due to the limited reserve and high cost of noble metals, some transitional metal oxides and hydroxides as alternatives, like Co_3O_4[8], NiO[9], $Ni(OH)_2$[10], MnO_x[11, 12] have brought about the interest on electro-oxidation activity for methanol in alkaline. Based on our literature, the Ni-Co hydroxides and Ni-Co oxides were used as electrodes for MOR, and the following key issues needed to be solved. (1) A systematic investigation needs to be done on the Ni/Co ratio in Ni-Co hydroxides and oxides for MOR activity. (2) In MOR process, the Ni effect in Ni-Co hydroxides and oxides needs to be revealed. (3) A comparison between Ni-Co hydroxides and Ni-Co oxides for MOR needs to be conducted.

Motivated by these key issues, Ni-Co hydroxides and Ni-Co oxides with different Ni/Co ratios were prepared on stainless steel meshes by tuning the Ni/Co ratio in electrolyte. It is found that Ni-Co oxides presented a better MOR activity than Ni-Co hydroxides. The increase of Ni content in Ni-Co hydroxides promoted MOR activity. The MOR activity on Ni-Co oxides exhibited a volcano-shaped trend with the optimal atomic Ni/Co ratio 46/54. The Ni effect in Ni-Co hydroxides and Ni-Co oxides was ascribed to increasing the intermediate product adsorption ability.

4.2 Experimental Methods

4.2.1 Electrode Preparation

The Ni-Co hydroxides were prepared on stainless steel meshes (0.5 cm × 1.0 cm) by electrodeposition method in $Ni(NO_3)_2$ and $Co(NO_3)_2$ mixed solution. The total concentration of metal ions was kept at 0.1 M. The Ni/Co ratio in Ni-Co hydroxide was controlled by tuning the ratio of Ni^{2+}/Co^{2+} in electrolyte. The electrodeposition potential was hold at -0.85 V vs. SCE at room temperature. The passing charge was fixed at 0.3 C

passed through the working electrode. The Ni-Co oxides were synthesized by calcinating the corresponding Ni-Co hydroxides at 300 °C in air. The formation process of Ni-Co hydroxides and oxides can be explained according to the Equations 3.2-3.7. The electrodeposition and the following electrochemical tests were conducted with Bio-Logic electrochemical station (SP150) with a built-in EIS analyzer.

4.2.2 SEM, EDX, and XRD

JSM-7600F and 6340F were used to obtain SEM images and EDX data. Shimadzu (x2) with Cu K_α radiation was used to characterize the crystal structure of samples.

4.2.3 Morphology Factor and MOR CV

The morphology factors of Ni-Co hydroxides and Ni-Co oxides were obtaining by measuring the double layer capacitance of Ni-Co hydroxides and Ni-Co oxides. A Hg/HgO (1 M KOH, aqueous) electrode and Pt wire were used as reference and counter electrodes, respectively. The double layer capacitances of Ni-Co hydroxides and Ni-Co oxides were calculated by consecutive CV scans at the range 0.46 ~ 0.53 V and 0.01 ~ 0.06 V vs. Hg/HgO in 1.0 M KOH solution, respectively. The scan rate increased from 1 to 250 mV s-1. The current at 0.47 V in the reverse scan for Ni-Co hydroxides and the current at 0 V in the reverse scan for Ni-Co oxides were chosen to figure out the capacitance at the difference potential range. The total double layer capacitance and outer capacitance were obtained by linear fitting the current vs. scan rate curve at the scan rate from 1 to 14 mV s-1 and at the scan rate higher than 200 mV s-1. MOR CV tests were carried out in 1.0 M KOH from -0.1 to 0.6 V vs. Hg/HgO at 10 mV s^{-1} in the absence and presence of 0.5 M methanol.

4.2.4 EIS

EIS tests were conducted at different bias potential from 0.50 to 0.60 V consecutively against Hg/HgO electrode with 10 mV ac amplitude. 0.02 V was a potential step. The

frequency range changed from 200 kHz to 10 mHz. The bias potential before EIS tests was hold for 120 s to make the MOR stable during each EIS test.

4.3 The Principle Outcome

4.3.1 Materials

The atomic Ni content in Ni-Co hydroxides and Ni-Co oxides can be determined by using EDX (Figure 4.1a). It is noticed that the Ni content in sample was lower than that in solution. Based on the EDX test, the Ni contents in Ni-Co hydroxides and oxides were 0%, 15%, 27%, 46%, 75%, and 100%, respectively. The average mass loadings of Ni-Co hydroxides and Ni-Co oxides are shown in Figure 4.1b. Ni-Co hydroxides had a similar mass loading from 0.40 to 0.42 mg except $Ni(OH)_2$, suggesting that the electrodeposition rate of $Co(OH)_2$ was faster than that of $Ni(OH)_2$. The average mass loadings of corresponding oxides show this trend.

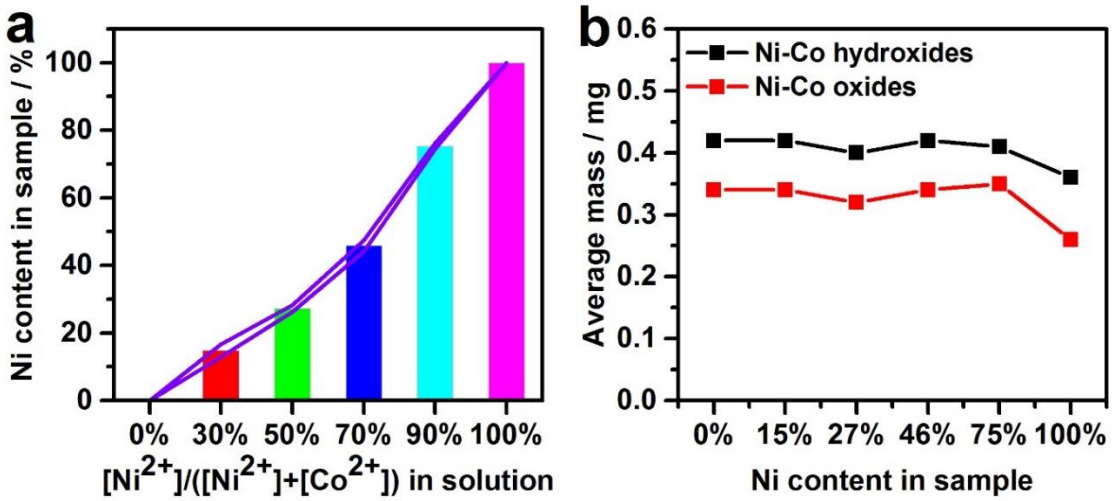

Figure 4.1 (a) The relationship of Ni content between in solution and in sample; (b) the average mass of Ni-Co hydroxides and Ni-Co oxides.

Figure 4.2 shows the morphologies of Ni-Co hydroxides and Ni-Co oxides. As Ni contents increased, the morphologies changed from nanosheets to nanorods, and from loose structure to dense structure. There was no obvious morphology change between Ni-Co hydroxides and their corresponding oxides.

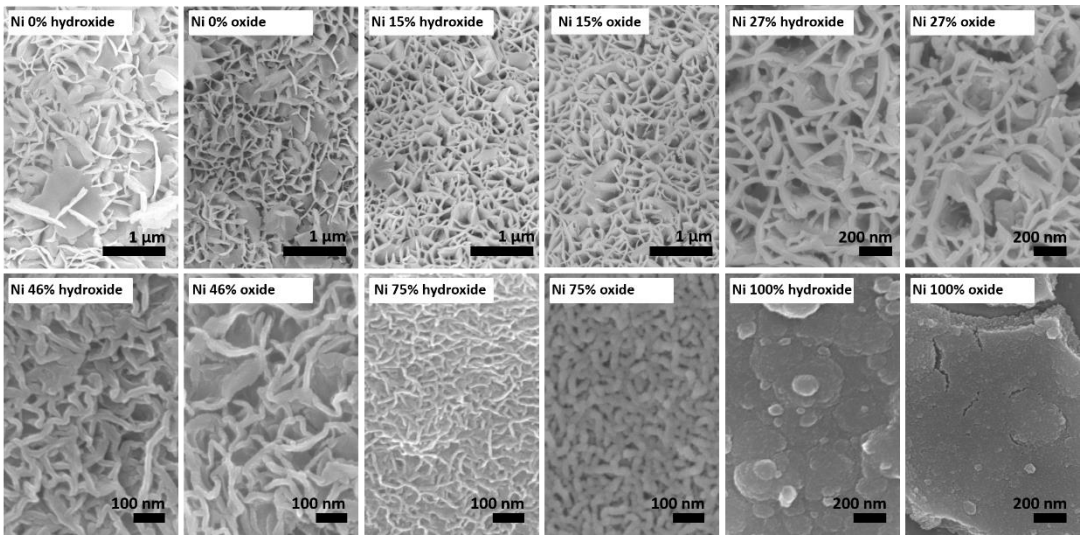

Figure 4.2 FESEM images of Ni-Co hydroxides and Ni-Co oxides with different Ni contents.

The crystal structure of Ni-Co oxides are shown in Figure 4.3. When Ni content was lower than 46%, all peaks from XRD patterns could be indexed as Ni-Co oxides cubic spinel structure. No additional peaks such as NiO were found. As Ni content was higher than 46%, only NiO cubic structure (JCPDS 47-1049) was found obviously. The crystal structure was considered to change from spinel structure to spinel and rocksalt structure, and to rocksalt structure based our result and previous reports[13-16].

4.3.2 Morphology Factor

The morphology factor can be obtained by measuring the double layer capacitance currents at different scan rates (e.g. Figure 4.4a and b). In Figure 4.4d, as the increase of Ni amount, the total capacitance of Ni-Co hydroxides almost increased from 142 to 595 F g^{-1}, and the outer capacitance first increased from 77 to 145 and then 101 F g^{-1}. As contrast, the total capacitance of Ni-Co oxides first increased from ~25 to 51 F g^{-1} and then decreased to ~22 F g^{-1}. Their outer capacitance also increased from ~18 to 40 and then decrease to zero. It is well known that the double layer capacitance is proportional to the electrochemical surface area. It suggests that in Ni-Co hydroxides, the addition of Ni can increase the surface area of materials dramatically, whereas it is not obvious for Ni-Co oxides. From Figure 4.5, as Ni contents increased, the morphology factor of Ni-Co hydroxides first decreased from 0%

Ni to 15% Ni and then increased from 15% Ni to 100% Ni. The morphology factors of Ni-Co oxides first decrease and then increased with the smallest value at 46% Ni, indicating that the Ni-Co oxide with 46% Ni had the lowest porosity and the most compacted structure among these Ni-Co oxides. The Ni increase in spinel structure promoted the morphology factor decrease. When the Ni content was higher than 46%, the NiO cubic structure would lead to the morphology factor increase. When comparing the capacitance between Ni-Co hydroxides and Ni-Co oxides, it can be found that Ni-Co hydroxides had a higher capacitance than Ni-Co oxides though the Ni-Co hydroxides and their corresponding oxides had the similar morphology. The morphology factor of Ni-Co oxides was smaller

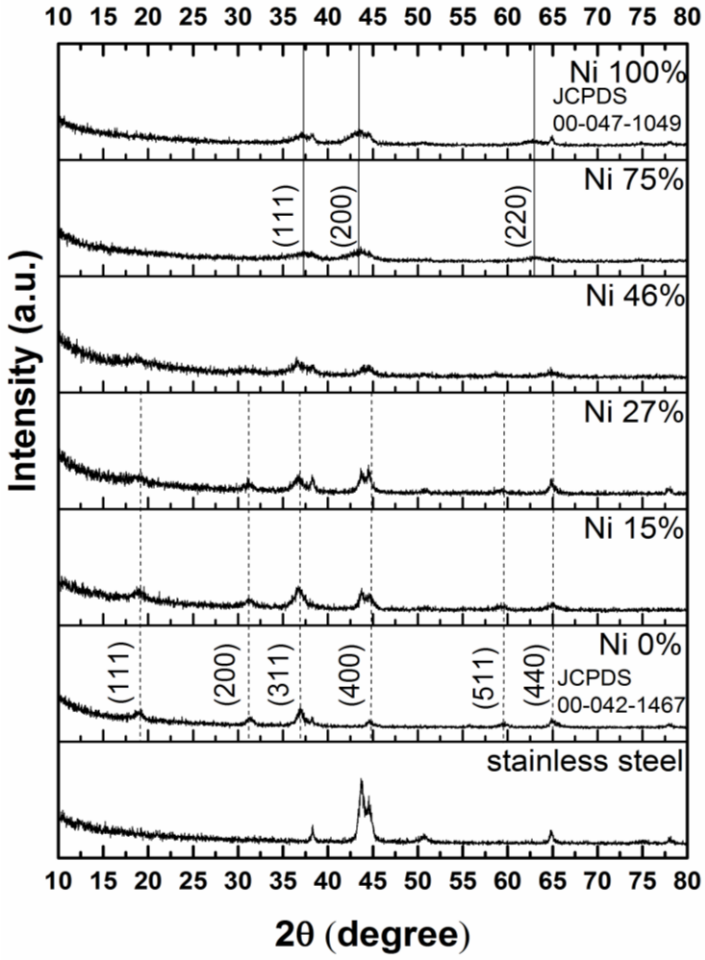

Figure 4.3 XRD patterns of stainless steel and Ni-Co oxides with different Ni contents.

than their corresponding Ni-Co hydroxides except for pure NiO and $Ni(OH)_2$, suggesting that structure of Ni-Co oxides were more compressed than their corresponding Ni-Co

hydroxides in spite of similar morphologies. All of these suggest that the morphology change cannot be used to estimate the change of electrochemical surface area.

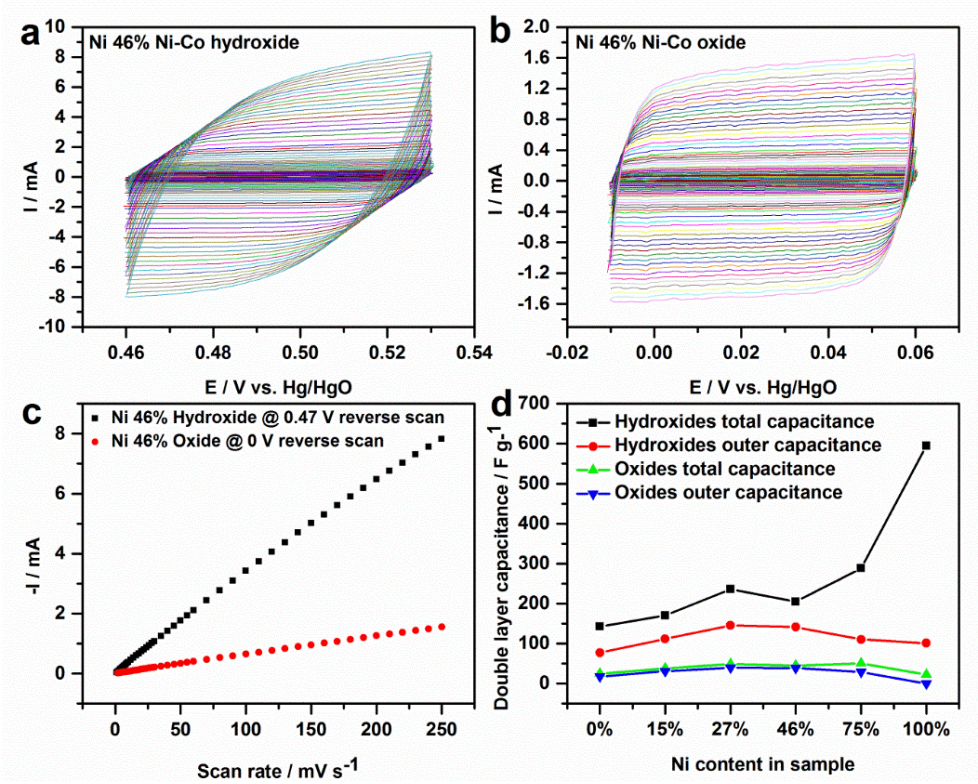

Figure 4.4 CV curves at different scan rates of (a) Ni-Co hydroxide (Ni 46%) and (b) Ni-Co oxides (Ni 46%) in 1.0M KOH in the double layer region; (c) the relationship between the currents and scan rates; (d) summary for double layer capacitance of Ni-Co hydroxides and oxides.

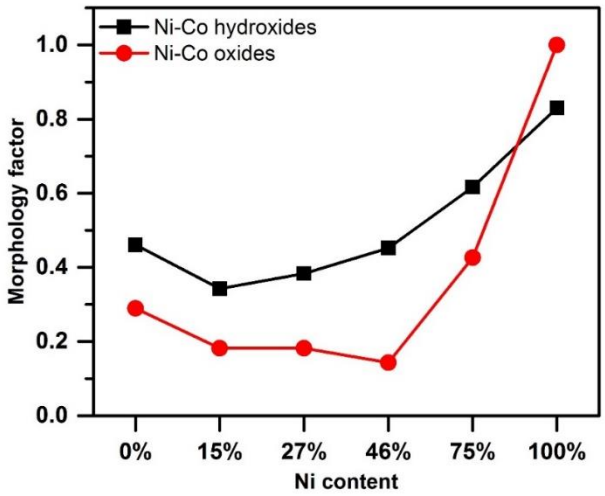

Figure 4.5 The morphology factor of Ni-Co hydroxides and Ni-Co oxides.

4.3.3 MOR CV

The Ni-Co hydroxide CV curves in 1.0 M KOH solution are shown in Figure 4.6a. As for $Co(OH)_2$, a pair of redox peaks $Co(OH)_2$/CoOOH can be observed at ~0.195 V and ~0.137.[17, 18] As for $Ni(OH)_2$, a pair of redox peaks $Ni(OH)_2$/NiOOH can be observed at ~0.530 V and ~0.376 V.[19, 20] As Ni contents increased, the oxidation peaks gradually moved to the high potential direction, which is consistent with the previous report.[21] Only a little change in the reduction peak location can be observed when the Ni content changed from 0% to 15%, to 27%, similar with that of $Co(OH)_2$. When the Ni content increased to 46%, there appeared a broader reduction peak. Note that only one oxidation peak and no individual $Co(OH)_2$ and $Ni(OH)_2$ oxidation peaks were observed in Ni-Co hydroxides, consistent with previous reports.[21] Figure 4.6c shows the CV curves of Ni-Co oxides. One oxidation peak at ~0.535 V can be observed on Co_3O_4. Different reports gave different attribution on the oxidation peak of Co_3O_4. Some researchers ascribed it to the Co^{3+} to Co^{4+} transition.[22-24] A pair of redox peaks assigned NiO/NiOOH transition can be observed at ~0.437 V and ~0.510 V. As oxygen evolution occurred on NiO, the oxidation peak at 0.510 V was not obvious. When Ni and Co coexisted in oxides, a broad oxidation peak can be observed.[8] Figure 4.6b and d show Ni-Co hydroxide and Ni-Co oxide CV curves in 1.0 M KOH + 0.5 M methanol solution, respectively. Obviously, the current had a dramatic increase at 0.60 V in the presence of methanol. Meanwhile, due to the reduction of Ni and Co with high valence state by methanol, the reduction peaks decreased.[25]

Figure 4.6e summarizes the relationship between the MOR current densities on Ni-Co hydroxides and Ni-Co oxides at 0.60 V. The background current was deducted to eliminate the current influence from capacitance and oxidation evolution, and thus the net current densities (methanol oxidation current density - background current density) were used to investigate the composition dependence of MOR activity. As Ni contents increased, MOR current densities increased on Ni-Co hydroxides. Small amount of nickel did not affect dramatically on the current density until the Ni content reached 27%. Compared with MOR on Ni-Co hydroxides, Ni-Co oxides (except for Co_3O_4 and NiO) exhibited a higher MOR current densities. With the increase of Ni contents, MOR current densities displayed a

volcano shape with the highest current density at Ni content 46%. Among Ni-Co oxides, Co_3O_4 exhibited the lowest MOR current density. NiO had a similar current density to Ni-Co oxide (Ni 27%). These suggest that Ni-Co oxides had a higher MOR activity than Co_3O_4 and NiO. Also, increasing Ni content in Ni-Co oxide spinel structure enhanced the MOR activity when Ni contents were lower than 46%. When Ni contents were higher than 46%, the Ni-Co oxides did not persist spinel structure and spinel and rocksalt mixed structure formed. Meanwhile, the MOR activity started to decrease. Another parameter, onset potential is also used to characterize MOR activity. Here, the potential at 10 A g^{-1} was chosen as the onset potential to compare MOR activity on different electrodes. The onset potentials of Ni-Co hydroxides and Ni-Co oxides were shown in Figure 4.6f. The MOR trend from onset potential trend was similar to that from current density. Obviously as the Ni content increased in Ni-Co hydroxides, the MOR onset potential gradually decreased from 0.536 V to 0.464 V. Small amounts of Ni did not change the MOR onset potential obviously. When the Ni content was higher than 27%, the onset potential started to have an obvious decrease. However, the MOR onset potential on Ni-Co oxides did not exhibit a decreasing tendency as Ni contents increased. It presents a quasi- inverted volcano-shaped tendency. When the Ni content was 27% or 75%, Ni-Co oxides had lower onset potential. When the Ni content was 46%, the onset potential was slightly higher than that of Ni 27% and Ni 75%. All MOR onset potentials on Ni-Co oxides were smaller than that on pure Co_3O_4 and NiO.

4.3.4 EIS

EIS was employed to deeply investigated Ni effect during MOR process on Ni-Co hydroxides and Ni-Co oxides. Nyquist plots of MOR on Ni-Co hydroxides with different Ni contents are shown in Figure 4.7a, d, g, j, m, and p. When Ni contents were not more than 27%, an obvious depressed semi-circle in the middle frequency region was observed. When Ni contents were more than 46%, another semi-circle in high frequency region appeared, especially at low bias potential, like 0.50 and 0.52 V. The semicircles became more obvious with the increase of Ni content. As bias potential increased, the semicircle diameters in high frequency region decreased and even disappeared. Investigations show

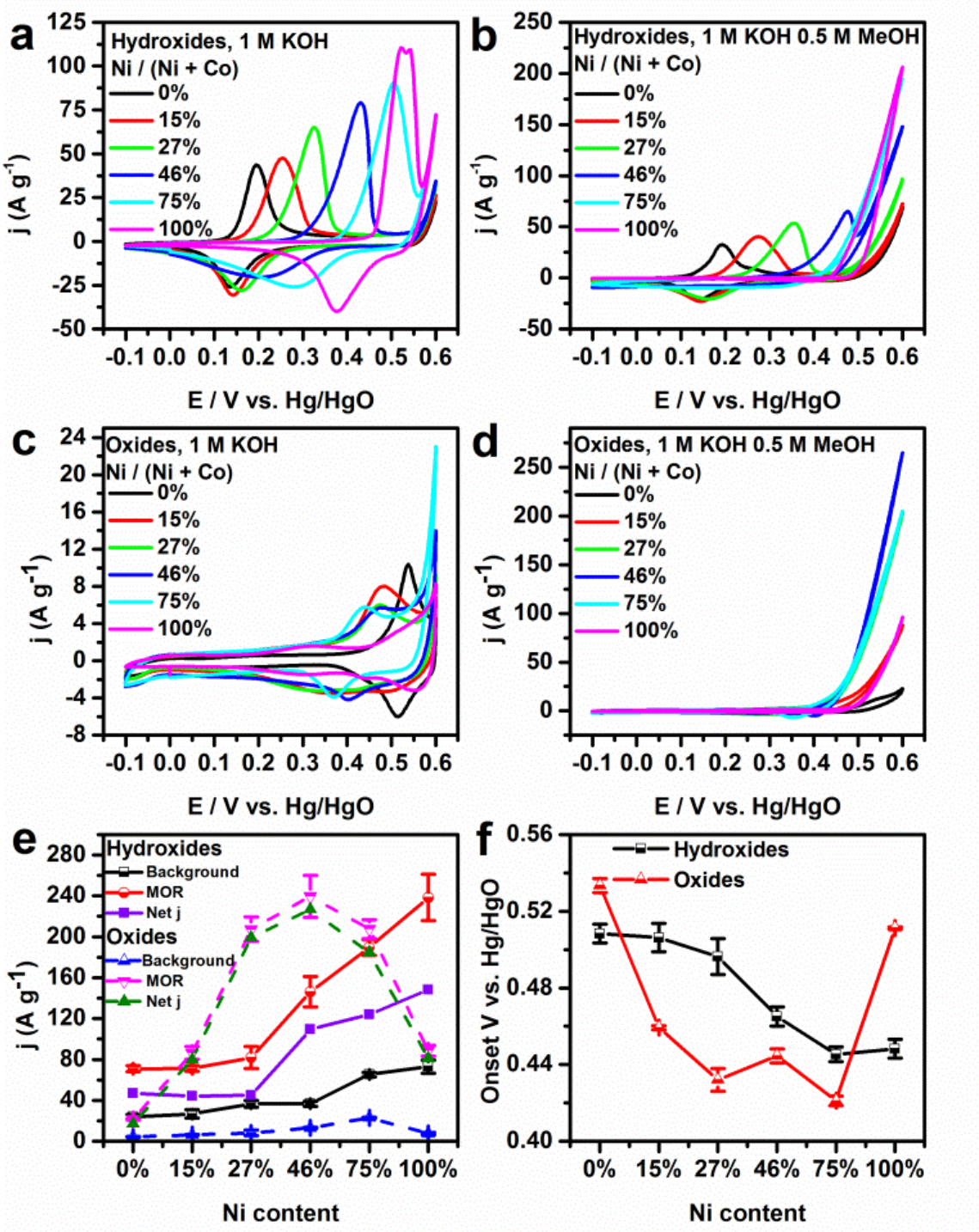

Figure 4.6 CV curves of (a) Ni-Co hydroxides and (c) Ni-Co oxides in 1.0 M KOH; CV curves of (b) Ni-Co hydroxides and (d) Ni-Co oxides in 1.0 M + 0.5 M methanol; (e) summary for the background, MOR and the net current densities; (f) summary for the MOR onset potentials.

that during methanol oxidation process the semicircles were ascribed to the combination

of charge transfer resistance and double layer capacitance and charge transfer resistance, along with the intermediate product adsorption represented by the combination of the adsorption resistance and adsorption capacitance (R_{ads}).When the semicircle appeared in the fourth quadrant, it could be related to inductor.[25] Besides, the semicircle in high frequency region is also related to the combination of resistance and capacitance of electrodes.[26] Here, the attribution of these semicircles can be determined by Bode-Phase plot. When the Ni content was less than 46% shown in Figure 4.7b, e and h, there was only one obvious peak observed in the middle frequency region when bias potential increased. This peak corresponded to the one depressed semicircles. The peak in the middle frequency region still existed when the Ni content was more than 46%. These peaks in the middle frequency region in Bode phase plot were equivalent with the ramp in Bode-Z plot. These peaks would decrease and shift to high frequency with the bias potential increase. When the Ni content was higher than 27%, there was a new peak in the high frequency region. As the Ni content increased, the new peak became significant. As the bias potential increased, the new peak decreased and gradually disappeared. In the high frequency region, the peak change in Bode-Phase plot showed the similar trend with the semicircle change in Nyquist plots in the high frequency region. Our results show that the semicircle in the high frequency region originated from the intermediate product adsorption and the semicircle in the middle and low frequency regions originated from the combination of double layer capacitance and charge transfer resistance. The reason is as follow. First, when the Ni content was lower than 46%, there was one major semicircle in Nyquist plot and one peak in Bode-Phase plot. Obviously, it is due to the combination of double layer capacitance and charge transfer resistance. When the Ni content was equal to or more than 46%, the peaks in the middle frequency in Bode-Phase plot still existed and a new peak appeared. Whereas, it is noticed that with the increase of bias potential, this peak in the middle frequency region disappeared. If this peak was attributed to the combination of double layer capacitance and charge transfer resistance, it should be independent on the bias potential. The gradual disappearance of this peak at high bias potentials suggests that there was no the combination of charge transfer resistance and double layer capacitance. With the increase of bias potential, the semicircles in the high frequency region in Nyquist plots gradually disappeared. A higher potential promoted the oxidation of the adsorbed

intermediate products, and the resistance and capacitance from intermediate products adsorbed on the electrode surface would drop and eventually disappear. This adsorption effect increased when Ni contents increased. From the Bode-Z plot in Figure 4.7c, f, i, l, o and r, this phenomenon can be also observed. The value of lg(|Z|) would start to ramp when the lg(f) decreased to some certain frequency. When Ni contents were low, the straight line in the middle frequency region could be related to the contribution from the combination of double layer capacitance and charge transfer resistance. Nevertheless, with the increase of Ni content, this ramp started from higher frequency and deviated from a straight line. Two ramps can be found in different frequency regions (Figure 4.7o and r). With the increase of bias potential, this deviation gradually disappeared. Hence, this ramp in the high frequency region could also attributed to another interaction from resistance and capacitance, i.e. the combination of the intermediate product capacitance and adsorption resistance. As for Ni-Co oxides, EIS results of MOR are shown in Figure 4.8. The trend was similar to that on Ni-Co hydroxides. The difference lay in that the adsorption phenomenon was not obvious until Ni contents reached 75%. Back to the crystal structure, when the Ni content reached 75%, the crystal structure of Ni-Co oxide was composed of cubic spinel structure and cubic rock salt structure. NiO with rock salt structure might enhance the adsorption of intermediate products. However, such enhanced adsorption probably could not eventually lead to the enhanced MOR activity due to the higher onset potential (Figure 4.6f) and higher MOR R_{ct} on NiO.Two types of equivalent circuits were commonly used to analyze EIS data. As shown in Figure 4.9, R_s, R_{ct}, and R_{ads} represent the solution resistance, charge transfer resistance, and adsorption resistance of intermediate products, respectively. Constant phase elements, CPE1 and CPE2 are related to the capacitance from double layer and intermediate product adsorption, respectively. The principle of simulation is based on the equivalent circuit shown in Figure 4.9a. If the deviation is big, the equivalent circuit shown in Figure 4.9b is employed. The detailed information on EIS fitting was shown in Table A.1-12 in Appendix.

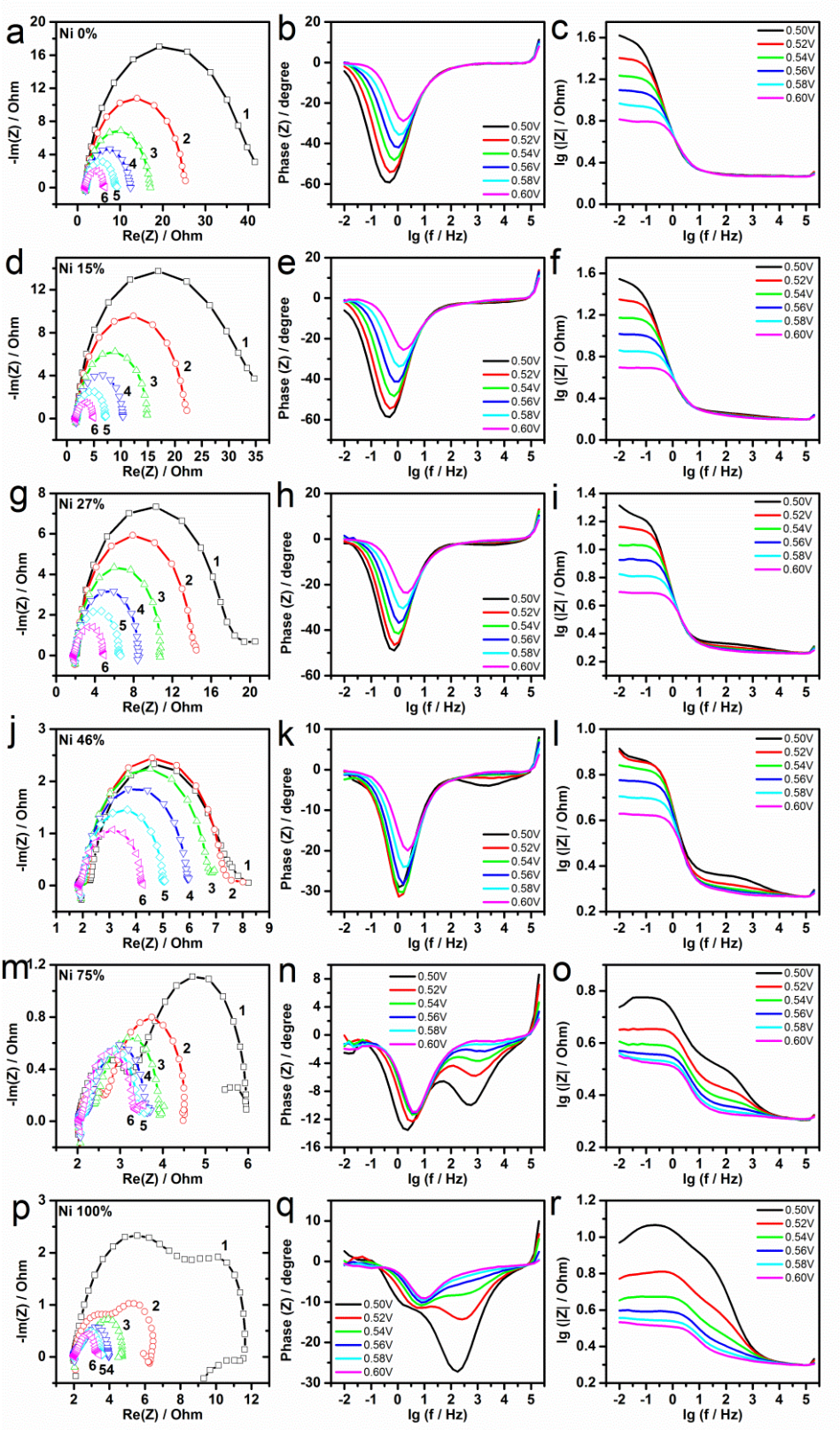

Figure 4.7 EIS results of methanol oxidation on Ni-Co hydroxides with various Ni contents: 0% (a-c), 15% (d-f), 27% (g-i), 46% (j-l), 75% (m-o) and 100% (p-r).

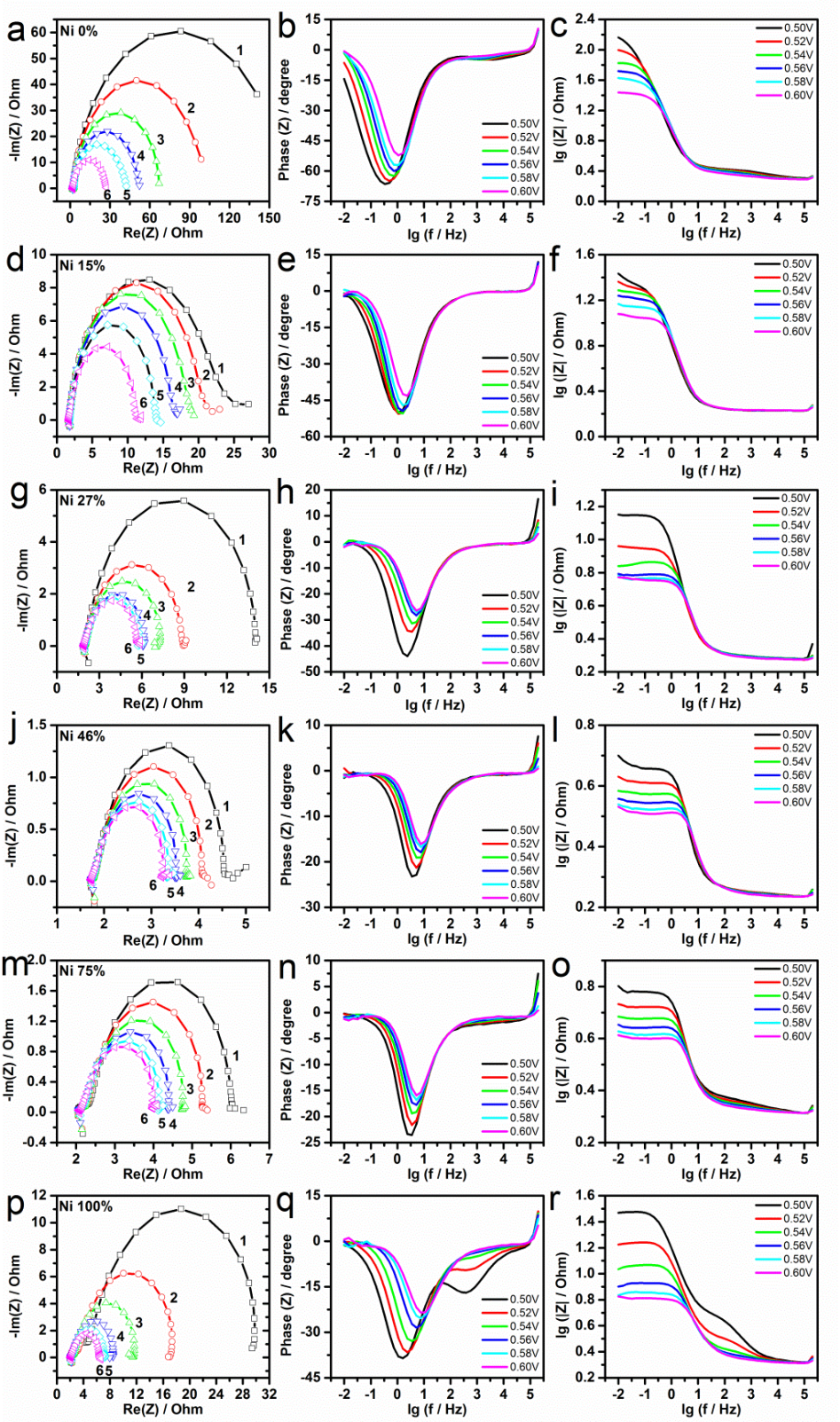

Figure 4.8 EIS results of methanol oxidation on Ni-Co oxides with various Ni contents: 0% (a-c), 15% (d-f), 27% (g-i), 46% (j-l), 75% (m-o) and 100% (p-r).

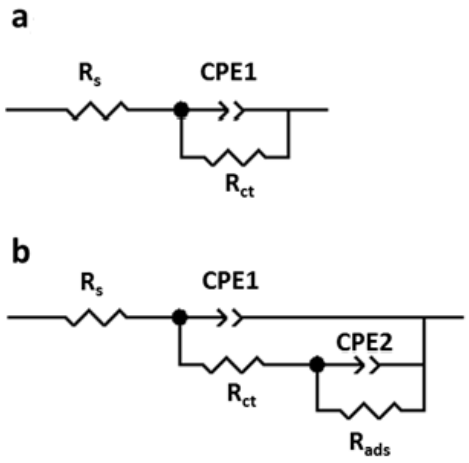

Figure 4.9 Equivalent circuits for simulating MOR on Ni-Co hydroxides and Ni-Co oxides.

Besides, for Ni-Co oxides, the change of crystal structure would also affect the catalytic activity. There are two factors. One is from the active site. When Ni content was less than 46%, it is obvious that the activity increased with the increase of Ni content. At this range, the crystal structure is spinel. Thus, it suggests that in $Ni_xCo_{3-x}O_4$ spinel structure, Ni is the active sites. When nickel amount was higher than 46%, NiO formed. Compared with Ni-Co oxides except Co_3O_4, NiO has a lower activity for methanol oxidation. It is a direct evidence that more NiO lowered methanol oxidation activity. The other factor is the conductivity of materials. Based literature review[27], it is clear that with the increase of Ni in $Ni_xCo_{3-x}O_4$ spinel structure, the conductivity increases, whereas NiO is an insulator. Since the catalyst in this thesis is a kind of carbon-free catalyst and belongs to self-support catalyst, the electron will go through the catalyst to the anode collector. Thus, a good conductivity will become an important factor of a good catalyst. Compared with Ni-Co oxides with spinel structure, Co_3O_4 and NiO have a poor conductivity, which lowers the utilization degree of catalysts in the electrocatalytic process, especially for the regions far away from the current collector.[27] In addition to electrode conductivity, the morphology change is also a crucial factor to affect the catalytic activity, because the electrochemical process is mainly limited to the surface. Porous electrodes with large accessible surfaces are highly desirable. The morphology of catalysts changed from sheet to plate with the increase of Ni amount. The accessible surfaces of electrode can be compared by using their corresponding double layer capacitance. From Figure 4.4d, as the Ni amount increase, the double layer capacitance of Ni-Co hydroxides changed from 142, 170, 236, 205, 288, to

595 F g^{-1}. It almost exhibits an increasing capacitance with the increase of Ni amount. Thus, it can be assumed that Ni doping increases the active sites in Ni-Co hydroxides, which result in an enhanced activity. For Ni-Co oxides, the capacitance first increased and then decreased from 25, 38, 49, 45, 51, to 22 F g^{-1} with the increase of Ni amount. When the oxidation currents were corrected by double layer capacitance, the activity of Ni-Co hydroxides was very low compared with that of Ni-Co oxides, which also exhibited a volcano-shaped trend (Figure 4.10). Thus, as Ni amount increased, the activity enhancement on Ni-Co hydroxides can be assumed due to the increase of active sites, whereas the contribution from the increase of active sites to the volcano can be excluded.

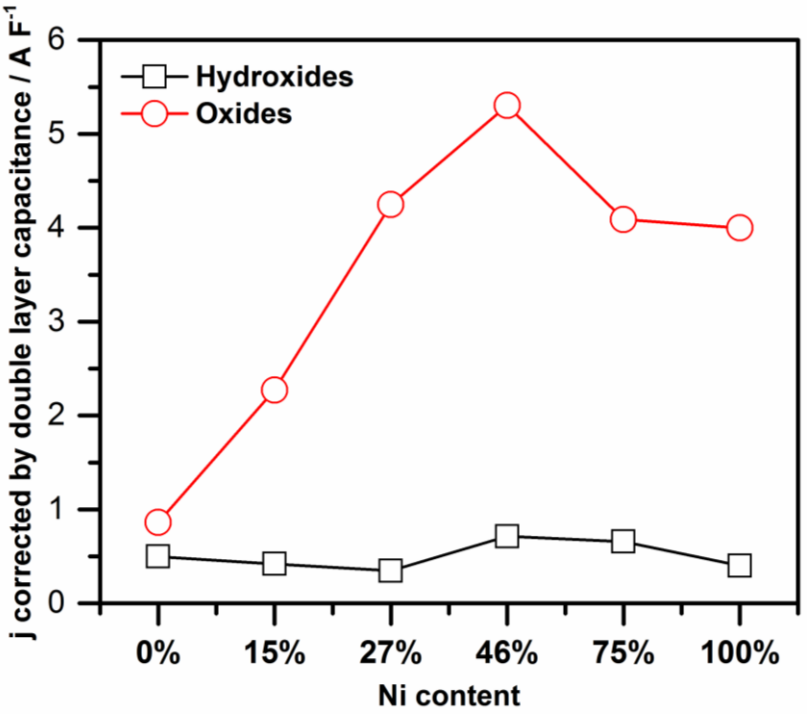

Figure 4.10 The relationship between double layer capacitance corrected current and Ni content.

4.3.5 CA Results

To further investigate the MOR activity on Ni-Co hydroxides and Ni-Co oxides, the polarization current density from EIS measurements were also compared (Figure 4.11). Figure 4.11a-d show the j-t curves of MOR on Ni-Co hydroxides and oxides at 0.56 V and 0.60 V. At each bias potential EIS test, the first 120 seconds was used to make MOR current

density stable and then the bias potential + 10 mV × sinωt was applied to the electrode. All j-t curves were stable except for NiO. MOR current density on NiO showed a slight increase with time. The relationship between current density and Ni content was shown in Figure 4.10c and d. The current density values were collected at 120th second during

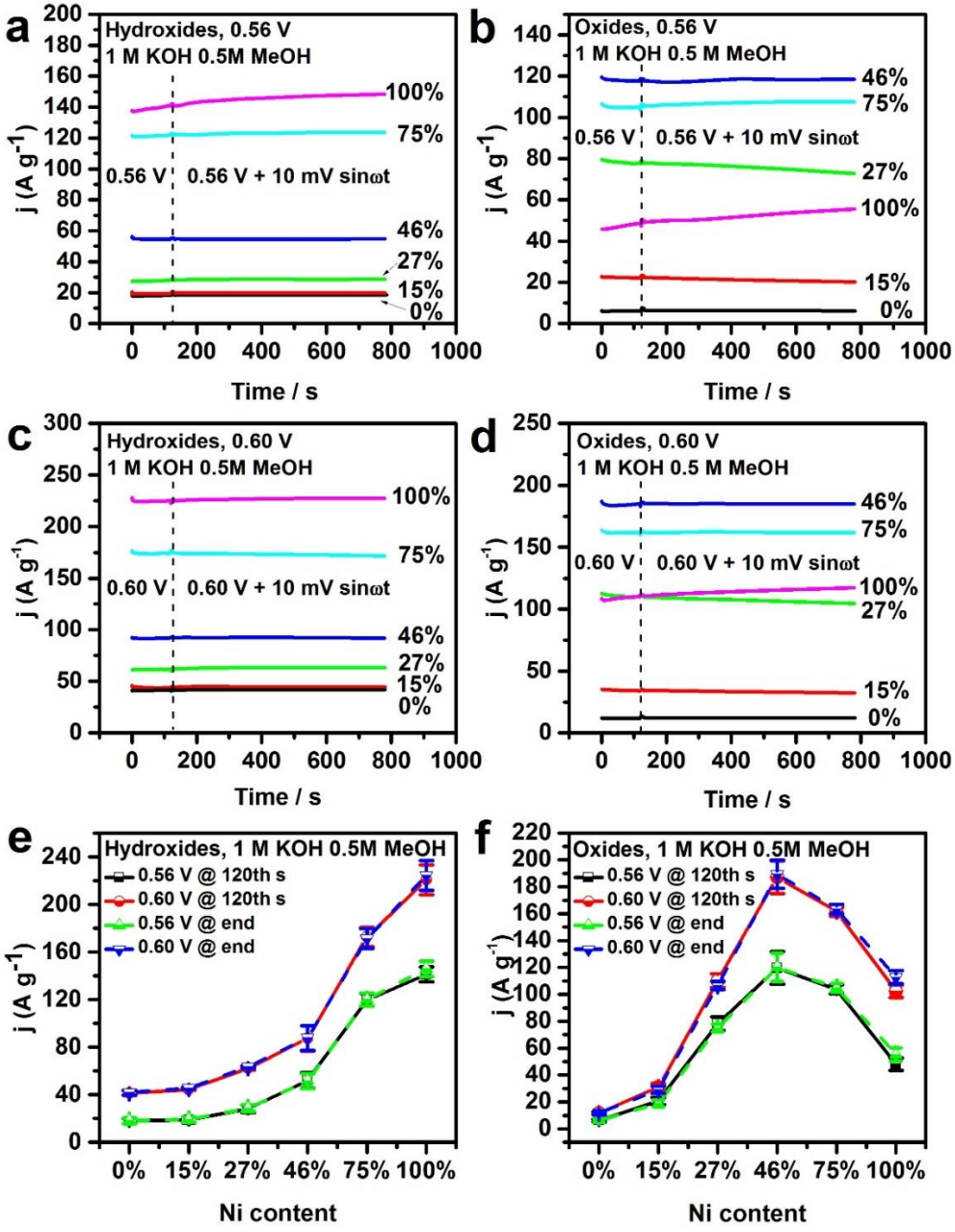

Figure 4.11 The MOR j-t curves on Ni-Co hydroxides (a) and Ni-Co oxides (b) from EIS at 0.56 V; the MOR j-t curves on Ni-Co hydroxides (c) and Ni-Co oxides (d) from EIS at 0.60 V; summary of current densities on Ni-Co hydroxides (e) and Ni-Co oxides (f) with various Ni contents at the 120th second (solid lines) and 780th second (dash lines).

polarization and the last second during the EIS test at 0.56 and 0.60 V, respectively. With the increase of Ni content, MOR current densities on Ni-Co hydroxides exhibited an increasing trend. The current densities of MOR on Ni-Co oxides manifested a volcano-shaped trend and the best activity appeared at Ni 46%. The current densities were almost the same at the 120th second and at the end of EIS test. The trends of MOR on Ni-Co hydroxides and oxides from polarization are similar to the results from CV tests.

4.4 Conclusions

In this chapter, Ni-Co hydroxides and Ni-Co oxides with different Ni contents were prepared on stainless steel meshes by electrodeposition for MOR. Ni-Co oxides showed spinel structure when Ni contents were not higher than 46%. Further increasing the Ni content resulted in the formation of NiO with a rock salt structure. The increase of Ni contents in Ni-Co hydroxides and Ni-Co oxides enhanced the adsorption of intermediates in MOR. The MOR activity on Ni-Co hydroxides showed an increasing tendency with the increase of the Ni content. The MOR activity on Ni-Co oxides displayed a volcano shape with a highest activity point at the atomic ratio of Ni / (Ni + Co) = 46%.

References:

[1] J. M. Ogden, M. M. Steinbugler and T. G. Kreutz. *Journal of Power Sources*. **1999**, 79, 143–168.

[2] D. K. Ross. *Vacuum*. **2006**, 80, 1084-1089.

[3] A. B. Stambouli and E. Traversa. *Renewable and Sustainable Energy Reviews*. **2002**, 6, 433-455.

[4] T. Iwasita. *Electrochimica Acta*. **2002**, 47, 3663-3674.

[5] E. Antolini, J. R. C. Salgado and E. R. Gonzalez. *Applied Catalysis B: Environmental*. **2006**, 63, 137-149.

[6] H. Liu, C. Song, L. Zhang, J. Zhang, H. Wang and D. P. Wilkinson. *Journal of Power Sources*. **2006**, 155, 95-110.

[7] S. Wasmus and A. Kuver. *Journal of Electroanalytical Chemistry*. **1999**, 461, 14-31.

[8] L. Qian, L. Gu, L. Yang, H. Yuan and D. Xiao. *Nanoscale*. **2013**, 5, 7388-7396.

[9] P. K. Shen, C. Xu, R. Zeng and Y. Liu. *Electrochemical and Solid-State Letters*. **2006**, 9, A39-A42.

[10] J. Taraszewska and G. Roslonek. *Journal of Electroanalytical Chemistry*. **1994**, 364, 209-213.

[11] M.-W. Xu, G.-Y. Gao, W.-J. Zhou, K.-F. Zhang and H.-L. Li. *Journal of Power Sources*. **2008**, 175, 217-220.

[12] G.-Y. Zhao and H.-L. Li. *Applied Surface Science*. **2008**, 254, 3232-3235.

[13] Y.-M. Wang, Xu. Zhang, C.-Y. Guo, Y.-Q. Zhao and H.-L. Li. *Journal of Materials Chemistry A*. **2013,** 1, 13290-13330.

[14] J.-W. Lang, L.-B. Kong, M. Liu, Y.-C. Luo and L. Kang. *Journal of The Electrochemical Society*. **2010,** 157, A1341-A1346.

[15] W. J. King and A. C. C. Tseung, *Electrochemica Acta*. **1974,** 19, 485-491.

[16] C.-C. Hu, Y.-S. Lee and T.-C. Wen, *Materials Chemistry and Physics,* **1997,** 48, 246-254.

[17] V. Gupta, T. Kusahara, H. Toyama, S. Gupta and N. Miura. *Electrochemistry Communications*. **2007**, 9, 2315-2319.

[18] V. Gupta, S. Gupta and N. Miura. *Journal of Power Sources*. **2008**, 175, 680-685.

[19] M. Gao, W. Sheng, Z. Zhuang, Q. Fang, S. Gu, J. Jiang and Y. Yan. *Journal of the American Chemical Society*. **2014**, 136, 7077-7084.

[20] A. A. El-Shafei. *Journal of Electroanalytical Chemistry*. **1999**, 471, 89-95.

[21] M. Vidotti, M. R. Silva, R. P. Salvador, S. I. C. d. Torresi and L. H. Dall'Antonia. *Electrochimica Acta*. **2008**, 53, 4030-4034.

[22] Z. Zhuang, W. Sheng and Y. Yan. *Advanced materials*. **2014**, 26, 3950-3955.

[23] Y. Wang, T. Zhou, K. Jiang, P. Da, Z. Peng, J. Tang, B. Kong, W.-B. Cai, Z. Yang and G. Zheng. *Advanced Energy Materials*. **2014**, 4, 1400696-1400702.

[24] Y. Cao, F. Yuan, M. Yao, J. H. Bang and J.-H. Lee. *CrystEngComm*. **2014**, 16, 826-833.

[25] I. Danaee, M. Jafarian, F. Forouzandeh, F. Gobal and M. Mahjani. *International Journal of Hydrogen Energy*. **2009**, 34, 859-869.

[26] M. E. G. Lyons and M. P. Brandon. *Journal of Electroanalytical Chemistry*. **2010**, 641, 119-130.

[27] Y. Li, P. Hasin, Y, Wu. *Advanced Materials.* **2010,** 22, 1926-1929.

Chapter 5*

Ethylene Glycol and Ethanol Oxidation Reaction on Ni-Co Oxides

This chapter discusses ethanol (EtOH) and ethylene glycol (EG) oxidation on Ni-Co oxides with various Ni contents. It is found that the best oxidation rate of ethanol and ethylene glycol happened on Ni-Co oxide with 46% Ni. This is similar to what has been found in methanol oxidation. The relationship between oxidation currents and C2 alcohols' concentration has been analyzed and revealed. The EtOH and EG oxidation products were analyzed by NMR, indicating that the oxidation process was a functional group conversion from hydroxyl group to carboxyl group.

* This chapter published substantially as Sun et al., Ethylene Glycol and Ethanol Oxidation on Spinel Ni-Co Oxides in Alkaline, *Journal of The Electrochemical Society*, **2016**, 163 (2) H99-H104.

5.1 Introduction

Based on the result on methanol oxidation on Ni-Co oxides, methanol oxidation reaction activity on Ni-Co oxides exhibited a volcano-shaped trend as Ni contents increases. The best Ni content was 46% for methanol oxidation. This conclusion intrigues us to investigate that whether this trend can be applied to other alcohols. Thus, the electro-oxidation of C2 alcohols (ethylene glycol and ethanol) was discussed in this chapter. Based on the previous reports, formate was the major methanol oxidation product on non-noble metal oxides. It indicates that the hydroxyl group was converted to carboxyl group, suggesting that when only hydroxyl group was oxidized, it is the only source to contribute the oxidation current. Comparing the molecular structure of ethanol and ethylene glycol, both ethanol and ethylene glycol have two carbon atoms in one molecule, and ethylene glycol has one more hydroxyl group than ethanol. When ethanol and ethylene glycol are the same concentration, whether the oxidation current of ethylene glycol is twice than that of ethanol needs to be investigated. In methanol oxidation reaction section, the Ni effect has been determined to facilitate the adsorption and oxidation of intermediate products, and during ethanol and ethylene glycol oxidation process, it is also necessary to investigate the Ni effect by using EIS spectra.

5.2 Experimental Methods

5.2.1 Electrode Preparation

The Ni-Co oxides were prepared by electrodepositing Ni-Co hydroxides on stainless steel meshes followed by annealing in air. The stainless steel meshes (500 mesh, 1.0 × 1.0 cm, SSM) were chosen as substrates. The electrolyte was the same with the electrolyte mentioned in Chapter 4. The electrodeposition potential was fixed at -0.85 V vs. SCE. The passing charge was controlled at 0.6 C.

5.2.2 CV for EG and EtOH Oxidation

The three-electrode system was employed to characterize NCOs/SSM, with Hg/HgO (1.0 M KOH, aqueous) electrode and Pt plate (~ 1.0 cm × 3.0 cm) as reference and counter electrodes. CV, DPV, and EIS were employed to investigate the EG and EtOH oxidation on NCOs. The CV tests were carried out from −0.1 ~ 0.6 V at the scan rates from 80, 40, 20, 10, 5, to 2 mV s^{-1} in the absence and presence of EG and EtOH, respectively. The DPV tests were conducted at 10 mV s^{-1} and with a 2.5 mV of pulse height. EIS tests were done at bias potentials from 0.48, 0.51, 0.54, 0.57 to 0.60 V consecutively at 10 mV amplitude. The frequency applied from 1 MHz to 10 mHz and the data were collected and analyzed from 100 kHz to 10 mHz.

5.2.3 EIS for EG and EtOH oxidation

EIS measurements were taken at bias potentials of 0.48, 0.51, 0.54, 0.57, and 0.60 V consecutively with 10 mV amplitude. The frequency ranged from 1 MHz to 10 mHz and the data were collected and processed from 100 kHz to 10 mHz.

5.2.4 DPV for EG and EtOH oxidation on NCO-46

The DPV was carried on based on the anodic sweep at 10 mV s^{-1} and with the pulse height 2.5 mV in 1.0 M KOH with different concentrations of alcohols.

5.2.5 CA for EG and EtOH oxidation on NCO-46

The multi-step CA was conducted on NCO-46 in 1.0 M KOH + 0.5 M alcohols according to the following procedure. First, the working electrode was held at 0 V for 2 min. Then, it was held for 10 min at 0.48, 0.51, 0.54, 0.57, 0.60, 0.57, 0.54, 0.51, and 0.48 V, respectively.

5.2.6 NMR

Bruker Advance 300 (300 MHz) NMR spectrometer was used to test the EG and EtOH oxidation product after long time electrolysis.

5.3 The Principle Outcomes

5.3.1 Materials

Figure 5.1a shows the relationship of atomic Ni / (Ni + Co) between in NCOs and in the precursor solutions. In this chapter, the Ni-Co oxides with 0% Ni, 15% Ni, 27% Ni, 46% Ni, 75% Ni, and 100% Ni are named NCO-0, NCO-15, NCO-27, NCO-46, NCO-75, and NCO-100, respectively. As the Ni contents increased, the mass loading of NCOs decreased (Figure 5.1b). As for preparing pure NiO, the passing charge was fixed at 0.8 C to maintain the similar mass loading to other Ni-Co oxides. The error bars in Figure 5.1 were based on three independent experiments. It can be noticed that the change of Ni ratio in NCOs and the NCO mass loading was small, which indicated that these electrodes have high reproducibility.

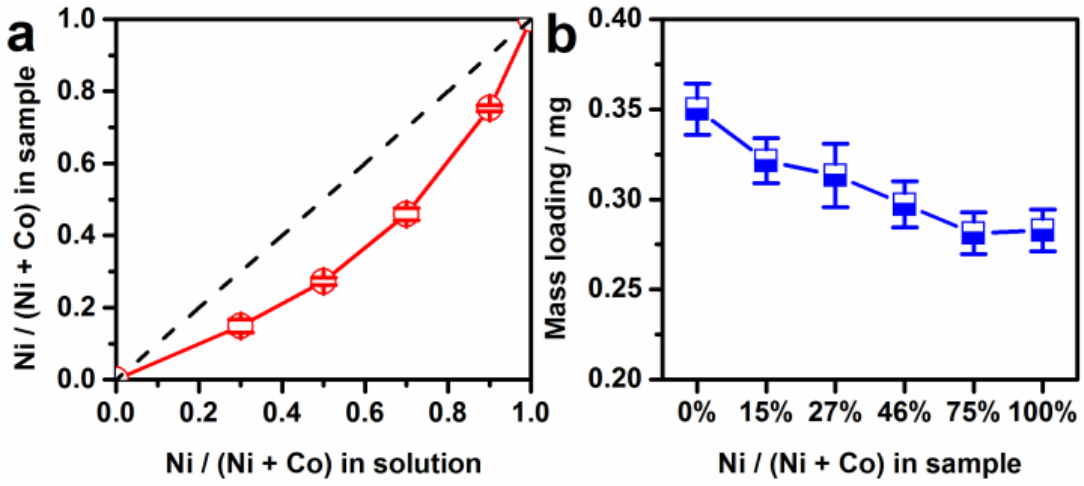

Figure 5.1 (a) The relationship of Ni content between in solution and in sample; (b) the mass loadings of Ni-Co oxides on stainless steel meshes.

5.3.2 CV for EG and EtOH Oxidation

Figure 5.2a shows the CV curves of Ni-Co oxides in 1.0 M KOH solution. These Ni-Co oxide CV curves have been discussed in Chapter 4. The CV curves of electro-oxidation of EG and EtOH are shown in Figure 5.2b and c, respectively. The concentration of EG and EtOH was kept at 0.5 M. Figure 5.2d displays the currents at 0.6 V from CV curves of EG and EtOH oxidation. Obviously, with the increase of Ni contents, EG and EtOH oxidation currents firstly increased and then decreased. NCO-46 gave the highest oxidation activity. This trend is consistent with what we have observed in methanol oxidation in Chapter 4.

In Figure 5.2, the oxidation currents from CV curves were obtained at 10 mV s^{-1}. During oxidation process, EG and EtOH near the electrode surfaces were consumed, and meanwhile EG and EtOH in bulk diffused to the surface of the electrodes. The concentration of EG and EtOH were influenced by the oxidation rates and diffusion rates. The Ni-Co oxides with various Ni contents exhibit different oxidation rates. The high oxidation rate corresponds to fast alcohol consumption, and the low oxidation rate corresponds to low alcohol consumption. At different scan rates, the duration is not the same in the oxidation region, resulting in the different consumptions near the electrode surface.

Thus, it is necessary to investigate whether the oxidation currents from CV curves depend on scan rates. Since NCO-46 has a best oxidation activity for EG and EtOH, the oxidation current-scan rate relationship was investigated on NCO-46. The scan rates changed from 80, 40, 20, 10, 5 to 2 mV s^{-1}. The CV curves of EG and EtOH oxidation at different scan rates were shown in Figure 5.3.

In Figure 5.3, it is noticed that in the capacitance region from -0.10 to 0.35 V, the current increased with the increase of scan rates, which is consistent with basic knowledge of CV test.[1-3] In the EG and EtOH electro-oxidation region from 0.40 ~ 0.60 V, as for EG, the oxidation current at the high scan rate was a little higher than that at the low scan rate, while as for EtOH, the oxidation currents were almost the same at different scan rates.

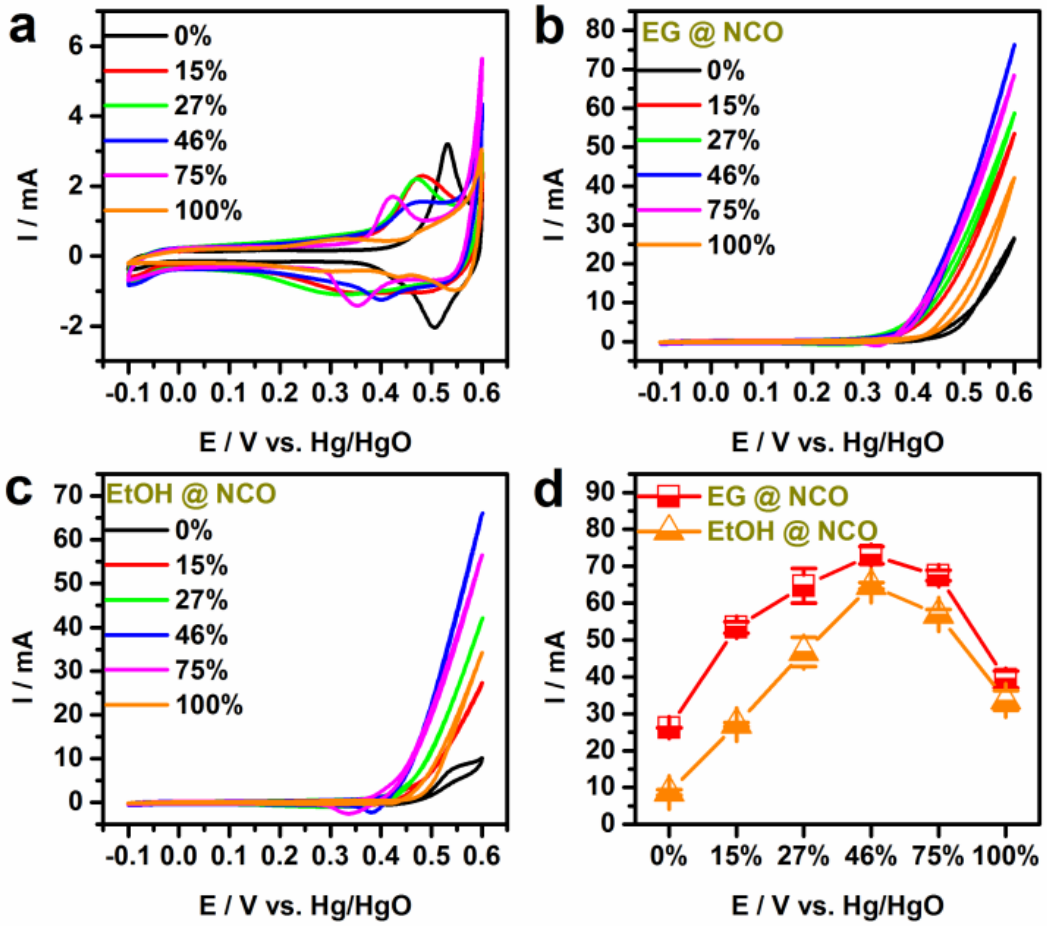

Figure 5.2 (a) NCO CV curves in 1.0 M KOH solution; NCO CV curves in 1.0 M KOH + 0.5 M EG (b) or 0.5 M EtOH (c); (d) summary for currents at 0.60 V against the Ni content.

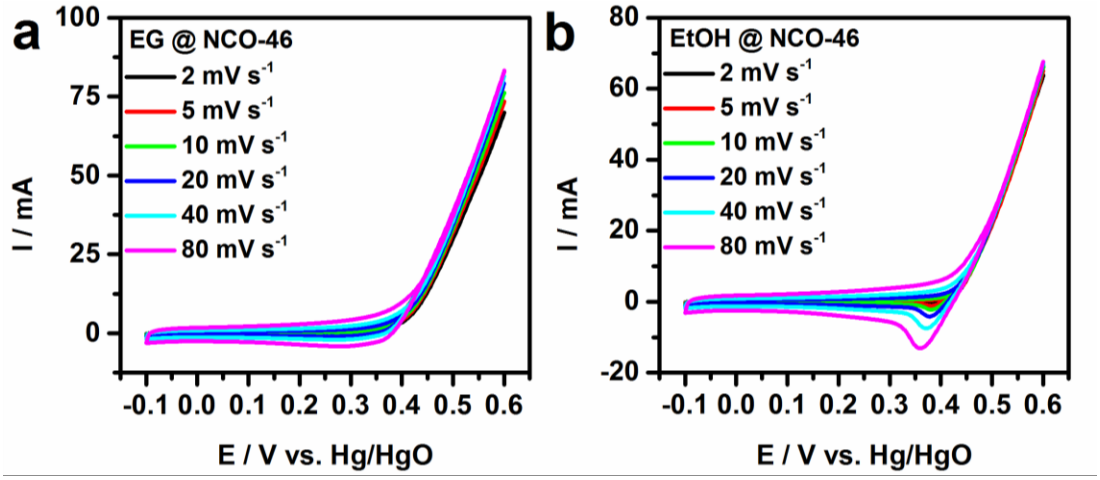

Figure 5.3 CV curves of (a) EG and (b) EtOH oxidation on NCO-46 at different scan rates in 1.0 M KOH solution.

It suggests that EtOH oxidation currents were independent on scan rates when the potential higher than some certain value (~0.50 V in Figure 5.3b). The reason that EG oxidation current decreased with the decrease of scan rate may be the slow diffusion of EG and the oxidation products or the adsorption of intermediate products. Though the EG oxidation changed when the scan rate changed, the change range was still small. It indicates that when using the current at 0.6 V of CV test at 10 mV s^{-1} is appropriate to estimate and compare the oxidation activity for and EG and EtOH.

5.3.3 EIS for EG and EtOH Oxidation

EIS tests were employed to further investigate EG and EtOH oxidation on NCOs. Figure 5.4 shows the Nyquist plots and Bode plots of EG oxidation on NCOs. There are some data points below zero in EG oxidation Nyquist plots on NCO-15 (Figure 5.4d), NCO-27 (Figure 5.4g), and NCO-46(Figure 5.4j), which are often attributed to the inductive behavior. Such inductive behavior is related to the adsorption, regeneration, and readsorption of intermediate products on active sites.[4-6] No obvious data points below zero were observed in the Nyquist plot of EG oxidation on Co_3O_4 (Figure 5.4a). Perhaps It is owing to the oxidation product adsorption and no new active site re-generated. For EG oxidation on NCO-75, below zero almost no data points can be found in the Nyquist plot (Figure 5.4m). It suggests that the charge transfer and intermediate product adsorption were more key steps than the adsorption and regeneration of active sites. The EG oxidation on NiO shows two depressed semicircles in the Nyquist plot (Figure 5.4p). With the increase of bias potential, these two semicircles' diameters became smaller. It can be assumed that these two depressed semicircles indicated two step reactions. In the low frequency region, the depressed semicircles can be attributed to the oxidation from EG to intermediate products along with adsorption. In the high frequency region, the depressed semicircles corresponded to the process from intermediate products to final products. In Figure 5.4p, with the increase of potential, the depressed semicircles' diameters decreased, indicative of that the oxidation rate of EG intermediate products absorbed on NiO can be promoted by high potential. It is observable that as Ni contents were higher than 46%, the data points below zero as representative of adsorption and regeneration of active sites could not be

found (Figure 5.4m and p) and data points in the low frequency region as representative of the adsorption of intermediate products became distinct (Figure 5.4p). Combining with CV results (Figure 5.2d), the composition dependence of NCOs for EG oxidation can be suggested. As Ni contents gradually increased to 46%, EG oxidation activities increased. It suggested that the higher Ni content can promote the overall oxidation reaction through facilitating the processes from EG to the intermediate products and from intermediate products to final products. Whereas, probably the promotion rate from intermediate products to final products was not dramatic in comparison with that from EG to intermediate products, resulting in the accumulation of excessive intermediate products. Thus, the regeneration of active sites became unobvious. Only at Ni 46%, the rates of two reaction processes were balanced, thus leading to the highest activity.

Figure 5.5 exhibits the EIS results of EtOH oxidation on NCOs. An obvious intermediate product adsorption of EtOH oxidation can be observed on NCO-0 (Figure 5.5a), NCO-15 (Figure 5.5d), and NCO-27 (Figure 5.5g). For EtOH oxidation on NCO-0 (Co_3O_4), the strong adsorption resulted in the gradual diameter increase of the depressed semicircles at 0.51, 0.54, and 0.57 V in Figure 5.5a, which was probably due to that the increase of potential led to more adsorbed intermediate products from EtOH oxidation to block the reaction. At 0.60 V, the smaller diameter of depressed semicircle indicated that EtOH was further oxidized (Figure 5-5a). In Figure 5.5d and g, although the potential increased from 0.51 to 0.57 V, only a little change can be observed in the diameter, indicative of almost no change in impedance. It further suggests that the intermediate product adsorption hindered the decrease of resistance.

The relationship between impedance Z and bias potential was summarized for EG and EtOH oxidation on NCOs (Figure 5.6). With the increase of bias potential, all the EG and EtOH oxidation impedance on NCOs became smaller except for EtOH oxidation on Co_3O_4. Generally, the impedance decrease is due to the promoted oxidation reaction caused by the bias potential increase. In Figure 5.6b, Co_3O_4 did not exhibit this trend for EtOH oxidation. At the potential from 0.48 to 0.51 V, the impedance decreased; at the potential from 0.51 to 0.57 V, the impedance increased; at the potential range 0.57 to 0.60 V, the impedance

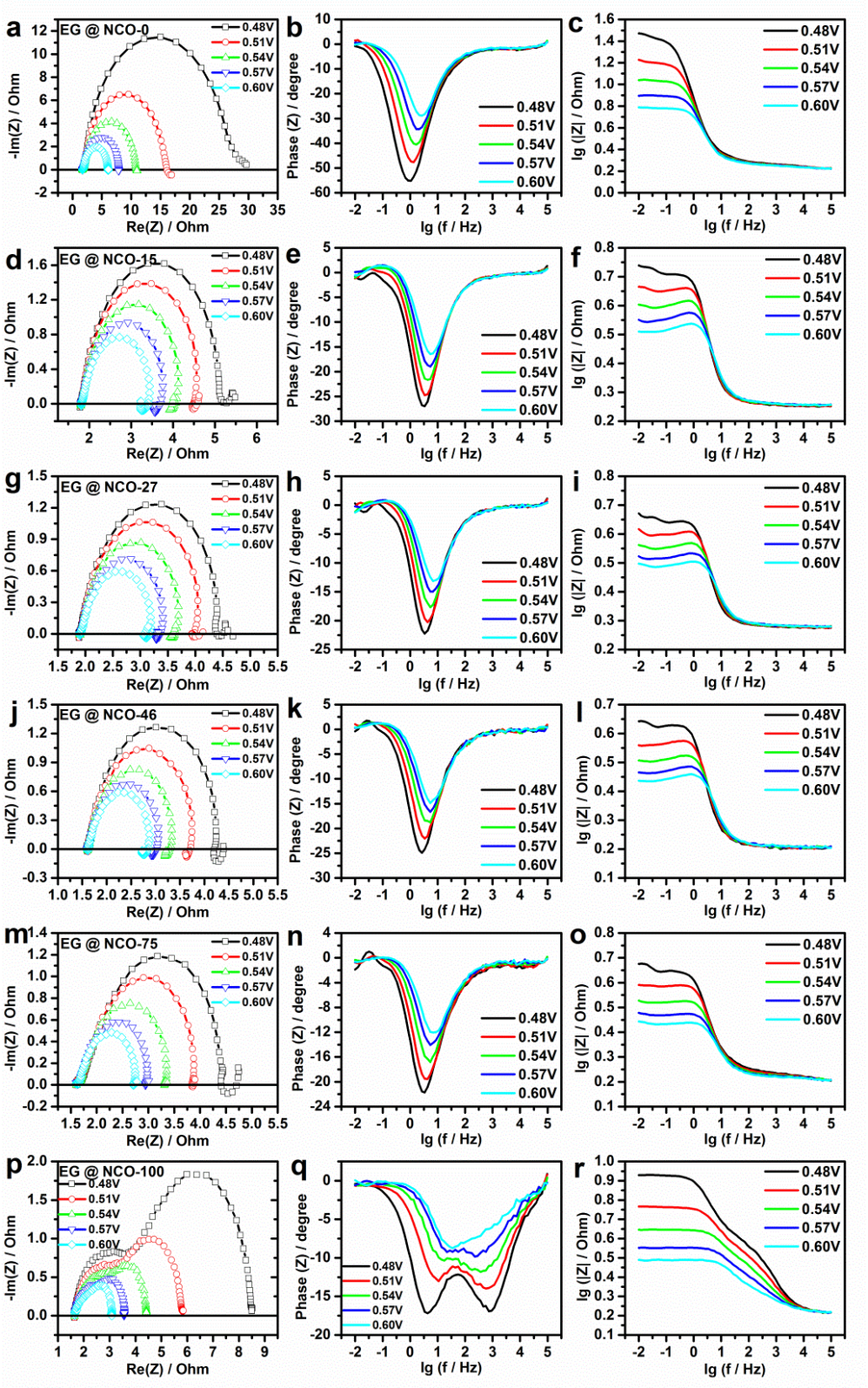

Figure 5.4 EIS results of EG oxidation on NCOs: NCO-0 (a-c), NCO-15 (d-f), NCO-27 (g-i), NCO-46 (j-l), NCO-75(m-o) and NCO-100 (p-r).

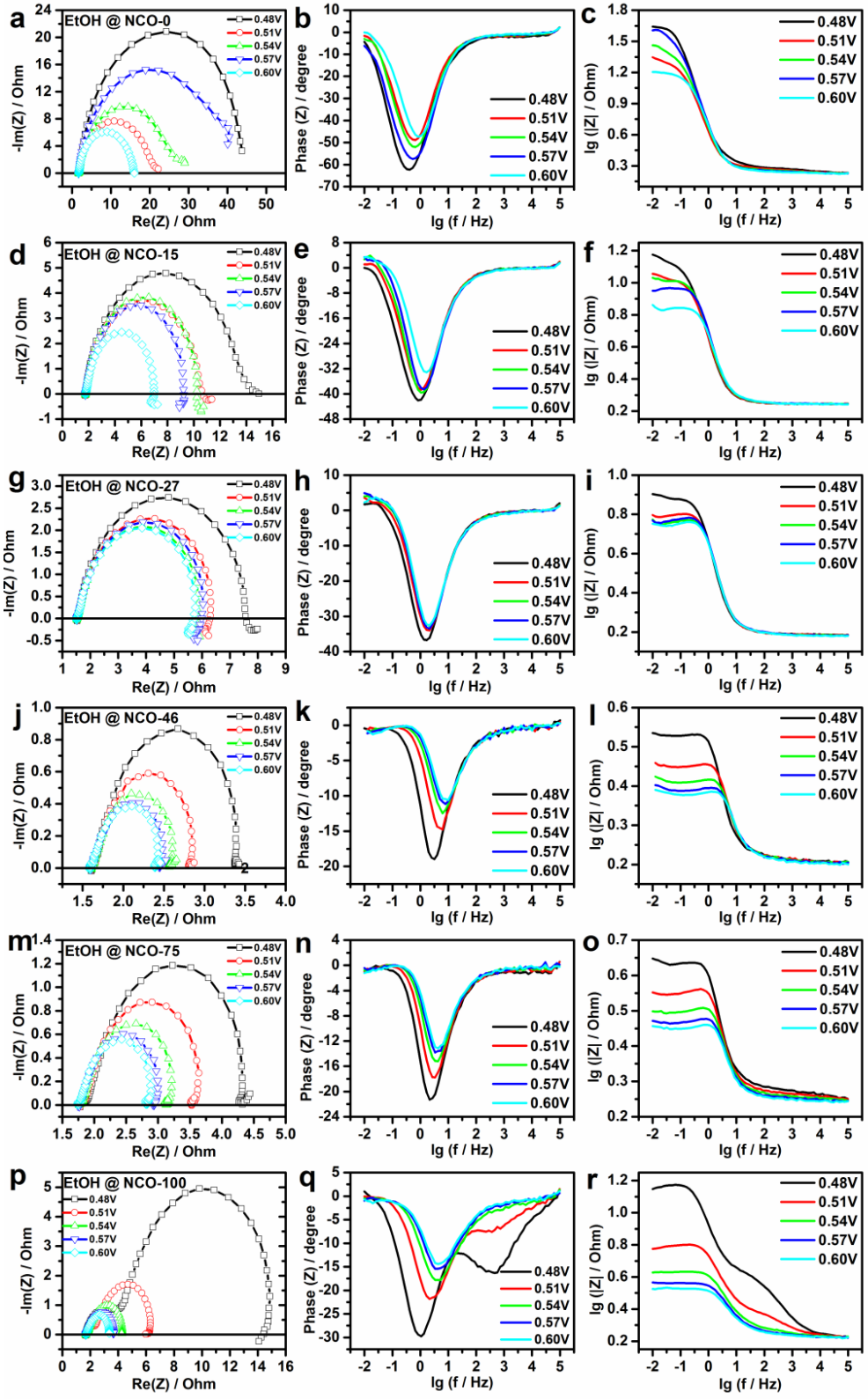

Figure 5.5 EIS results of EtOH oxidation on NCOs: NCO-0 (a-c), NCO-15 (d-f), NCO-27 (g-i), NCO-46 (j-l), NCO-75(m-o) and NCO-100 (p-r).

decreased. The irregular ErOH oxidation impedance change on Co_3O_4 may be attributed to the intermediate product accumulation at potential higher than 0.51 V. As the potential increased, intermediate products accumulated on the electrode surface, which made the reaction gradually blocked until 0.6 V. At 0.6 V, the intermediate products would be fully oxidized, and thus a cleaned surface was ready for more reactions. Whereas, this phenomenon was not observed in EG oxidation on Co_3O_4 (Figure 5.6a). It means the intermediate products from EtOH oxidation was more difficult than those from EG oxidation. Such an assumption should be possible. One EG molecule has two hydroxyl groups at each end, and thus the difficulty in oxidizing the two hydroxyl groups simultaneously is reduced. Only in the presence of Ni, the further oxidation of the intermediate products in EtOH oxidation can be facilitated. Thus, NCOs did not display such an impedance change trend as Co_3O_4 did.

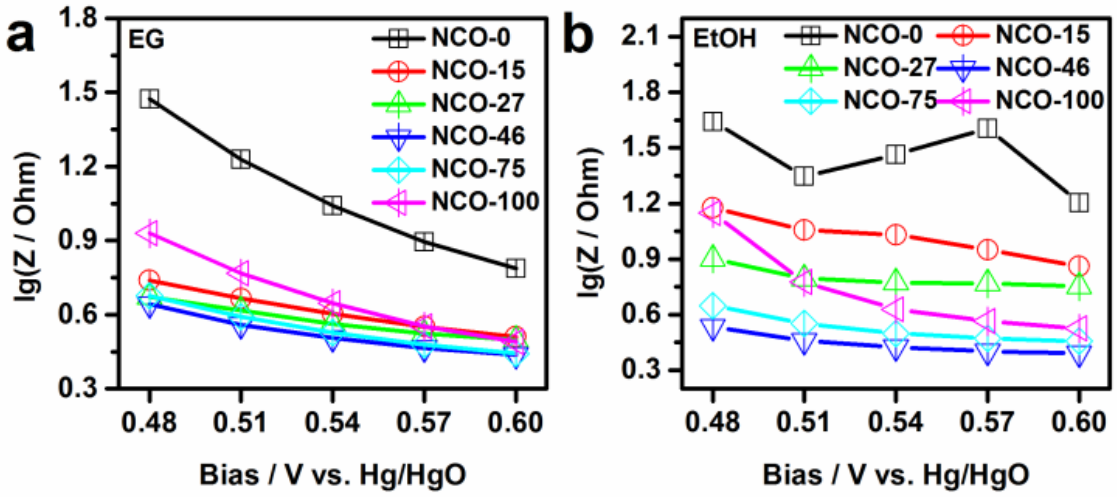

Figure 5.6 The impedance Z vs the bias potential for EG (a) and EtOH (b) oxidation on NCOs.

5.3.4 EG and EtOH Oxidation on NCO-46

The best electrode for EG and EtOH oxidation, NCO-46, was chosen to investigate the concentration effect in EG and EtOH oxidation process. The LSV curves in Figure 5.7 exhibit EG oxidation on NCO-46 when the EG concentration increased from 0 to 1.0 M. Obviously, the oxidation currents increased with the increase of EG concentration. At low EG concentration, the oxidation peak of NCO-46 in was obvious. At high EG concentration,

the current curve ramped along the anodic sweep direction. This phenomenon can be also observed in DPV curves (Figure 5.7d). With the increase of EG concentration, the DPV currents increased, and meanwhile, the DPV peaks became broader and shifted to the higher potential region. The relationship between the potential at 2 mA and the EG concentration was displayed in Figure 5.7c. As EG concentration increased, the potential decreased, indicative of that the EG reaction rate can be promoted by an increasing EG concentration. Figure 5-8b gives a summary on the current at 0.60 V in Figure 5.7a. When EG concentrations ranged from 0 to 0.04 M, the current increased approximately linearly with EG concentrations. When the EG concentration was between 0.04 and 0.20 M, the current kept increasing. As the EG concentration was close to 0.20 M, the current did not increase and reached a saturated state. At EG concentration higher than 0.20 M, increasing concentration resulted in a slight decreasing current. Comparing Figure 5.7b and Figure 5.7c, the potential at 2 mA decreased gradually as the EG concentration increased (Figure 5.7c), while the current at 0.6 V firstly increased and then slightly decreased. Here, the potential (Figure 5.7c) was collected at a relatively small current 2 mA and the current (Figure 5.7b) was collected at a relatively high potential 0.60 V. The relationship between oxidation current and EG concentration (Figure 5.7b) can be explained as follow. At low EG concentration (< 0.20 M), the oxidation rate was determined by EG concentration. Thus, an increasing EG amount facilitated the oxidation rate. At high EG concentration (> 0.20 M), the OH^- supply ability to the electrode surface cannot satisfy EG oxidation rate. Thus, the EG oxidation rate cannot be further facilitated. Additionally, a slight current decrease can be observed as EG concentration continued increasing, which was probably due to the viscosity increase of the solution.[7] Based on the relationship between diffusion coefficient (D) and viscosity (η),

$$D = RT/6\pi a\eta N_A \quad (5.1)$$

where R, T, a, and N_A are the gas constant, thermodynamic temperature, and hydrodynamic radius, and Avogadro's number.[8, 9] The increase of solution viscosity resulted in the decrease of EG diffusion coefficient. The relationship between EtOH oxidation current and EtOH concentration is shown in Figure 5.8. EtOH oxidation currents reached saturated at ~1.25 M EtOH. Comparing EG oxidation, EtOH oxidation showed a higher current at high concentration. For instance, at 0.60 V and alcohol concentration 1.0 M, EtOH oxidation

current was ~80 mA, while EG oxidation current was ~71 mA. Such a difference is probably due to that EtOH has a lower viscosity and thus better EtOH diffusion.

5.3.5 NMR on EG and EtOH Oxidation

The EG and EtOH oxidation products on NCO-46 were detected by using NMR. The electrolysis of EG and EtOH were carried out at 0.60 V for 12 hours and 18 hours, respectively. Figure 5.9 demonstrated the NMR spectra of the solution after EG and EtOH oxidation. In Figure 5.9a, the peaks at 62.7 and 171.0 ppm can be assigned to EG and oxalate, respectively.[10] In Figure 5.9b, the peaks at 16.9 and 57.3 ppm can be assigned to EtOH, and the peaks at 23.3 and 181.0 ppm can be assigned to acetate.[10]

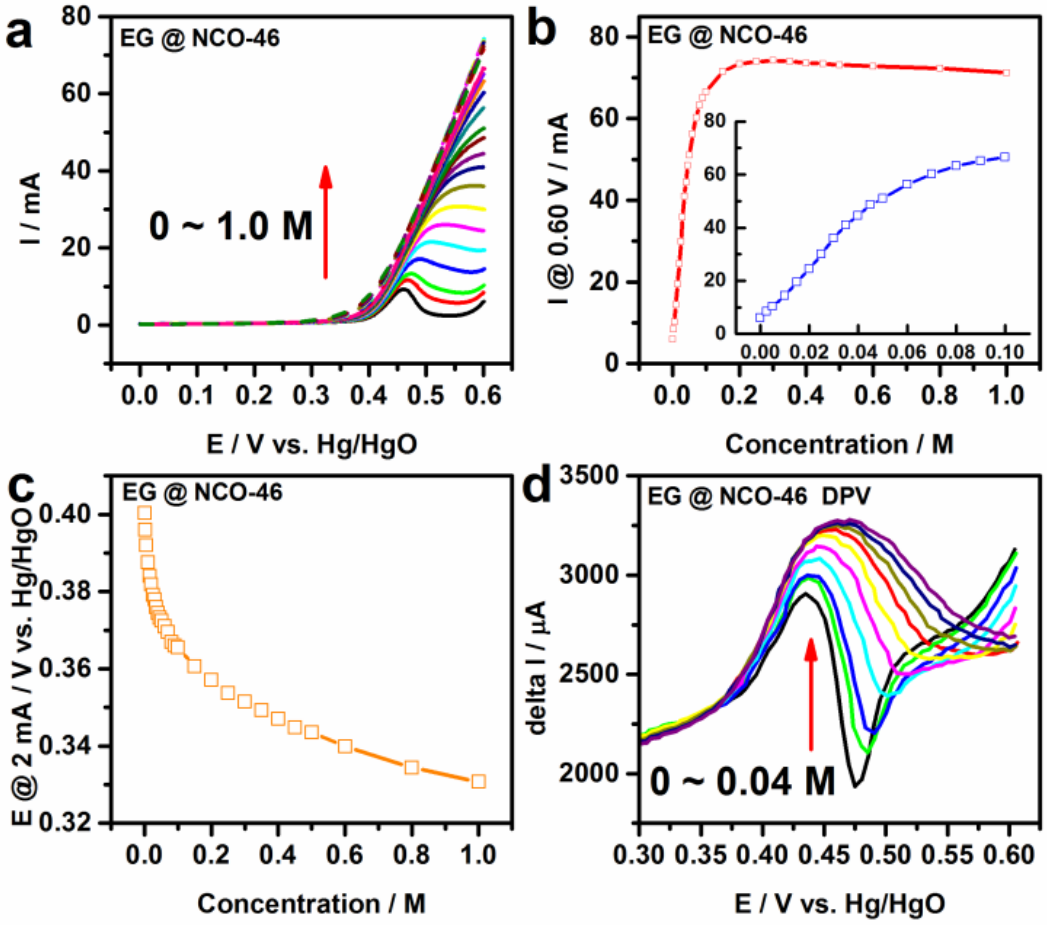

Figure 5.7 Different concentrations of EG oxidation on NCO-46: (a) LSV curves; (b) the current at 0.60 V vs. concentration; (c) the potential at 2 mA vs. concentration; (d) DPV curve.

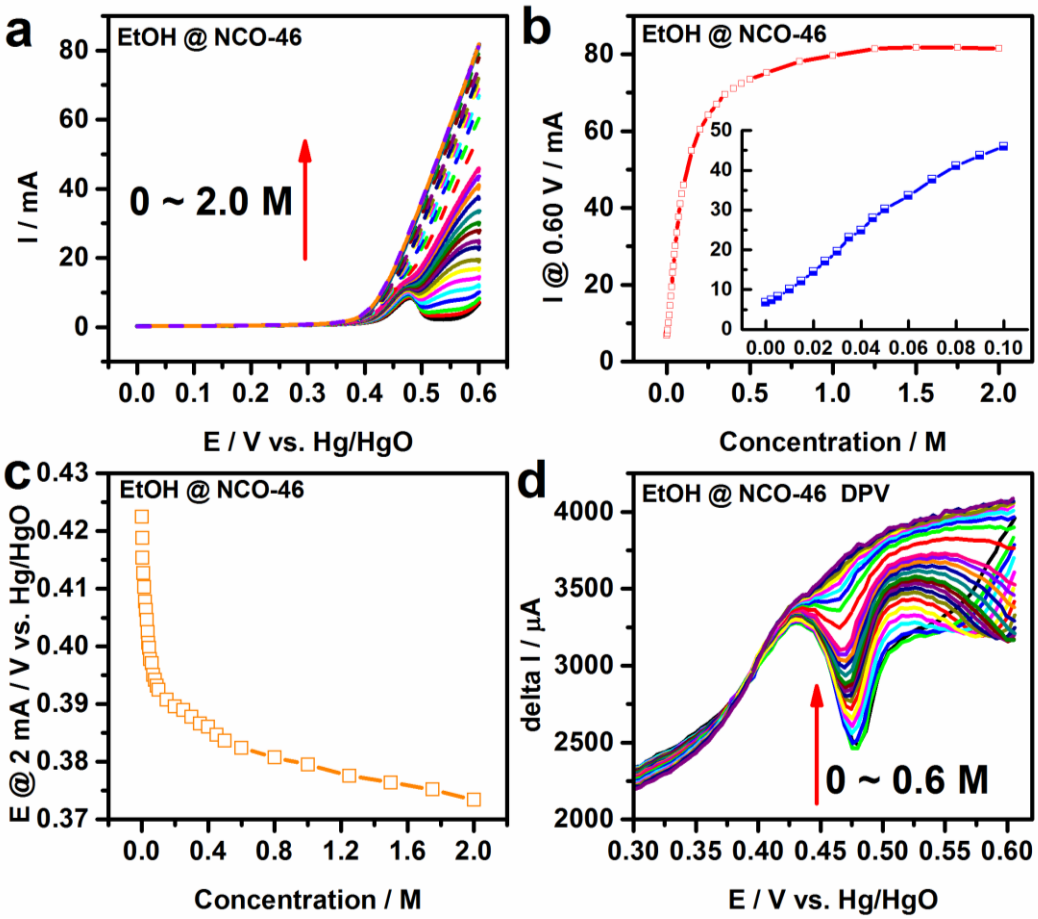

Figure 5.8 Different concentrations of EtOH oxidation on NCO-46: (a) LSV curve; (b) the current at 0.60 V vs. concentration; (c) the potential at 2 mA vs. concentration; (d) DPV curves.

The peak at 168.3 ppm in Figure 5.9a and b are assigned to carbonate[11], which may come from the adsorption CO_2 adsorption in the solution. The theoretical study has indicated that in C2 alcohol oxidation, the CO_2 formation from C-C bond cleavage is difficult.[12] Several studies have also indicated that no cleavage of C-C bond was observed in EtOH oxidation[13-17], and the cleavage of C-C bond only occurred on some noble metals.[18, 19] Accordingly, the small peak at 168 ppm should be attributed to carbonate due to CO_2 adsorption. NMR results indicates that oxalate was the EG oxidation major products and the major products, and acetate was the EtOH oxidation major products, respectively. Some aldehyde compounds such as glyoxal, acetaldehyde, etc. are the possible intermediate products. However, these intermediate products were not detected in the solution, indicating that these aldehyde intermediate products only existed on the electrode surface in oxidation process. Given NMR results and above analysis, the EG and EtOH oxidation

process can be expressed as follows:

EG oxidation to oxalate:

$CH_2OH\text{-}CH_2OH + 4OH^- \rightarrow CHO\text{-}CHO + 4H_2O + 4e^-$ (5.2)

$CHO\text{-}CHO + 6OH^- \rightarrow {}^-OOC\text{-}COO^- + 4H_2O + 4e^-$ (5.3)

EtOH oxidation to acetate:

$CH_3\text{-}CH_2OH + 2OH^- \rightarrow CH_3\text{-}CHO + 2H_2O + 2e^-$ (5.4)

$CH_3\text{-}CHO + 3OH^- \rightarrow CH_3\text{-}COO^- + 2H_2O + 2e^-$ (5.5)

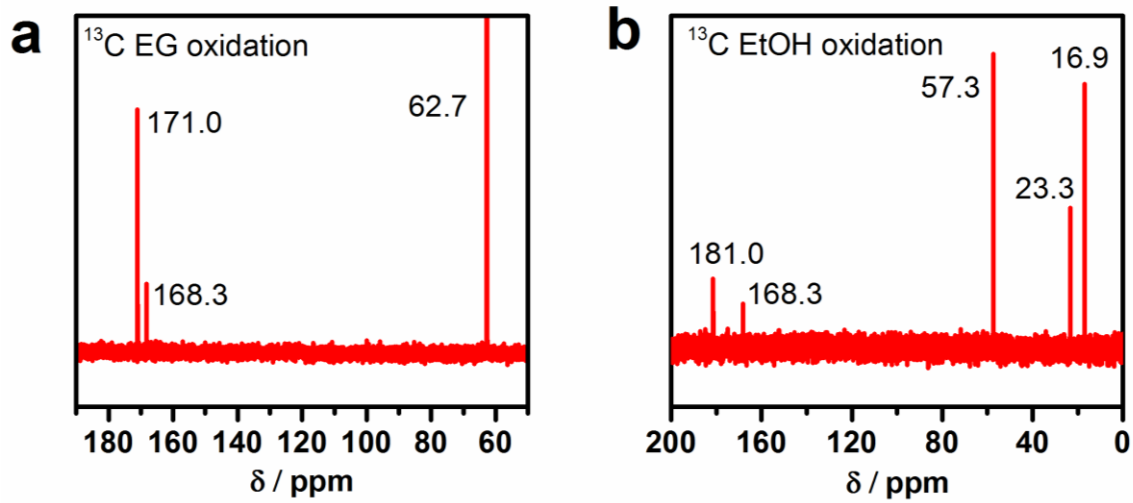

Figure 5.9 The ^{13}C NMR spectra of solution after EG (a) and EtOH (b) oxidation.

5.3.6 Comparison of Reaction Charge between EG and EtOH Oxidation

Based on NMR results, the oxidation degrees of hydroxyl groups in EG and EtOH are further compared. Both EG and EtOH are C2 alcohols. One EG molecule has two hydroxyl groups, while one EtOH molecule has one. Here the reaction charge (Q) was used to describe and compare the oxidation degree of hydroxyl groups in EG and EtOH on NCO-46. Q(EG) and Q(EtOH) can be obtained by integrating I-t curves at different potentials in Figure A.1 in Appendix. From Figure 5.10a, Q(EG) almost equaled to Q(EtOH) at the relatively high potential like 0.54, 0.57, and 0.60 V, while at low potential step like 0.48 and 0.51 V, Q(EG) was higher than Q(EtOH). Figure 5.10b shows Q(EG)/Q(EtOH) ratios were demonstrated in Figure 5.10a. At low potential steps (0.48 V and 0.51 V), Q(EG)/Q(EtOH) ratio was between one and two. At high potential steps (0.54 V, 0.57 V,

and 0.60 V), Q(EG)/Q(EtOH) ratio was nearly one. Two possibilities can be proposed to explain that Q(EG)/Q(EtOH) had different value ranges at low and high potential step, respectively. Different diffusion rates of EG and EtOH can be considered as one factor. EG and EtOH fluid mechanics can be compared by using viscosity (η), diffusion coefficient (D), and Schmidt number (Sc) can be used. From Table A.13, compared with EtOH, EG has a bigger viscosity, smaller diffusion coefficient, and bigger Schmidt number in water.[20] Thus, compared with EtOH, EG is more difficult to diffuse. When EG and EtOH were consumed fast at high potential step, EtOH had a high supply rate than EG, leading to more EtOH oxidized and the similar reaction charge at high potential steps. At low potential steps, due to the slow consumption of EG and EtOH, the supply of EG and EtOH was sufficient for the oxidation reaction. Thus, the reaction charge involved in EG and EtOH oxidation was determined more by the number of hydroxyl group. Another possibility is that not both hydroxyl groups in one EG molecule were oxidized simultaneously. To further analyze these two possibilities, reaction charges from the anodic sweeps in CV curves (Figure 5.3) at 80mV s^{-1} were compared with those from CA curves. The purpose to employing the CV test at high scan rates is to avoid the influence of the consumption of EG and EtOH. The reaction charge (Q) from CV tests can be calculated by the equation

$$Q = (1/v) \int i \, du \qquad (5.6)$$

where i, u, and v represent the current, the potential, and the scan rate in anodic sweep in CV curves, respectively. Figure 5.10c demonstrates that the net Q (net Q = Q(EG) – Q(background)) from 0.42 V to some specific potential. As the specific potential increased, Q increased. It is obvious that Q(EG) was higher than Q(EtOH). Figure 5.10d shows that the two types of Q(EG)/Q(EtOH). One was the value from 0.42 V to the specific potential and the other one was the value at every 0.03 V step, like the step 0.42 ~ 0.45 V and the step 0.45 ~ 0.48 V. It can be found that in general Q(EG)/Q(EtOH) value was bigger than 1. At low potential range, Q(EG)/Q(EtOH) value was bigger than 2. This result is not the same with the result from CA curves. It further indicates that the charge in EG and EtOH oxidation was prominently dominated by EG and EtOH supply through diffusion. The difference of EG and EtOH diffusion properties determines the difference in reaction charges. At low potentials, the influence from the reactant consumption was little and thus, the reaction charge in EG and EtOH oxidation was dominated by the number of hydroxyl

groups on each molecule.

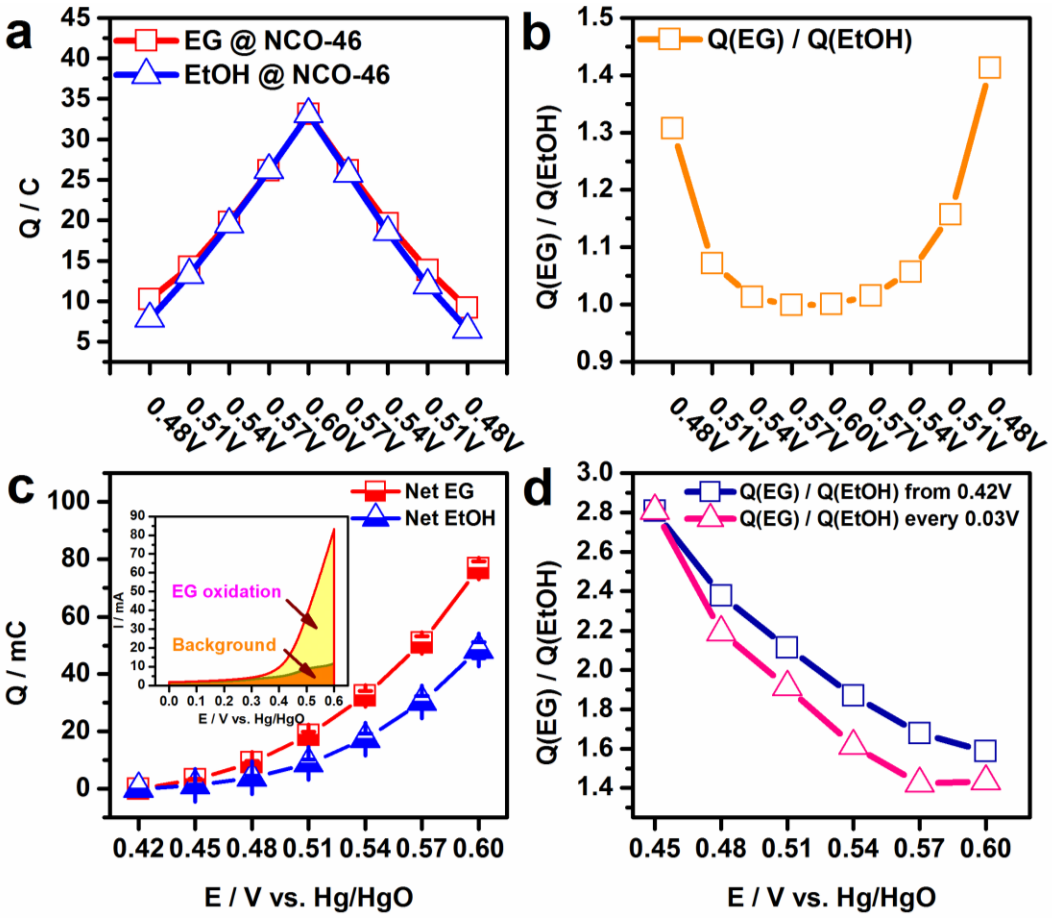

Figure 5.10 (a) The Q obtained from the CA tests in Figure A.1; (b) the Q(EG)/Q(EtOH) value from Figure 5.10a; (c) the net Q(EG) and net Q(EtOH) from 0.42 V to each specific potential. The inset: CV anodic sweeps of NCO-46 in the absence and the presence of EG at 80 mV s^{-1}; (d) the value of the net Q(EG) / net Q(EtOH) from 0.42 V to each specific potential (blue line) and the value of the net Q(EG) / net Q(EtOH) within every 0.03 V step from 0.42 V (pink line).

5.4 Conclusions

In this chapter, the electro-oxidation of EtOH and EG on Ni-Co oxides (NCOs) were investigated systematically. NCO-46 was found to have the best oxidation activity for both EtOH and EG. Having more Ni would facilitate the oxidation reaction as evidenced by EIS tests. The promotion on facilitating the step from intermediate products to final products was not significant, which led to the accumulation of produced excessive intermediate

products. The NCO-46 with the best oxidation activity can be attributed to the balance of the two oxidation rates between the step from alcohol to intermediate products and the step from intermediate products to final products. The NMR result shows that the EtOH and EtG oxidation process is a conversion process from hydroxyl groups to carboxyl groups.

References:

[1] A. J. Bard and L. R. Faulkner. Electrochemical Methods-Fundamentals and Applications Second edition.

[2] V. Augustyn, P. Simon and B. Dunn. *Energy & Environmental Science*. **2014**, 7, 1597.

[3] J. P. Zheng. *Electrochemical and Solid-State Letters*. **1999**, 2, 359-361.

[4] I. Danaee, M. Jafarian, F. Forouzandeh, F. Gobal and M. Mahjani. *International Journal of Hydrogen Energy*. **2009**, 34, 859-869.

[5] F. Seland, R. Tunold and D. A. Harrington. *Electrochimica Acta*. **2006**, 51, 3827-3840.

[6] I. Danaee, M. Jafarian, F. Forouzandeh, F. Gobal and M. G. Mahjani. *Electrochimica Acta*. **2008**, 53, 6602-6609.

[7] F. S. Jerome, J. T. Tseng and L. T. Fan. *Journal of chemical & engineering data*. **1968**, 13, 496-496.

[8] D. J. Scott, S. E. Harding and D. J. Winzor. *Analyst*. **2014**, 139, 6242-6248

[9] G. K. Batchelor. *J. Fluid Mech.*. **1976**, 74, 1-29.

[10] H. E. Gottlieb, V. Kotlyar and A. Nudelman. *The Journal of Organic Chemistry*. **1997**, 62, 7512-7515.

[11] S. Moret, P. J. Dyson and G. Laurenczy. *Dalton transactions*. **2013**, 42, 4353-4356.

[12] H.-F. Wang and Z.-P. Liu. *The Journal of the American Society*. **2008**, 130, 10996-11004.

[13] F. Hu, C. Chen, Z. Wang, G. Wei and P. K. Shen. *Electrochimica Acta*. **2006**, 52, 1087-1091.

[14] F. Hu, F. Ding, S. Song and P. K. Shen. *Journal of Power Sources*. **2006**, 163, 415-419.

[15] P. Cox and D. Pletcher. *Journal of Applied Electrochemistry*. **1991**, 21, 11-13.

[16] Z. X. Liang, T. S. Zhao, J. B. Xu and L. D. Zhu. *Electrochimica Acta*. **2009**, 54, 2203-2208.

[17] G. A. Camara and T. Iwasita. *Journal of Electroanalytical Chemistry*. **2005**, 578, 315-321.

[18] C. Xu, Y. Hu, J. Rong, S. P. Jiang and Y. Liu. *Electrochemistry Communications*. **2007**, 9, 2009-2012.

[19] J. Liu, J. Ye, C. Xu, S. P. Jiang and Y. Tong. *Electrochemistry Communications*. **2007**, 9, 2334-2339.

[20] D. R. Lide. *CRC Press LLC*. **2002**, 6-181.

Chapter 6*

C3 saturated alcohol oxidation on Co_3O_4

This chapter discusses C3 saturated alcohols' oxidation on the Co_3O_4 electrode. It is found that the oxidation rate of C3 saturated alcohols followed the sequence: glycerol > 1,2-propanediol > 1,3-propanediol >1-propanol > 2-propanol in 1.0 M KOH solution. The oxidation rate will strongly be affected by KOH concentration, especially for the alcohols bearing secondary hydroxyl group. The NMR results show that at adjacent hydroxyl groups, the corresponding C-C bond can be easily broken.

* This chapter published substantially as Sun et al., Electrochemical oxidation of C3 saturated alcohols on Co_3O_4 in alkaline, *Electrochimica Acta*, **2017**, 228, 183–194.

6.1 Introduction

In Chapter 4 and Chapter 5, the electro-oxidation of C1 alcohol (methanol) and C2 alcohols (ethylene glycol and ethanol) has been investigated on Ni-Co oxides. In those reactions, it has been found that the hydroxyl group can be converted into the carboxyl group. As for EG and EtOH oxidation, no cleavage of C-C bond can be observed. When carbon atom increases to three, the electro-oxidation of corresponding alcohols is more interesting due to the increase of complexity in molecule structure and types. The oxidation of C3 alcohols are very attractive not only in fuel cell field[1-5], but also for value-added C3 products.[6] For example, 1,2,3-propanetriol, also called glycerol (GLY), is one of the by-products from biomass conversion.[6] Based on its C-C-C structure, GLY is promising to be used for converting into C3 value-added products like dihydroxy acetone (DHA), tartronic acid (TA), mesoxalic acid (MA), dihydroxymalonic acid (DMA) etc.[7-10] Except glycerol, other C3 alcohols such as 1,2-propanediol[11-13], 1,3-propanediol[14-16] are attracting much attention. Thus, in this chapter, five kinds of C3 saturated alcohols, glycerol (GLY), 1,2-propanediol (1,2-P), 1,3-propanediol (1,3-P), 1-propanol (1-P), 2-propanol (2-P) were chosen as objective.Based on EG and EtOH oxidation results, comparing the cleavage of C-C bond, the hydroxyl group can be easily oxidized to carboxyl group. According to previous report[5], Ni has the ability to break the C-C bond, and thus Ni-free Co_3O_4 and Ni-free graphite paper were chosen as catalyst and substrate, respectively, to guarantee the non-cleavage of C-C bond to the largest extent. In this Chapter, it is assumed that the oxidation from C-OH to C=O will occur before the cleavage of C-C bond. Thus, to compare the oxidation rate, the same hydroxyl group concentration for these five alcohols (GLY, 1,2-P, 1,3-P, 1-P, and 2-P) was fixed at the concentration of 0.50, 0.75, 0.75, 1.50, and 1.50 M, respectively.

6.2 Experimental Methods

6.2.1 Electrode Preparation

The Co_3O_4 electrodes were prepared by electrodeposition of $Co(OH)_2$, followed by annealing at 300 °C in air for 2 hours. The graphite paper (1.0 cm × 1.0 cm) was used as

substrate to avoid the contribution from metal substrates to oxidation product. The electrodeposition was carried out in 0.1 M $Co(NO_3)_2$ solution. The potential was held at -0.85 V until the passing charge reached 1.8 C.

6.2.2 CV for C3 saturated Alcohol Oxidation

The three-electrode system was employed to characterize the working electrode Co_3O_4, with a Hg/HgO (1.0 M KOH, aqueous) reference electrode and a Pt plate (~ 1.0 cm × 3.0) counter electrodes. The CV tests of C3 saturated alcohols were conducted in 1.0 M KOH solution at 10 mV s^{-1}. The Tafel plots were fitted by 1 mV s^{-1} of CV curves. To investigate the KOH concentration effect on C3 alcohol oxidation, 0.5, 1.0, 3.0, and 5.0 M KOH solutions were used.

6.2.3 XANES

The XANES test was done to determine the Co valence state during alcohol oxidation. During the oxidation process, the potential was hold at 0.2, 0.3, 0.4, 0.5, and 0.6 V, consecutively, and meanwhile the XANES test was conducted. The XANES characterization was carried out at XAFCA beamline of Singapore Synchrotron Light Source (SSLS).

6.2.4 NMR

Bruker Advance 300 (300 MHz) NMR spectrometer was used to test the C3 saturated alcohol oxidation product after long time electrolysis.

6.3 Principle Outcomes

6.3.1 CV for C3 saturated Alcohol Oxidation

Figure 6.1 shows 100 continuous C3 alcohol oxidation CV cycles on Co_3O_4. Figure 6.1a shows the 100 continuous CV cycles of Co_3O_4 in 1.0 M KOH solution. No obvious change can be found during 100 cycles, indicative of the stability of Co_3O_4 in alkaline. Figure 6.1b-f exhibit the CV cycles of Co_3O_4 in the mixed solution of KOH and alcohols. Generally, the electro-oxidation started at ~0.4 V. In following CV cycles, the oxidation currents of C3 saturated alcohols firstly decreased and then became steady except for that of 2-P. The 2-P oxidation displayed an increasing current within the first three cycles and then the current dropped since the forth cycle. The obvious oxidation current drop for all alcohols suggested that the oxidation products gradually adsorbed and accumulated on Co_3O_4 surface until the adsorption and desorption of oxidation products reached equilibrium during CV cycling.

Figure 6.2a demonstrates the first CV cycle of C3 alcohol oxidation. Clearly, the oxidation rate of C3 saturated alcohol on Co_3O_4 follows the order: GLY > 1,2-P > 1,3-P > 1-P > 2-P. The potential at 5 mA is summarized in Figure 6.2b. Here, this potential is denoted as the oxidation potential. The oxidation potential follows the order: GLY < 1,2-P < 1,3-P < 1-P < 2-P. GLY is the alcohol that can be oxidized at the lowest potential (~ 0.37 V) and 2-P is the most difficult to be oxidized most difficultly among these five alcohols. It indicates that C3 saturated alcohols bearing more hydroxyl groups were easier to be oxidized. Both 1,2-P and 1,3-P have two hydroxyl groups. 1,2-P had a lower oxidation potential than 1,3-P. It means that the alcohol bearing adjacent hydroxyl groups was easier to be oxidized than that bearing only primary hydroxyl groups at two sides. There is one primary hydroxyl group in one 1-P or 2-P molecule. 1-P had a lower oxidation potential than 2-P, which suggests that C3 alcohol with one primary hydroxyl group was easier to be oxidized than that with one secondary hydroxyl group in 1.0 M KOH solution. Based on the proposed mechanism on cobalt-based materials for alcohol oxidation, cobalt cations with high valence states play a critical role in alcohol oxidation process. However, it has also been reported that both Co^{3+} and Co^{4+} contributed to alcohol oxidation reaction. From CV results (Figure 6.2a), different C3 saturated alcohols began their oxidation reactions at different cobalt valence states. For example, GLY and 1,2-P oxidation happened from ~0.30 V and ~0.35 V, respectively, where Co^{2+} at the electrode surface have been oxidized

to Co^{3+}. 1,3-P, 1-P, and 2-P began to be oxidized at ~0.4 V, where Co^{3+} began to be oxidized to Co^{4+}. Figure 6.2c summarizes the oxidation currents at 0.60 V for C3 saturated

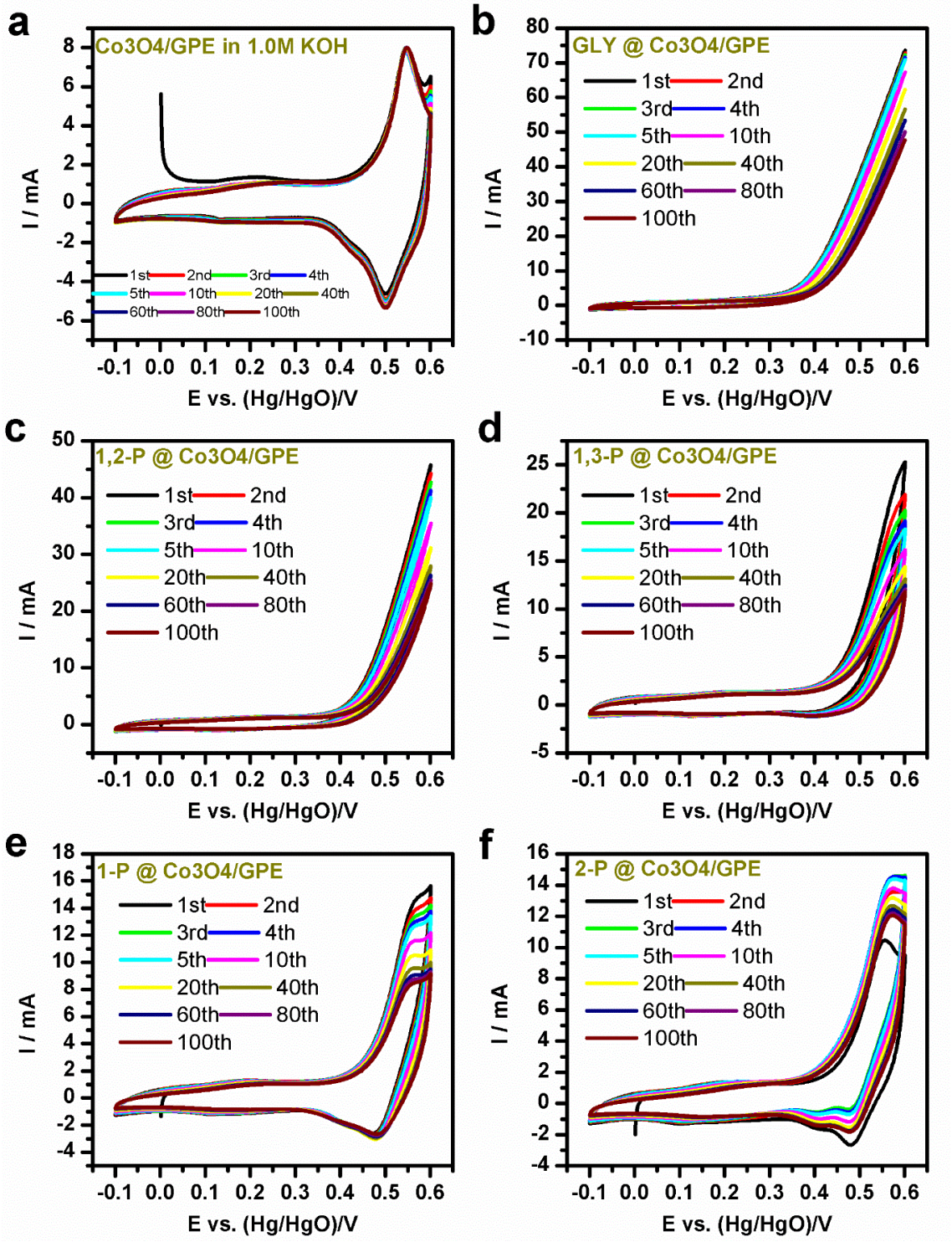

Figure 6.1 The continuous CV cycles of Co_3O_4 in 1.0 M KOH in the absence (a) and the presence (b-f) of C3 saturated alcohols.

alcohols. The oxidation current followed the order: GLY > 1,2-P > 1,3-P > 1-P > 2-P. Besides, the reduction peak was not observed in CV curves of GLY and 1,2-P oxidation. However, the reduction peak was observed in CV curves of 1,3-P, 1-P, and 2-P oxidation. The reduction peak heights followed the order 2-P > 1-P > 1,3-P, indicating that the reduction from Co^{4+} to Co^{3+} occurred in GLY and 1,2-P oxidation reactions. In terms of 1,3-P, 1-P, and 2-P oxidation, the existence of this reduction peak means that an insufficient oxidation reaction occurred. From another perspective, it means that the electron transfer from 1,3-P, 1-P, and 2-P to Co_3O_4 was more difficult than that from GLY and 1,2-P to Co3O4 at high potential. Figure 6.2d exhibits the Tafel plots for C3 saturated alcohol oxidation. The Tafel slopes of GLY, 1,2-P, 1,3-P, 1-P, and 2-P oxidation were 79, 72, 99, 87, 45 mV dec^{-1}, respectively, demonstrating the order 2-P < 1,2-P < GLY < 1-P < 1,3-P. It indicates that increasing potential led to a greater oxidation rate promotion for those alcohols bearing secondary hydroxyl group.

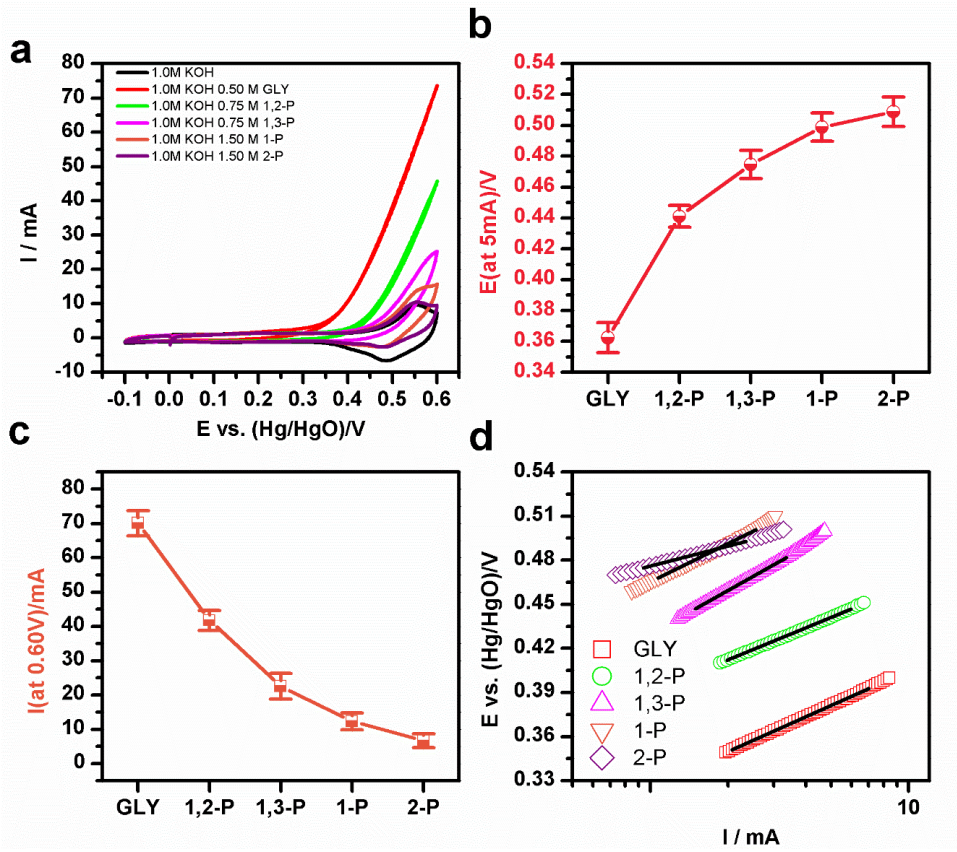

Figure 6.2 (a) CV curves of C3 saturated alcohol oxidation. (b) The oxidation potentials for C3 saturated alcohols. (c) The oxidation currents for C3 saturated alcohols. (d) Tafel plots of C3 saturated alcohol oxidation.

6.3.2 Co Valence State Change during Oxidation Process

In general, the alcohol oxidation process on cobalt-based oxides is believed as follow: (1) Co is oxidized from low to high valence state; (2) Co with high valence state oxidizes alcohol molecules.[17-21] It is necessary to investigate the change of Co valence state in the oxidation reaction. Here, GLY was chosen as objective for in situ X-ray absorption characterization. Figure 6.3 exhibits the XANES spectra for Co K-edge recorded on Co_3O_4 in the absence and the presence of GLY. In Figure 6.3a and b, generally it can be seen that the Co K-edge absorption edge shifted to higher energies as potential increased, indicating that Co_3O_4 were gradually oxidized no matter there was GLY or not. At 0.60 V, when comparing the oxidation degree of Co_3O_4 in the absence and the presence of GLY (Figure 6.3c and d), there was no obvious difference. It is believed that the oxidation of GLY was through the electron transfer from GLY to Co cations with high valance state. The electron transfer to Co cations should be able to reduce Co to a lower valence state. However, there was no obvious difference observed when GLY was being oxidized.

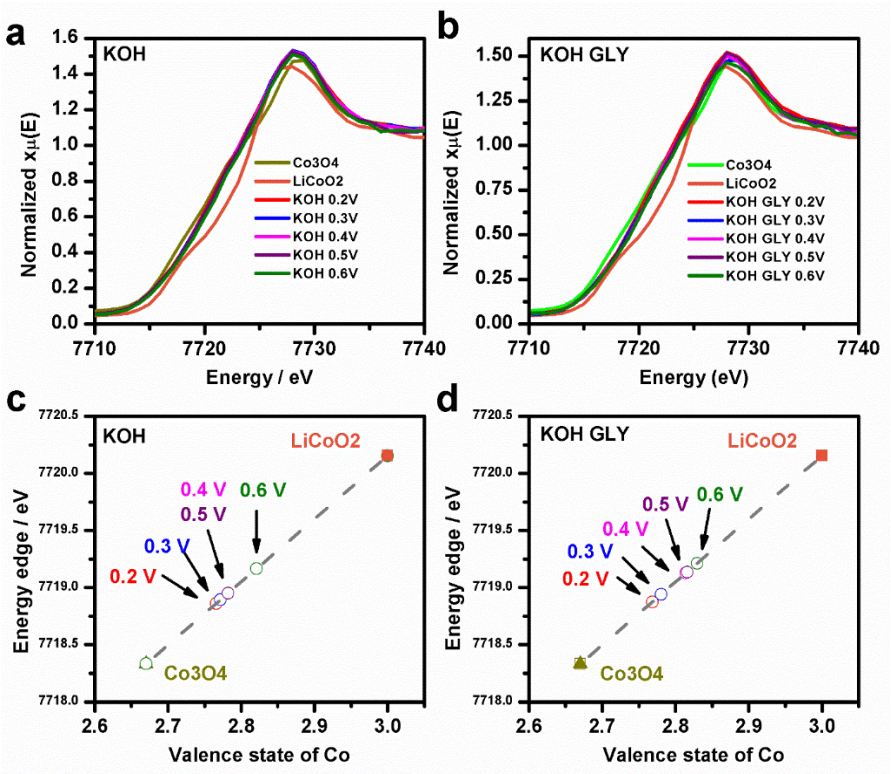

Figure 6.3 XANES profiles of Co_3O_4 under electrochemical conditions: Co_3O_4 in 1.0 M KOH solution (a) and KOH and GLY solution (b) at various potential; the relationship between energy

edge and valence state of cobalt in 1.0 M KOH solution without (c) and with (d) GLY at various potential.

6.3.3 NMR for Oxidation Products

To analyze the oxidation products of the C3 saturated alcohols on Co_3O_4, the oxidation experiment was carried out in 1.0 M KOH solution at 0.60 V for 24 hours. To prevent the reduction of oxidation products at counter electrode, an anion exchange membrane was used to separate the anode and cathode. NMR was used to detect the oxidation products. Figure 6.4 shows the NMR spectra of the electrolyte solutions after the oxidation of C3 saturated alcohols. In the electrolyte of GLY oxidation, the formate can be determined by the signal 8.37 ppm in ^{1}H NMR spectra (Figure 6.3a) and 171.04 ppm in ^{13}C NMR spectra (Figure 6.3b). The signal at 168.44 ppm (Figure 6.3b) can be assigned to the CO_3^{2-}, which may be attributed to the adsorption of CO_2 by alkaline solution.[22, 23]

However, it is noticed that this signal was not observed in the electrolytes during the oxidation of 1,2-P (Figure 6.3d), 1-P (Figure 6.3e), 1,3-P (Figure A.2a and b) and 2-P (Figure A.2c and d). These observations indicate that the CO_3^{2-} was the most likely to be one of GLY oxidation products. Moreover, formate was detected as the major oxidation product, suggesting that the C-C bond of GLY can be cleaved in the oxidation reaction. The C-C bond cleavage is a key step for CO_2 formation in the non-C1 alcohol oxidation reaction. Interestingly, trace amount of acetate can be also found based on 1.83 ppm in ^{1}H NMR spectrum (Figure 6.3a) and 179.93 ppm in ^{13}C NMR spectrum (Figure 6.3b).[23] It suggests that trace amount of $-CH_2OH$ or -OH was substituted by H in GLY oxidation. The signal at 1.25 ppm in ^{1}H NMR spectra (Figure 6.3a) is unknown. Figure 6.3c and d show the ^{1}H NMR and ^{13}C NMR spectra of solution after 1,2-P oxidation. The signals at 8.35 ppm in ^{1}H NMR spectrum (Figure 6.3c) and 171.04 ppm in ^{13}C NMR spectrum (Figure 6.3d) are attributed to formate. The signals at 1.81 ppm in ^{1}H NMR spectrum (Figure 6.3c) and 181.29, and 23.25 ppm in ^{13}C NMR spectrum (Figure 6.3d) are attributed to acetate.[23]

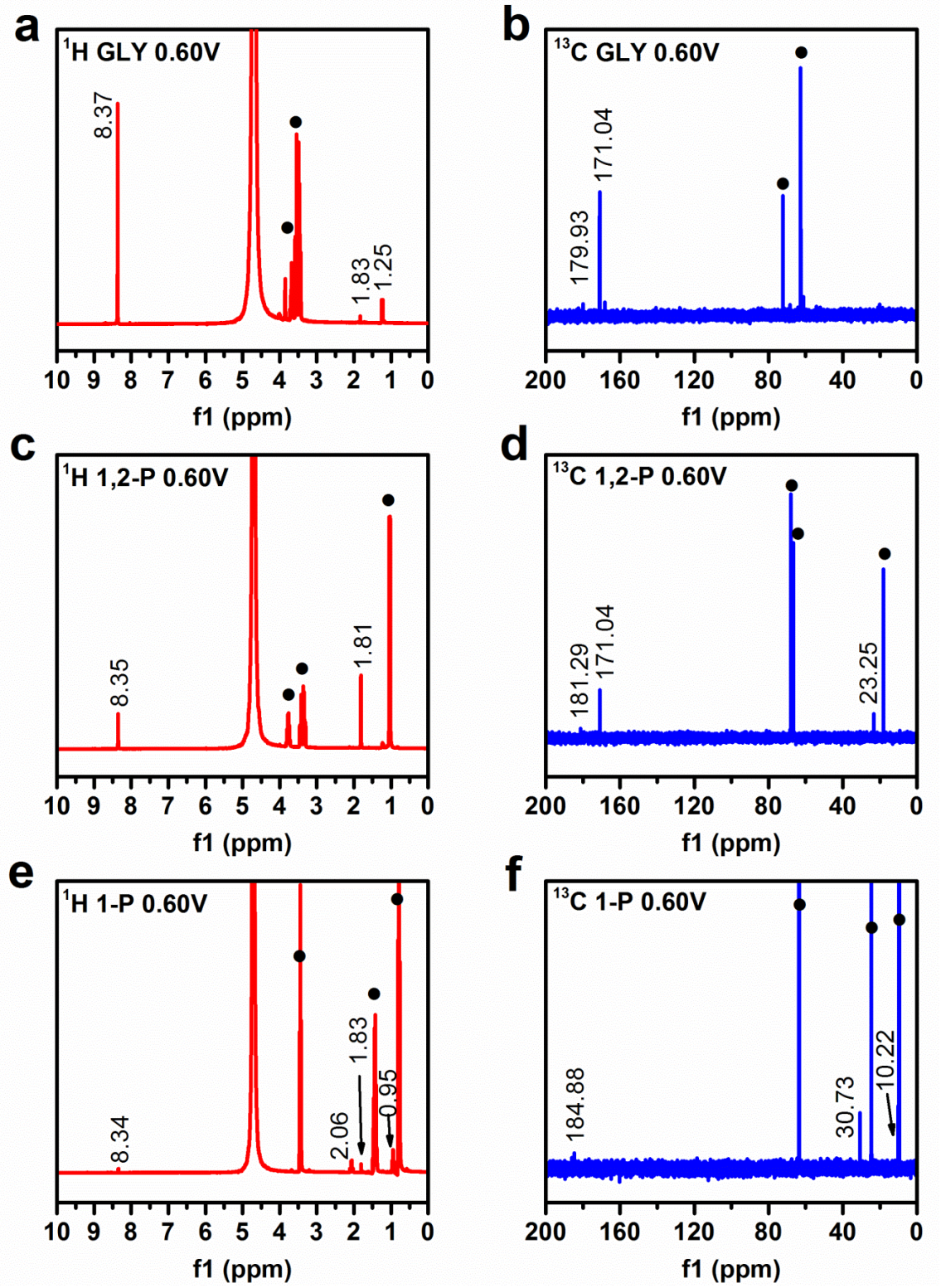

Figure 6.4 The ^{1}H (a, c, e) and ^{13}C (b, d, f) NMR spectra of the electrolyte solutions after 24-hour oxidation of GLY, 1,2-P and 1-P at 0.60 V. The dots represent the peaks from alcohol substrates.

The observations observed above indicate that formate and acetate were the major products in 1,2-P oxidation. Figure 6.3e and f exhibit the ^{1}H NMR spectrum and ^{13}C NMR spectrum of the solution after 1-P oxidation. The signals at 0.95 and 2.06 ppm in ^{1}H NMR spectrum (Figure 6.3e) and 10.22, 30.73, 184.88 ppm in ^{13}C NMR spectrum (Figure 6.3f) indicate that propionate was the major product. Moreover, the trace signal of formate and acetate can also be detected in ^{1}H NMR spectrum (Figure 6.3e). The above results reveal that the adjacent hydroxyl groups facilitated the cleavage of C-C bond. For instance, the major oxidation product of GLY was formate, indicating that all C-C bonds were broken up. The major products of 1,2-P oxidation were formate and acetate, indicating that the cleavage of C-C bond occurred at the location where two adjacent hydroxyl groups were attached. Further the major product of 1-P oxidation was propionate, implying that hydroxyl group was oxidized to carboxylic group and the C-C bond cleavage seldom occurred. The NMR spectra of 1,3-P and 2-P are shown in Figure A.2. The 1,3-P oxidation products were difficult to be analyzed. Despite that, the existence of malonate can be ruled out. Acetone was found to be as one of the 2-P oxidation products based on the signal at 2.11 ppm in ^{1}H NMR spectrum (Figure A.3e) and the signal at 30.32 ppm in ^{13}C NMR spectrum (Figure A.3f).

6.3.4 Effect of KOH Concentration on C3 saturated Alcohol Oxidation

To investigate the effect of KOH concentration on C3 saturated alcohol oxidation, the concentration of KOH solution was changed from 0.5 to 5.0 M (Figure 6.5). The applied potentials in this section were converted to RHE. Figure 6.5a exhibits the CV curves of Co_3O_4 in different concentrations of KOH solution.[24-26] As KOH concentrations increased, Co^{2+}/Co^{3+} and Co^{3+}/Co^{4+} oxidation peaks shifted towards the negative potential direction, which indicates that increasing KOH concentration can promote the oxidation of Co^{2+} and Co^{3+} cations. Figure 6.5b-d show the CV curves of GLY, 1,2-P, and 1,3-P oxidation in different concentrations of KOH solution, revealing that increasing KOH concentration can promote GLY, 1,2-P, and 1,3-P oxidation. Figure 6.5e exhibits the 1-P oxidation in different KOH concentration electrolytes. From these CV curves of 1-P oxidation, the oxidation current increased with the increase of KOH concentration from 0.5 to 1.0 M,

whereas with the increase of KOH concentration from 1.0 to 3.0, and to 5.0 M, the oxidation current decreased. This can be explained as follow. With the increase of KOH concentration, the solubility of 1-P in KOH solution become less beyond 1.0 M. As KOH concentration increased, obvious liquid layer stratification was observed (Figure A.4). When KOH concentrations increased from 1.0, to 3.0, and to 5.0 M, the Co^{3+}/Co^{4+} oxidation peak shifted from ~1.50, to ~1.47, and to ~1.45 V, respectively. The Co^{3+}/Co^{4+} oxidation peak was not observed in CV curves in 0.5 M KOH solution (Figure 6.5e). This current increase from 0.5 to 1.0 M KOH means that the alcohol oxidation rate can be facilitated by increasing KOH concentration, which is in accord with previous reports.[21, 23, 27-31] However, as KOH concentrations further increased from 1.0 to 3.0, and to 5.0 M, the 1-P oxidation current did not increase rather decrease. Meanwhile, the Co^{3+}/Co^{4+} oxidation peak became weaker, and whereas the Co^{4+}/Co^{3+} reduction peak became stronger.

This phenomenon implies that when the KOH concentration was higher than 1.0 M, the amount of 1-P on the surface of the electrode was not enough to make Co^{4+} reduce to Co^{3+}. For 2-P oxidation, increasing KOH concentration can also facilitate 2-P oxidation (Figure 6.5f). When the KOH concentration increased from 0.5 to 1.0 M, the anodic sweep current increased and the cathodic sweep current decreased. Despite that, this reduction peak still existed. It also suggests that Co^{4+} was not fully reduced by 2-P. When KOH concentrations were 3.0 and 5.0 M, crossovers can be observed in CV curves and the cathodic sweep current was higher than anodic sweep current. It is probably because the intermediate products produced in anodic sweep continued to be oxidized. Meanwhile, no obvious Co^{4+}/Co^{3+} reduction peak was observed in CV curves, indicating that higher KOH concentration can promote the oxidation reaction and thus accelerate electron transfer from 2-P to electrode.

Figure 6.6a demonstrates the relationship of the oxidation potential against KOH concentration. Here the potential at 5 mA is donated as oxidation potential. It can be noticed that except for GLY, the oxidation potential decreased with the increase of KOH concentration. As KOH concentrations increased from 0.5 to 1.0 M, the oxidation potential of 1-P and 2-P decreased obviously, while 1,3-P oxidation potential exhibited a smaller

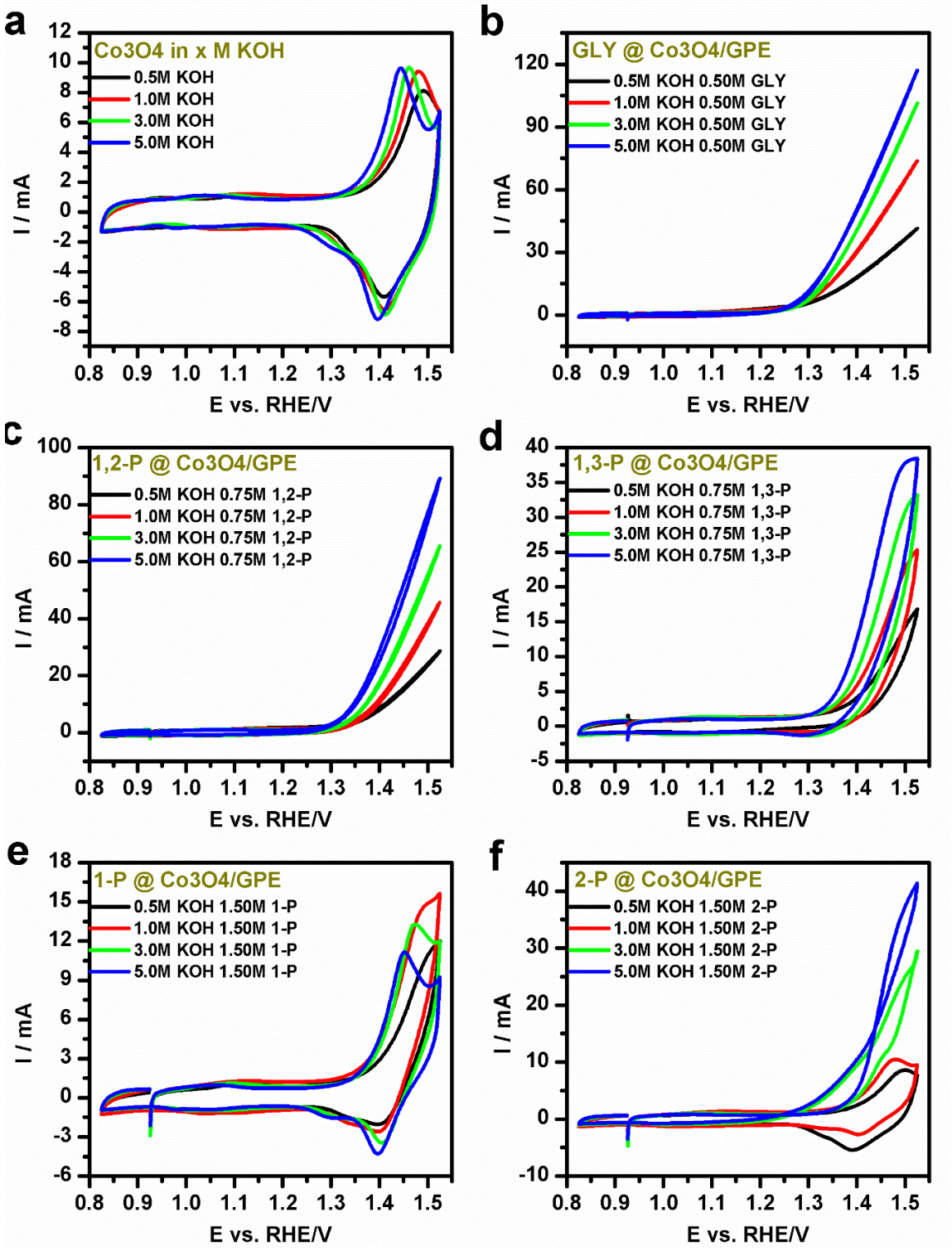

Figure 6.5 CV curves of C3 saturated alcohol oxidation on Co_3O_4 in different concentrations of KOH solution: (a) no alcohol; (b) GLY; (c) 1,2-P; (d) 1,3-P; (e) 1-P; (f) 2-P.

drop. The 1,2-P oxidation potential almost kept unchanged as KOH concentrations changed from 0.5 to 1.0 M. However, GLY oxidation potential in 0.5 M KOH was smaller than that in 1.0 M KOH. This phenomenon was not observed in GLY oxidation in other concentrations of KOH solution. It implies that the alcohol oxidation potential may be influenced by the oxidation peaks of Co_3O_4, especially when these two types of oxidation peaks were close to each other. Figure 6.6b demonstrates the relationship of the oxidation potential of C3 saturated alcohols in different concentrations of KOH solution. At the same KOH concentrations, a clear oxidation potential order can be observed. When KOH concentrations were 0.5 and 1.0 M, the oxidation potential sequence was GLY < 1,2-P < 1,3-P < 1-P < 2-P. In 3.0 M KOH solution, 2-P oxidation potential was similar to 1-P oxidation potential. In 5.0 M KOH solution, 2-P oxidation potential was lower than 1-P oxidation potential. These results demonstrate that the oxidation potential order could be varied in different concentrations of KOH solution.

Despite that, the oxidation potential order GLY < 1,2-P < 1,3-P < 1-P or 2-P remained. Besides, although KOH concentrations increased 10 times from 0.5 to 5.0 M, GLY oxidation potential change was less than 20 mV. It means that the KOH concentration effect on GLY oxidation potential was very little. Figure 6.6c exhibits the relationship between oxidation currents and KOH concentrations. The oxidation currents of GLY and 1,2-P increased obviously as KOH concentration increased from 0.5 to 5.0 M, compared to those of 1,3-P, 1-P, and 2-P. Such an obvious change is observed in Figure 6.6d. For example, for GLY oxidation, although the KOH concentration effect on GLY oxidation potential change can be neglected, the oxidation current increased obviously. 1,3-P oxidation current also increased as KOH concentrations increased. However, this increase of 1,3-P oxidation current was smaller than that of GLY and 1,2-P. As for 1-P oxidation, KOH concentration change did not bring about remarkable influence on the oxidation current. As for 2-P oxidation, when the KOH concentration was lower than 1.0 M, its oxidation current was smallest among these five saturated C3 alcohol, while when KOH concentrations were higher than 1.0 M, 2-P oxidation current increased abruptly, exceeding 1,3-P oxidation current. It should be noted that the KOH concentration effect on those

alcohols with secondary hydroxyl group was more dramatic than that on those alcohols only with primary hydroxyl group.

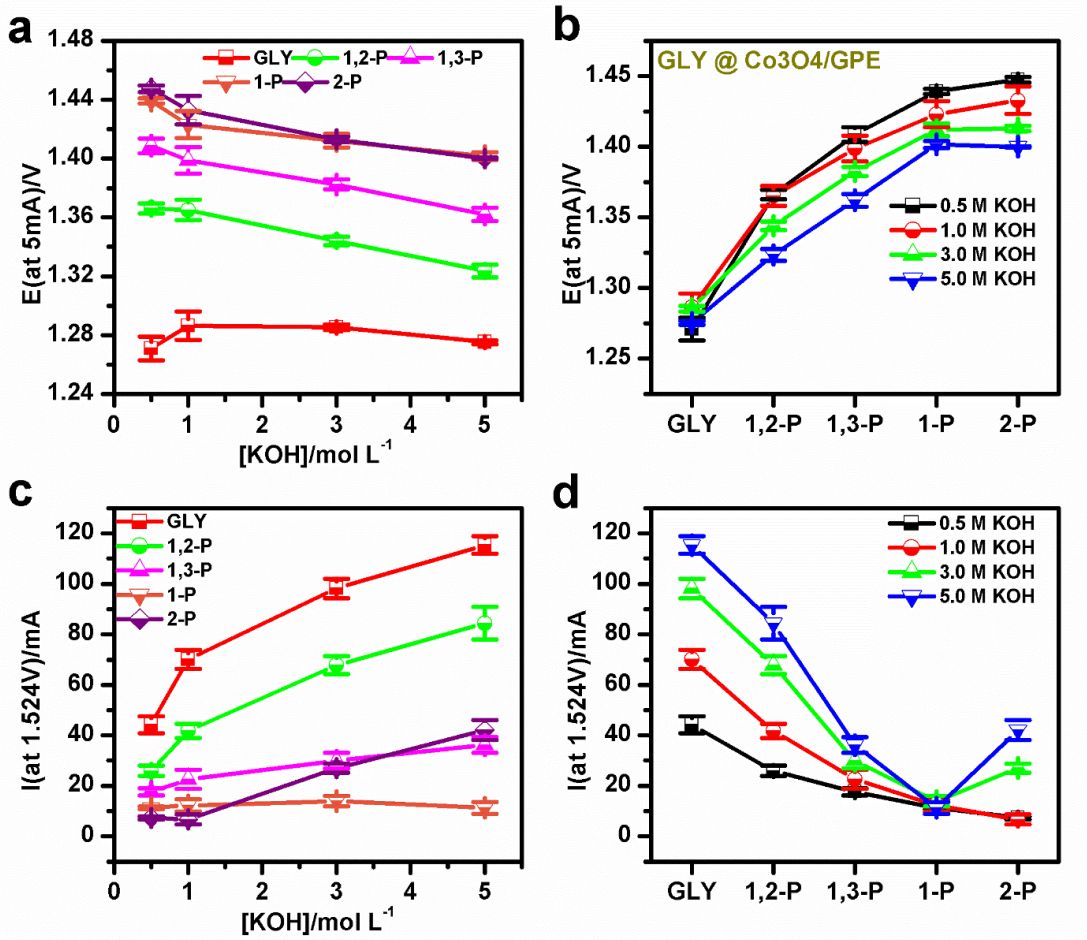

Figure 6.6 Summary of the relationship between (a) oxidation potentials and KOH concentrations; (b) oxidation potentials and C3 saturated alcohol; (c) oxidation currents (at 1.524 V vs. RHE) and KOH concentrations; (d) oxidation currents (at 1.524 V vs. RHE) for C3 saturated alcohols.

6.4 Conclusions

In this chapter, the electro-oxidation of C3 saturated alcohols on Co_3O_4 was conducted in 1.0 M KOH solution. The electro-oxidation rates of these alcohols were found to follow the order: GLY > 1,2-P > 1,3-P > 1-P > 2-P. Higher KOH concentration facilitates the oxidation reaction, especially for those alcohols with secondary hydroxyl group. The NMR

analysis found that the cleavage of C-C bond happened easily for alcohols with adjacent hydroxyl groups.

References:

[1] Z. Zhang, L. Xin and W. Li. *International Journal of Hydrogen Energy*. **2012**, 37, 9393-9401.

[2] J. Qi, L. Xin, Z. Zhang, K. Sun, H. He, F. Wang, D. Chadderdon, Y. Qiu, C. Liang and W. Li. *Green Chemistry*. **2013**, 15, 1133.

[3] Z. Zhang, L. Xin and W. Li. *Applied Catalysis B: Environmental*. **2012**, 119-120, 40-48.

[4] J. Wang, S. Wasmus and R. F. Savinell. *Journal of the Electrochemical Society*. **1995**, 142, 4218-4224.

[5] S.-C. Chang, Y. Ho and M. J. Weaver. *Journal of the American Chemical Society*. **1991,** 113, 9506-9513

[6] M. Pagliaro, R. Ciriminna, H. Kimura, M. Rossi and C. Della Pina. *Angewandte Chemie*. **2007**, 46, 4434-4440.

[7] B. Katryniok, H. Kimura, E. Skrzyńska, J.-S. Girardon, P. Fongarland, M. Capron, R. Ducoulombier, N. Mimura, S. Paul and F. Dumeignil. *Green Chemistry*. **2011**, 13, 1960.

[8] D. T. Johnson and K. A. Taconi. *Environmental Progress*. **2007**, 26, 338-348.

[9] S. Bagheri, N. M. Julkapli and W. A. Yehye. *Renewable and Sustainable Energy Reviews*. **2015**, 41, 113-127.

[10] Z. Gholami, A. Z. Abdullah and K.-T. Lee. *Renewable and Sustainable Energy Reviews*. **2014**, 39, 327-341.

[11] D. J. Chadderdon, L. Xin, J. Qi, B. Brady, J. A. Miller, K. Sun, M. J. Janik and W. Li, *ACS Catalysis*. **2015**, 5, 6926-6936.

[12] N. Dimitratos, J. A. Lopez-Sanchez, S. Meenakshisundaram, J. M. Anthonykutty, G. Brett, A. F. Carley, S. H. Taylor, D. W. Knight and G. J. Hutchings. *Green Chemistry*. **2009**, 11, 1209.

[13] J. L. Bott-Neto, A. C. Garcia, V. L. Oliveira, N. E. de Souza and G. Tremiliosi-Filho. *Journal of Electroanalytical Chemistry*. **2014**, 735, 57-62.

[14] C. S. Lee, M. K. Aroua, W. M. A. W. Daud, P. Cognet, Y. Pérès-Lucchese, P. L. Fabre, O. Reynes and L. Latapie. *Renewable and Sustainable Energy Reviews*. **2015**, 42, 963-972.

[15] J. Mahmoudian, M. Bellini, M. V. Pagliaro, W. Oberhauser, M. Innocenti, F. Vizza and H. A. Miller. *ACS Sustainable Chemistry & Engineering*. **2017**, 5, 6090–6098.

[16] M. E. M. Chbihi, D. Takky, H. F., H. H., J. M. Leger and L. C.. *Journal of Electroanalytical Chemistry*. **1999**, 463, 63-71.

[17] S. Sun and Z. J. Xu. *Electrochimica Acta*. **2015**, 165, 56-66.

[18] L. Qian, L. Gu, L. Yang, H. Yuan and D. Xiao. *Nanoscale*. **2013**, 5, 7388.

[19] M. Jafarian, M. G. Mahjani, H. Heli, F. Gobal, H. Khajehsharifi and M. H. Hamedi. *Electrochimica Acta*. **2003**, 48, 3423-3429.

[20] J. B. Wu, Z. G. Li, X. H. Huang and Y. Lin. *Journal of Power Sources*. **2013**, 224, 1-5.

[21] M. Asgari, M. G. Maragheh, R. Davarkhah, E. Lohrasbi and A. N. Golikand. *Electrochimica Acta*. **2012**, 59, 284-289.

[22] S. Moret, P. J. Dyson and G. Laurenczy. *Dalton transactions*. **2013**, 42, 4353-4356.

[23] S. Sun, Y. Zhou, B. Hu, Q. Zhang and Z. J. Xu. *Journal of The Electrochemical Society*. **2015**, 163, H99-H104.

[24] H. Y. Wang, S. F. Hung, H. Y. Chen, T. S. Chan, H. M. Chen and B. Liu. *J Am Chem Soc*. **2016**, 138, 36-39.

[25] A. Bergmann, E. Martinez-Moreno, D. Teschner, P. Chernev, M. Gliech, J. F. de Araujo, T. Reier, H. Dau and P. Strasser. *Nature communications*. **2015**, 6, 8625.

[26] N. Spataru, C. Terashima, K. Tokuhiro, I. Sutanto, D. A. Tryk, S.-M. Park and A. Fujishima. *Journal of The Electrochemical Society*. **2003**, 150, E337.

[27] Y. Kwon, K. J. P. Schouten and M. T. M. Koper. *ChemCatChem*. **2011**, 3, 1176-1185.

[28] Z. Zhang, L. Xin, J. Qi, Z. Wang and W. Li. *Green Chemistry*. **2012**, 14, 2150.

[29] J. Liu, J. Ye, C. Xu, S. P. Jiang and Y. Tong. *Electrochemistry Communications*. **2007**, 9, 2334-2339.

[30] Z. X. Liang, T. S. Zhao, J. B. Xu and L. D. Zhu. *Electrochimica Acta*. **2009**, 54, 2203-2208.

[31] Y. Wang, D. Zhang, W. Peng, L. Liu and M. Li. *Electrochimica Acta*. **2011**, 56, 5754-5758.

Chapter 7

Discussion and Future Work

This chapter gives a general discussion on the electro-oxidation of C1, C2, and C3 saturated alcohols. For C1 and C2 alcohols on Ni-Co oxides, Ni can promote the alcohol oxidation rate and increase the intermediate product adsorption. For C3 saturated alcohols, the oxidation rate ranks as GLY > 1,2-P > 1,3-P > 1-P > 2-P on Co_3O_4. The C-C bond is readily to be broken up when existing the hydroxyl groups. The Based on the current results, three aspects of future work can be carried out. (1) Alcohol Oxidation on Ni/Co in different Coordination; (2) Glycerol Oxidation on Co in different Coordination; (3) Dihydric Alcohols Oxidation on the Co_3O_4 electrode.

7.1 General Discussion

7.1.1 Methanol Oxidation on Ni-Co Hydroxides and Ni-Co Oxides

Based on the results of methanol oxidation in Chapter 4, an interesting phenomenon can be found that though Ni content increased both in Ni-Co hydroxides and Ni-Co oxides, the methanol oxidation activities exhibited different trends. As the Ni content increased, the methanol oxidation activity increased in Ni-Co hydroxides, while exhibited a volcano shape in Ni-Co oxides. It suggests that the composition dependence of methanol oxidation activity is related to the crystal structure. The Ni-Co hydroxide is a kind of structure, where Ni and Co atoms are coordinated with six oxygen atoms in octahedral sites at any Ni/Co ratio. Whereas, with the increase of Ni content in Ni-Co oxides, the crystal structure of Ni-Co oxides change from spinel structure to the mixture of spinel and rocksalt structure. It means that there is a maximum value of Ni accommodated in $Ni_xCo_{3-x}O_4$ spinel structure. Ni / (Ni + Co) 33% is the maximum value in our system, and this value corresponds to a relatively high methanol oxidation activity. When considering the Ni coordination environment, it is noticed that not all Ni ions occupy the octahedral sites in spinel structure. Thus, it is necessary to investigate the Ni contribution to methanol oxidation in a certain and independent coordination environment. Two coordination environments need to be considered, and they are tetrahedral sites and octahedral sites, respectively.

7.1.2 Ethylene Glycol and Ethanol Oxidation on Ni-Co Oxides

Based on the results in Chapter 5, it has been found that the electro-oxidation activity of ethylene glycol and ethanol on Ni-Co oxides exhibited a volcano-shaped trend with the increase of Ni content. The balance of the oxidation rates between from alcohol to intermediate products and from intermediate products to final products was considered the key factor to determine the overall oxidation rate. The role of Ni was considered to increase the intermediate product adsorption and oxidation rates from alcohol to intermediate products. However, excess Ni would lead to the accumulation of intermediate products, which block the active sites on the surface, and thus lower the alcohol oxidation activity.

In the study of comparing the oxidation of ethylene glycol and ethanol, it was found that the oxidation rate difference of ethylene glycol and ethanol were determined by the hydroxyl group number and the consumption and diffusion of alcohols. At low potentials, ethylene glycol had a higher oxidation rate than ethanol, which depended on the number of hydroxyl group on each molecule. At high potential, ethylene glycol and ethanol had similar oxidation rates, which was caused by the different diffusion rates.

7.1.3 C3 saturated Alcohol Oxidation on Co_3O_4

Based on the results in Chapter 6, it was found that the oxidation rates of C3 alcohols were related to the number and position of hydroxyl groups. The more hydroxyl groups the alcohol had, the higher oxidation rate it had. The alcohols with adjacent hydroxyl groups had a higher oxidation rate, and meanwhile the C-C bond was easier to break up. Increasing the KOH concentration can facilitate the alcohol oxidation rates, especially for those alcohols with secondary hydroxyl group.

7.2 Reconnaissance work

7.2.1 Alcohol Oxidation on Ni/Co in different Coordination

According to the Chapter 4 and 5, a volcano-shaped relationship between methanol, ethanol, and ethylene glycol oxidation activity and Ni/Co ratio can be found in Ni-Co oxides. It is also noticed that in Ni-Co oxides, as the Ni content increases, the structure of Ni-Co oxides changes from spinel structure to the mixed structure of spinel and rocksalt. Spinel is a very complex structure with stoichiometric AB_2O_4, having one tetrahedral site and two octahedral sites in one molecule structure. Meanwhile, the valence state of the metal element changes when the metal element occupies different sites. Generally, spinel structure is divided into two categories, normal spinel structure and inverse spinel structure, according to the occupation A and B cations. There are two different rules to judge the normal spinel and inverse spinel. One is based on the stoichiometry.[1] For example, one AB_2O_4 molecule has one A cation and two B cations. If one A cation is in the tetrahedral

site and two B cations are in the octahedral site, this spinel structure is called normal spinel structure. If one A cation is in the octahedral site and two B cations are distributed in the tetrahedral and octahedral sites equally, this spinel structure is called inverse spinel structure. The other rule is based on the valence state.[2] In AB_2O_4, if one A cation with +2 valence state occupies the tetrahedral site and two B cations with +3 occupies the octahedral sites, this spinel structure is called normal spinel structure. If one A cation with +2 occupies the octahedral sites and two B cations with +3 valence state are distributed in the tetrahedral and octahedral sites equally, this spinel structure is called inverse spinel structure. Here, we use the second rule to determine the spinel category. For example, Co_3O_4 has a normal structure because one Co^{2+} ion is in the tetrahedral site and Co^{3+} ions are in the octahedral sites in one Co_3O_4 molecule.[2-5] While, Fe_3O_4 has an inverse structure because one Fe^{2+} ion in the octahedral site and two Fe^{3+} ions are equally distributed in the tetrahedral and octahedral sites in one Fe_3O_4 molecule.[6, 7] Based on the report, in $NiCo_2O_4$, both Ni and Co ions are distributed in the tetrahedral and octahedral sites, and most Ni ions are in octahedral sites.[8-10] Though it can be determined that the electro-oxidation activity of methanol, ethanol, and ethylene glycol has a composition dependence in Ni-Co oxides, the occupation influence on alcohol oxidation is not excluded. In the future work, it is necessary to design a systematic investigation on Ni/Co ratio in the fixed occupation, the tetrahedral site or octahedral site, and the fixed occupation is not limited in the spinel structure.

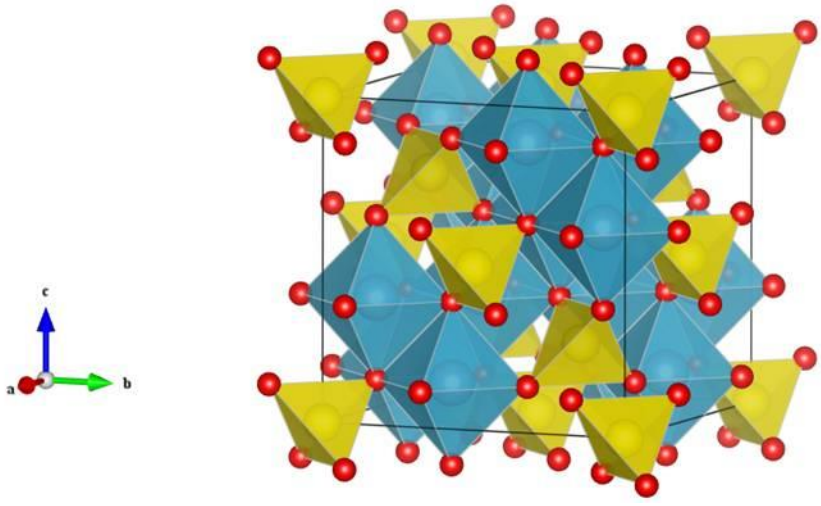

Figure 7.1 The crystal structure of AB_2O_4. The A atoms are located in the yellow tetrahedral sites and the B atoms are located in the blue octahedral site.[11]

To studying the effect of Ni/Co composition on methanol oxidation in tetrahedral sites of spinel structure, it is very important chose a series of materials, in which all Ni and Co can occupy the tetrahedral sites exclusively, and meanwhile the cations in other coordination environments are inactive to electro-oxidation of alcohols. Thus, we will choose $CoAl_2O_4$, $Ni_xCo_{1-x}Al_2O_4$, and $NiAl_2O_4$ as electrocatalysts. For $CoAl_2O_4$, the normal spinel structure can be obtained by choosing the proper synthesis method.[12] For $NiAl_2O_4$, the inverse structure often exists.[13, 14] Thus, it is necessary to choose an optimal temperature to maximize the occupation of Ni and Co in tetrahedral site. The sol-gel method can be used to synthesize a series of $Ni_xCo_{1-x}Al_2O_4$ by calcination at optimal temperature. Thus, the powder samples will be synthesized directly instead of film/substrate.

To investigate the Ni/Co composition effect on alcohol oxidation in the octahedral site of spinel structure, choosing a series of materials with Ni and Co occupying the octahedral site exclusively and inactive metal elements occupying tetrahedral sites is necessary. Thus, based on reports, the $ZnCo_2O_4$ of with a normal spinel structure[3, 15] will be used as matrix, and an increasing amount of Ni will be tried to dope into the octahedral site to substitute Co in the octahedral site. $ZnCo_{2-x}Ni_xO_4$ will be prepared.

Except for spinel, rocksalt and perovskite structures are also choices to guarantee Ni and Co to occupy the octahedral sites. In rocksalt-type structure, each of the two atom types forms a separate face-centered cubic lattice, with the two lattices interpenetrating so as to form a 3D checkerboard pattern. In the part, we have finished the sample synthesis by high-temperature decomposition method. The XRD patterns of $Ni_xCo_{1-x}O$ can be found in Figure 7.2. Perovskite structure is often written as ABO_3, where A represents the rare earth metal element and B represents the transition metal. In perovskite structure, the cations in A and B hardly exchange their position. Here $LaCo_{1-x}Ni_xO_3$ is a good choice due to the same symmetry of $LaCoO_3$ and $LaNiO_3$. Thus, a series of $LaCo_{1-x}Ni_xO_3$ will be used to investigate the Ni/Co composition effect on alcohol oxidation in octahedral sites. As this work, we have synthesized the $LaCo_{1-x}Ni_xO_3$ by sol-gel method, and the XRD patters are shown in Figure 7.3.

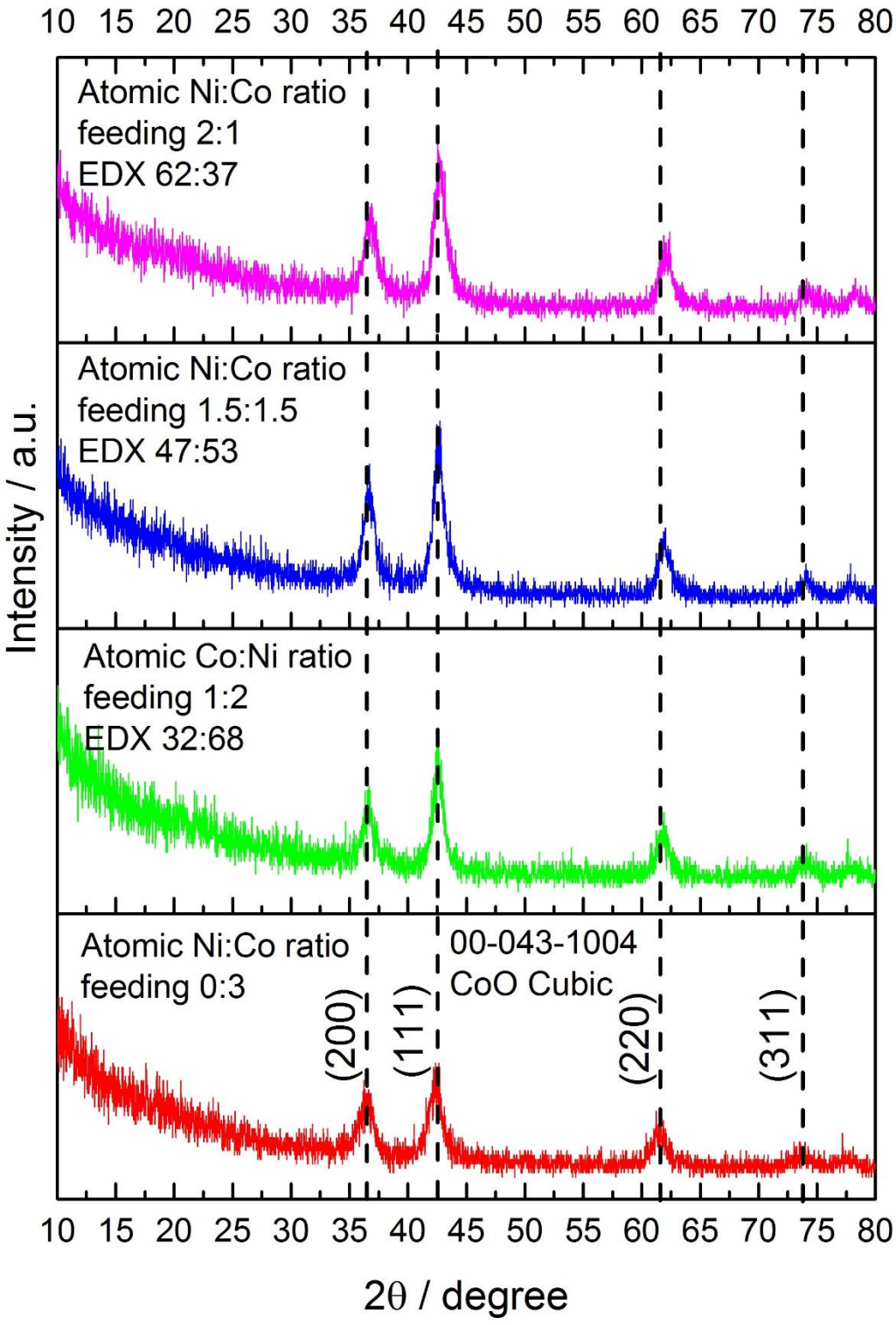

Figure 7.2 XRD patterns of $Ni_xCo_{1-x}O$.

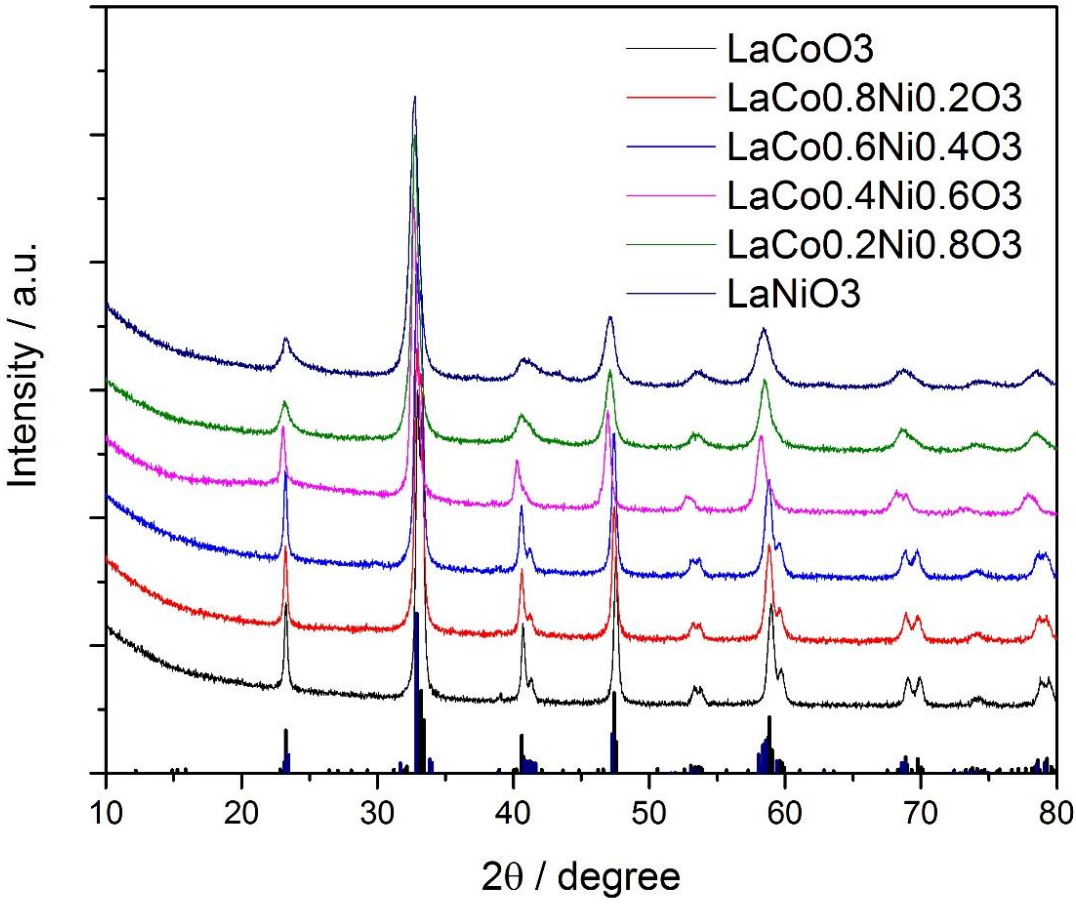

Figure 7.3 XRD patterns of $LaCo_{1-x}Ni_xO_3$.

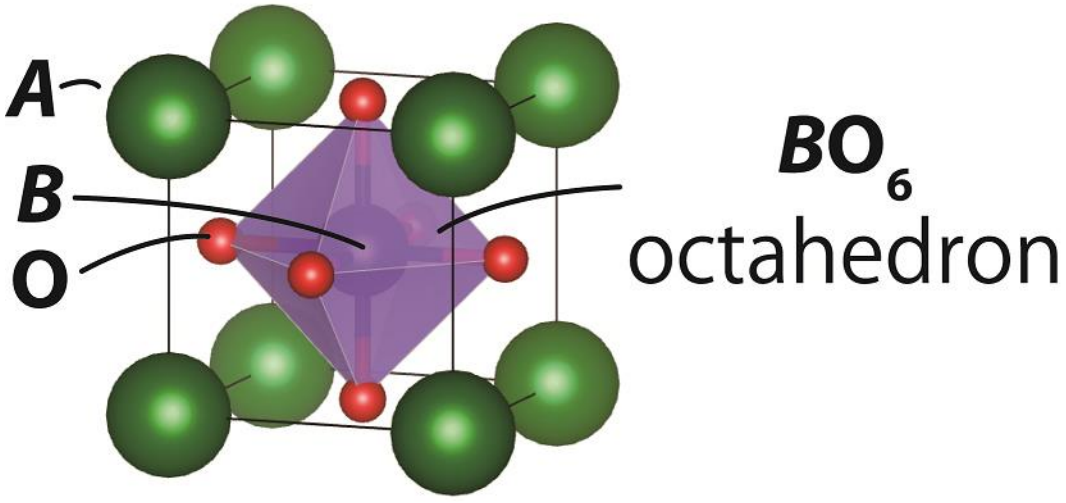

Figure 7.4 Ideal cubic ABO_3 perovskite-type structure[16]

7.2.2 Glycerol Oxidation on Co in different Coordination

From CV curves of glycerol oxidation on Co_3O_4, it can be found that the glycerol oxidation started to occur at 0.3 V vs, Hg/HgO in 1.0 M KOH solution, which corresponded to Co^{3+}. It is well known that Co_3O_4 has a spinel structure with Co^{2+} and Co^{3+} itself, with Co^{2+} in the tetrahedral site and Co^{3+} in the octahedral site. When the potential was 0.3 V, only the Co^{2+} ions in the tetrahedral site were oxidized to Co^{3+}, and the valence state of Co in the octahedral site did not change. It is assumed that the glycerol oxidation was easier to take place on Co in the tetrahedral site than in the octahedral site. To verify this assumption, a systematic comparison needs to be do. First, $CoAl_2O_4$, $ZnCo_2O_4$, and Co_3O_4 will be used as electrodes. In $CoAl_2O_4$ with normal spinel structure, Co^{2+} ions are in the tetrahedral site. In $ZnCo_2O_4$ with normal spinel structure, Co^{3+} ions are in octahedral sites. Based on our assumption, glycerol oxidation will start to occur on $CoAl_2O_4$ at the potential similar to Co_3O_4, and $ZnCo_2O_4$ will present a higher onset potential than $CoAl_2O_4$ and Co_3O_4 because no Co ions are in the tetrahedral site. Besides, another investigation needs to be conducted, which is on the oxidation activity on Co in different octahedral coordination. Thus, the rocksalt-type of CoO, spinel-type of $ZnCo_2O_4$, perovskite-type of ABO_3, and layer-type of $LiCoO_2$ and $Co(OH)_2$ will be chosen as catalyst. In the rocksalt-type of CoO, all the Co^{2+} ions are located in the corner-shared octahedral site. In the perovskite-type of ABO_3, all the Co^{3+} ions are located in corner-shared octahedral site. In the layer-type of $LiCoO_2$, all the Co^{3+} ions are located in the edge-shared octahedral site.

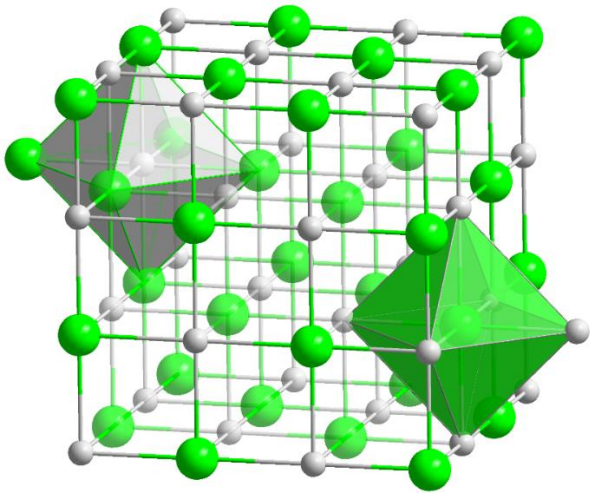

Figure 7.5 The crystal structure of rocksalt.[17]

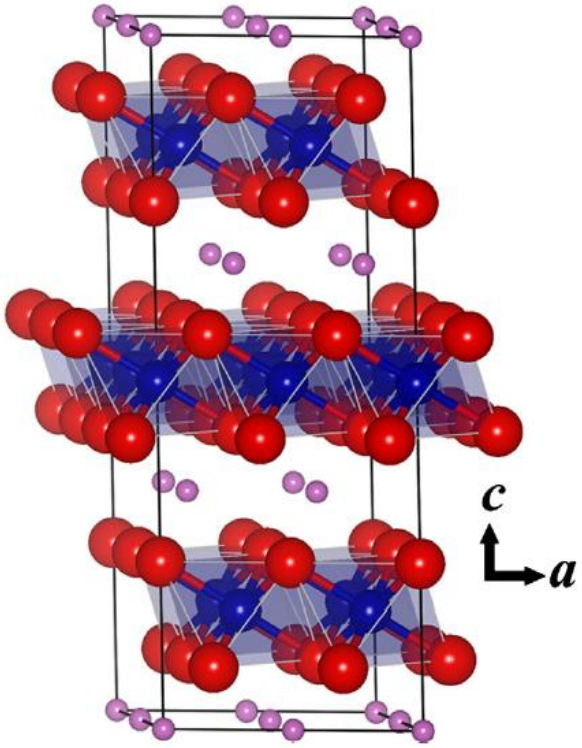

Figure 7.6 The crystal structure of $LiCoO_2$. The small (purples), mid-sized (blue) and large (red) spheres are Li, Co and O atoms, respectively.[18]

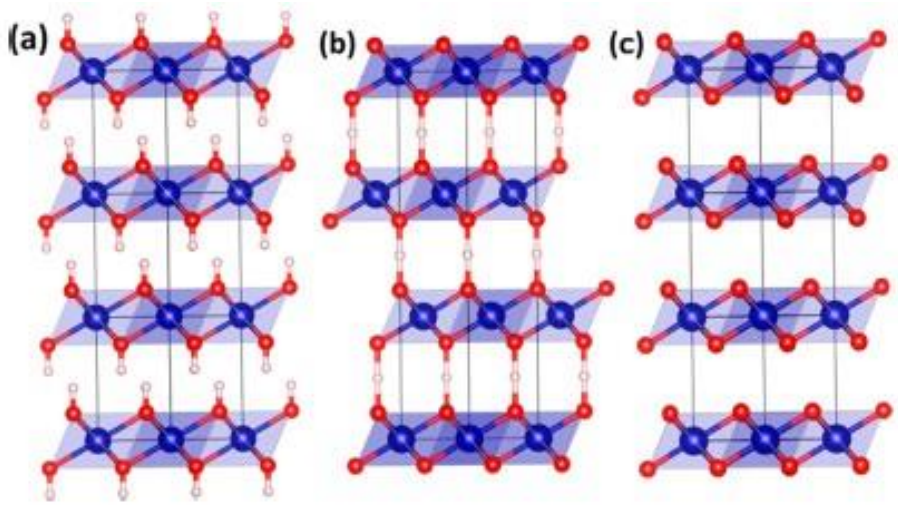

Figure 7.7 Layer structure of (a) $Co(OH)_2$, (b) CoO(OH), and (c)CoO_2.[19]

7.2.3 Dihydric Alcohols Oxidation on Co_3O_4

In C3 alcohol oxidation part, it has been found that the number and position of hydroxyl groups of carbon chain has a dramatic influence on the alcohol oxidation rate and product. It also be found that when there existed the adjacent hydroxyl groups, the corresponding C-C bond was easy to be broken up. Thus, based on our previous work, it is interesting and necessary to explore the electro-oxidation properties of dihydric alcohols and analyze the oxidation products. In this part, we will choose a series of dihydric alcohols, from C2 alcohol (ethylene glycol), C3 alcohols (1,2-propanediol and 1,3-propanediol), to C4 alcohols (1,2-butanediol, 1,3-butanediol, 1,4-butanediol, and 2,3-butanediol). From the investigation of this series of dihydric alcohols, two aspects of conclusions are expected. One is the hydroxyl group position effect in dihydric alcohols on electro-oxidation reactivity. The other one is when the hydroxyl groups were fixed, the carbon position number effect in dihydric alcohols on electro-oxidation reactivity.

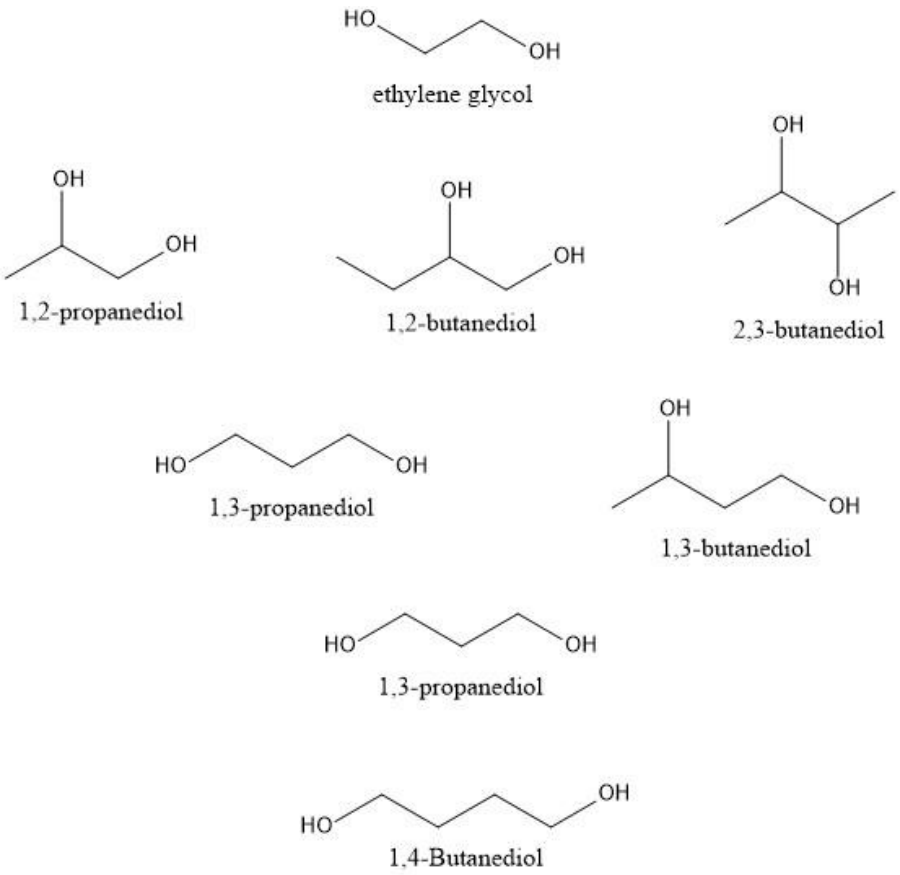

Figure 7.8 The structure of dihydric alcohols to be investigated in future work.

In this thesis, I have finished the methanol, ethanol, and ethylene glycol oxidation on Ni-Co oxides. An optimal Ni/Co ratio (46/54) for alcohol oxidation has been found, which is consistent with our hypothesis that there would be the optimal Ni/Co ratio value. The Ni effect on alcohol oxidation was studied and clarified. In the methanol oxidation part, the Ni effect was concluded as to increase the adsorption of intermediate products. In the ethylene glycol and ethanol oxidation part, the increase of Ni increased the oxidation rate from alcohols to intermediate products, and the optimal Ni/Co ratio made a balance between the oxidation rate from alcohol to intermediate products and from intermediate products to final products. Besides, it is also noticed that the structure had a big influence on the optimal Ni/Co ratio. For Ni-Co hydroxides, more Ni brought about higher oxidation activity. In the study on ethylene glycol and ethanol, we found that for the same electrocatalyst, the oxidation rate difference of ethylene glycol and ethanol depended on not only by the difference of molecule structures but also by the difference of diffusion rates. The major oxidation process of ethylene glycol and ethanol was determined as a conversion from hydroxyl group to carboxyl group. In the C3 saturated alcohol oxidation part, we found that the oxidation rates of C3 saturated alcohols was strongly related to the number and position of hydroxyl groups on the carbon chain. The C-C bond with adjacent hydroxyl groups was easier to be broken up. However, the expected value-added products were not obtained due to the C-C bond cleavage.

References:

[1] L. Suchow. *Journal of Chemical Education, New Jersey Institute of Technology, Newark. New Jersey. 07102*, 560-560.

[2] M. Casas-Cabanas, G. Binotto, D. Larcher, A. Lecup, V. Giordani and J.-M. Tarascon. *Chemistry of Materials*. **2009**, 21, 1939-1947.

[3] N. H. Perry, T. O. Mason, C. Ma, A. Navrotsky, Y. Shi, J. S. Bettinger, M. F. Toney, T. R. Paudel, S. Lany and A. Zunger. *Journal of Solid State Chemistry*. **2012**, 190, 143-149.

[4] K. M. Nam, J. H. Shim, D.-W. Han, H. S. Kwon, Y.-M. Kang, Y. Li, H. Song, W. S. Seo and J. T. Park. *Chemistry of Materials*. **2010**, 22, 4446-4454.

[5] Y. Ikedo, J. Sugiyama, H. Nozaki, H. Itahara, J. H. Brewer, E. J. Ansaldo, G. D. Morris, D. Andreica and A. Amato. *Physical Review B*. **2007**, 75. 054424.

[6] Z. Szotek, W. M. Temmerman, D. Ködderitzsch, A. Svane, L. Petit and H. Winter. *Physical Review B*. **2006**, 74. 174431.

[7] C. L. Shufeng Si, Xun Wang, Dapeng Yu, Qing Peng, and Yadong Li. *Crystal Growth & Design*. **2005**, 5, 391-393.

[8] R. Ding, L. Qi, M. Jia and H. Wang. *Catal. Sci. Technol.* **2013**, 3, 3207-3215.

[9] L. Qian, L. Gu, L. Yang, H. Yuan and D. Xiao. *Nanoscale*. **2013**, 5, 7388.

[10] Y. Li, P. Hasin and Y. Wu. *Advanced materials*. **2010**, 22, 1926-1929.

[11] https://crystallography365.files.wordpress.com/2014/09/spinel.jpg

[12] H. Y. Wang, S. F. Hung, H. Y. Chen, T. S. Chan, H. M. Chen and B. Liu. *J Am Chem Soc*. **2016**, 138, 36-39.

[13] E. Ustundag, B. Clausen and M. A. M. Bourke. *Applied Physics Letters*. **2000**, 76, 694-696.

[14] M. Khairy, *Journal of the Iranian Chemical Society*. **2016**, **13**, 671-677.

[15] T. W. Kim, M. A. Woo, M. Regis and K. S. Choi. *The journal of physical chemistry letters*. **2014**, 5, 2370-2374.

[16] https://www.kek.jp/en/NewsRoom/Release/20140516150000/

[17] https://chemistry.stackexchange.com/questions/23673/rock-salt-structure

[18] F. Ning, S. Li, B. Xu and C. Ouyang. *Solid State Ionics*, **2014**, 263, 46-48.

[19] J. Chen and A. Selloni. *The Journal of Physical Chemistry C*, **2013**, 117, 20002-20006.

APPENDIX

Table A.1 Equivalent circuit parameters of MOR on Co(OH)2 (Ni 0%)

E/V	R_s/Ω	R_{ct}/Ω	Q_1/F s^(a_1-1)	a_1	R_{ads}/Ω	Q_2/F s^(a_1-1)	a_2
0.50	1.860	36.77	0.04597	0.9758			
0.52	1.850	23.66	0.04489	0.9088			
0.54	1.850	15.24	0.04548	0.8978			
0.56	1.850	10.59	0.04725	0.8764			
0.58	1.850	7.064	0.04408	0.8939			
0.60	1.840	4.421	0.04092	0.8992			

Table A.2 Equivalent circuit parameters of MOR on Ni-Co hydroxide (Ni 15%)

E/V	R_s/Ω	R_{ct}/Ω	Q_1/F s^(a1-1)	a_1	R_{ads}/Ω	Q_2/F s^(a_1-1)	a_2
0.50	1.580	31.74	0.05359	0.9198			
0.52	1.580	20.11	0.05013	0.9607			
0.54	1.580	13.17	0.05157	0.9375			
0.56	1.580	8.584	0.05154	0.9381			
0.58	1.570	5.311	0.04855	0.9628			
0.60	1.580	3.136	0.04653	0.9639			

Table A.3 Equivalent circuit parameters of MOR on Ni-Co hydroxide (Ni 27%)

E/V	R_s/Ω	R_{ct}/Ω	Q_1/F s^(a_1-1)	a_1	R_{ads}/Ω	Q_2/F s^(a_1-1)	a_2
0.50	1.840	15.71	0.04695	0.9436			
0.52	1.840	12.12	0.04356	0.9565			
0.54	1.830	8.712	0.04102	0.9771			
0.56	1.830	6.404	0.04023	0.9904			
0.58	1.820	4.399	0.03983	1.0000			
0.60	1.820	2.902	0.03921	0.9905			

Table A.4 Equivalent circuit parameters of MOR on Ni-Co hydroxide (Ni 46%)

E/V	R_s/Ω	R_{ct}/Ω	Q_1/F s^(a_1-1)	a_1	R_{ads}/Ω	Q_2/F s^(a_1-1)	a_2
0.50	1.850	5.174	0.05646	0.9331			
0.52	1.850	5.143	0.04524	0.9671			
0.54	1.840	4.659	0.04583	0.9660			
0.56	1.840	3.917	0.04641	0.9641			
0.58	1.840	3.018	0.04532	0.9706			
0.60	1.840	2.214	0.04461	0.9873			

Table A.5 Equivalent circuit parameters of MOR on Ni-Co hydroxide (Ni 75%)

E/V	R_s/Ω	R_{ct}/Ω	Q_1/F s^(a_1-1)	a_1	R_{ads}/Ω	Q_2/F s^(a_1-1)	a_2
0.50	2.020	2.453	0.04867	0.9349			
0.52	2.030	1.727	0.04420	0.9569			
0.54	2.030	1.503	0.04020	0.9064			
0.56	2.030	1.335	0.04016	0.9194			
0.58	2.030	1.279	0.04259	0.9013			
0.60	2.030	1.228	0.04407	0.9075			

Table A.6 Equivalent circuit parameters of MOR on $Ni(OH)_2$ (Ni 100%)

E/V	R_s/Ω	R_{ct}/Ω	Q_1/F s^(a_1-1)	a_1	R_{ads}/Ω	Q_2/F s^(a_1-1)	a_2
0.50	1.990						
0.52	1.990						
0.54	1.980						
0.56	1.990	0.875	0.01105	0.6445	1.080	0.01552	1.0000
0.58	2.000	0.677	0.03037	0.5700	0.928	0.01158	1.0000
0.60	2.010	0.580	0.04337	0.5822	0.806	0.01234	1.0000

Table A.7 Equivalent circuit parameters of MOR on Co_3O_4 (Ni 0%)

E/V	R_s/Ω	R_{ct}/Ω	Q_1/F s^(a_1-1)	a_1	R_{ads}/Ω	Q_2/F s^(a_1-1)	a_2
0.50	2.020	163.6	0.02838	0.8740			
0.52	2.000	98.71	0.02297	0.8651			
0.54	1.990	64.38	0.02042	0.9038			
0.56	1.970	49.81	0.02063	0.8840			
0.58	1.960	40.27	0.02223	0.8592			
0.60	1.950	25.36	0.02264	0.8717			

Table A.8 Equivalent circuit parameters of MOR on Ni-Co oxides (Ni 15%)

E/V	R_s/Ω	R_{ct}/Ω	Q_1/F s^(a_1-1)	a_1	R_{ads}/Ω	Q_2/F s^(a_1-1)	a_2
0.50	1.690	21.03	0.02838	0.8740			
0.52	1.700	18.95	0.02297	0.8651			
0.54	1.700	16.79	0.02042	0.9038			
0.56	1.700	14.54	0.02063	0.8840			
0.58	1.700	12.30	0.02223	0.8592			
0.60	1.700	9.467	0.02264	0.8717			

Table A.9 Equivalent circuit parameters of MOR on Ni-Co oxides (Ni 27%)

E/V	R_s/Ω	R_{ct}/Ω	Q_1/F s^(a_1-1)	a_1	R_{ads}/Ω	Q_2/F s^(a_1-1)	a_2
0.50	1.900	11.94	0.01669	0.9472			
0.52	1.880	6.874	0.01819	0.9168			
0.54	1.900	5.244	0.01383	0.9685			
0.56	1.890	4.177	0.01395	0.9451			
0.58	1.890	3.770	0.01190	1.0000			
0.60	1.880	3.689	0.01358	0.9588			

Table A.10 Equivalent circuit parameters of MOR on Ni-Co oxides (Ni 46%)

E/V	R_s/Ω	R_{ct}/Ω	Q_1/F s^(a_1-1)	a_1	R_{ads}/Ω	Q_2/F s^(a_1-1)	a_2
0.50	1.720	2.715	0.02279	0.9712			
0.52	1.720	2.237	0.01931	0.9839			
0.54	1.720	1.917	0.01878	0.9848			
0.56	1.720	1.704	0.01762	0.9827			
0.58	1.720	0.609	0.00945	0.9905	0.991	0.01276	1.0000
0.60	1.730	0.271	0.00612	0.9360	1.311	0.01402	0.9817

Table A.11 Equivalent circuit parameters of MOR on Ni-Co oxides (Ni 75%)

E/V	R_s/Ω	R_{ct}/Ω	Q_1/F s^(a_1-1)	a_1	R_{ads}/Ω	Q_2/F s^(a_1-1)	a_2
0.50	2.060	3.654	0.02267	0.9651			
0.52	2.060	2.950	0.01947	0.9866			
0.54	2.060	2.505	0.02000	0.9738			
0.56	2.060	2.150	0.01786	0.9974			
0.58	2.070	1.911	0.02003	1.0000			
0.60	2.080	1.790	0.01779	1.0000			

Table A.12 Equivalent circuit parameters of MOR on NiO (Ni 100%)

E/V	R_s/Ω	R_{ct}/Ω	Q_1/F s^(a_1-1)	a_1	R_{ads}/Ω	Q_2/F s^(a_1-1)	a_2
0.50	2.080	26.11	0.01187	0.8812			
0.52	2.070	14.25	0.01150	0.9331			
0.54	2.070	8.868	0.01127	0.9660			
0.56	2.070	6.123	0.01083	0.9097			
0.58	2.050	4.895	0.01095	0.8816			
0.60	2.060	4.237	0.00957	0.8973			

Table A.13 ρ, η, D and Sc of EG and EtOH in water at 25 °C.

Liquid	ρ / g mL^{-1}	η / mPa s	D / 10^{-5} cm^2 s^{-1}	Sc / 10^3
EG	2.050	4.8950	0.010950	0.8816
EtOH	2.060	4.2370	0.009573	0.8973

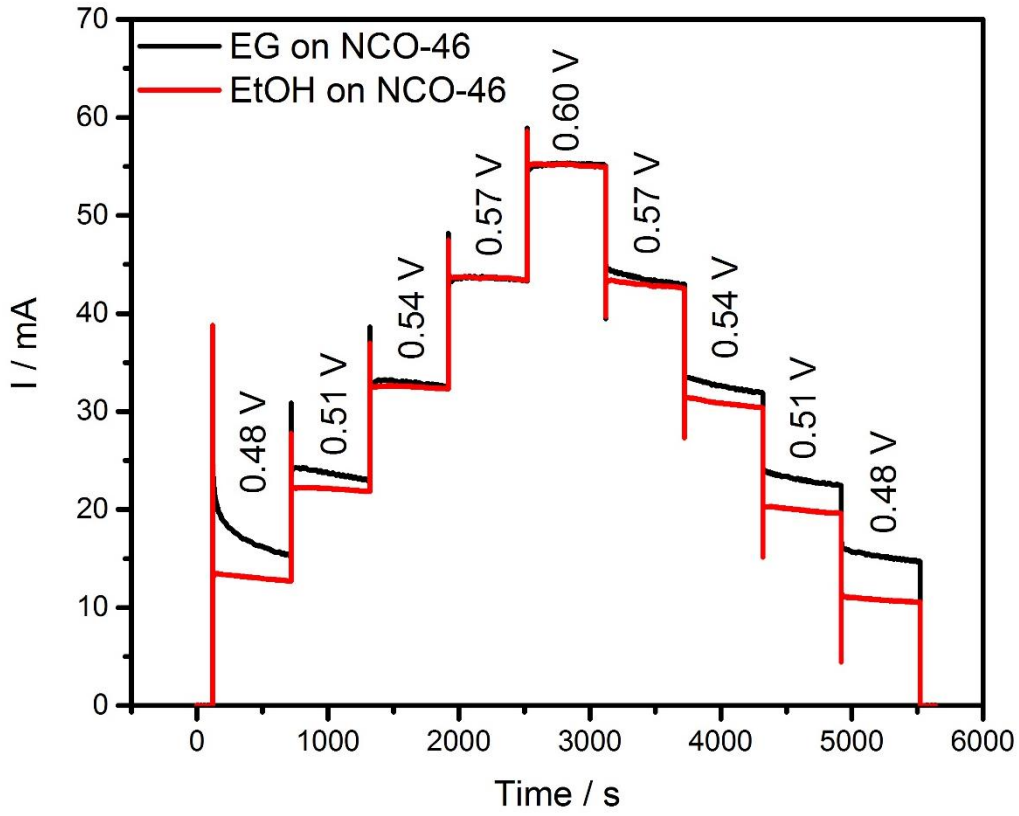

Figure A.1 The multi-step CA curves of EG and EtOH oxidation on NCO-46. It was conducted according to the following procedure. First, the working electrode was held at 0 V for 2 min. Then, it was held for 10 min at 0.48, 0.51, 0.54, 0.57, 0.60, 0.57, 0.54, 0.51, and 0.48 V, respectively.

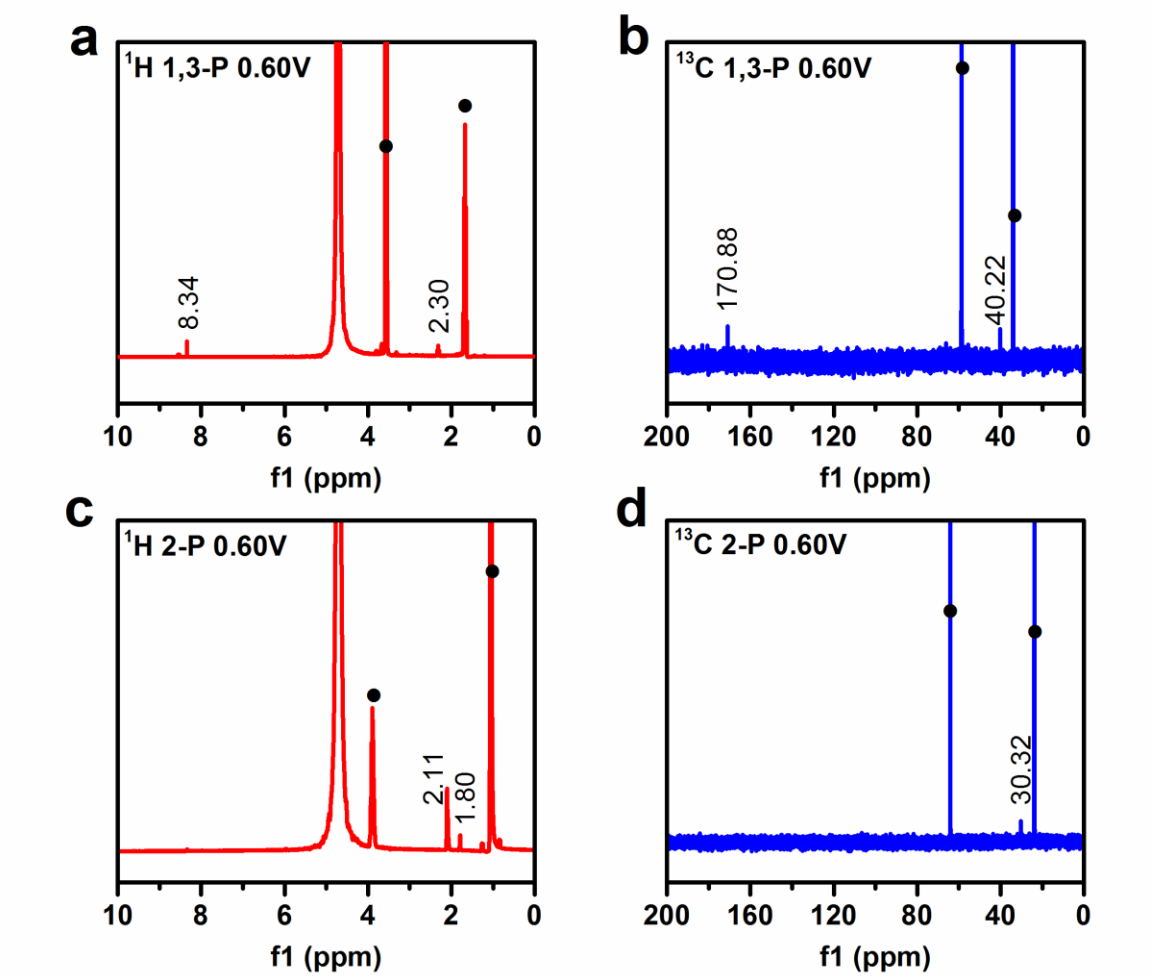

Figure A.2 The ^{1}H (a and c) and ^{13}C (b and d) NMR spectra of electrolyte solution after 24 hour oxidation of 1,3-P and 2-P. The dots represent the peaks from substrates.

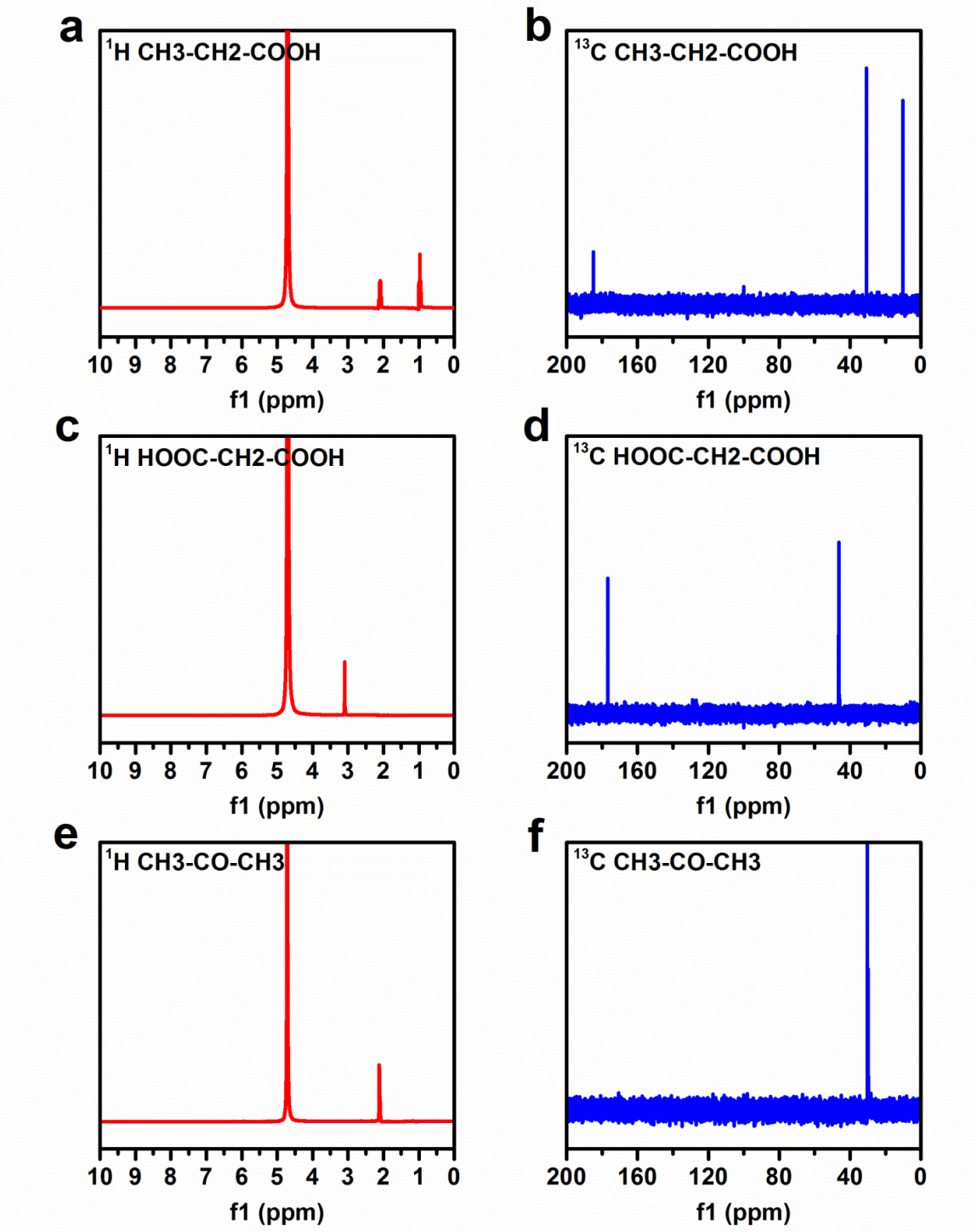

Figure A.3 The ^{1}H and ^{13}C NMR spectra of propionate (a and b), malonate (c and d), and acetone (e and f) in 1.0 M KOH aqueous solution.

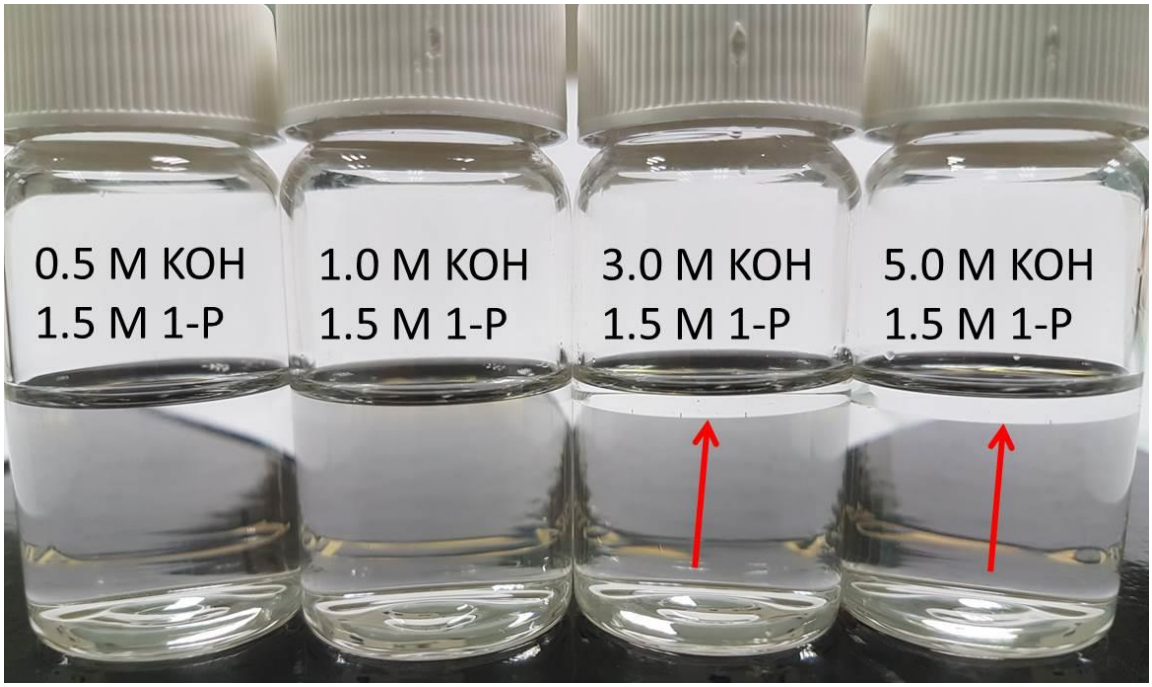

Figure A.4 The photographs of 1-propanol in different concentrations of KOH solution.